November 2017

Evaluating satellite and supercomputing technologies for improved coastal ecosystem assessments

Matthew James Mccarthy
University of South Florida, mjm8@mail.usf.edu

EVALUATING SATELLITE AND SUPERCOMPUTING TECHNOLOGIES FOR IMPROVED COASTAL ECOSYSTEM ASSESSMENTS

by

Matthew James McCarthy

A dissertation submitted in partial fulfillment
of the requirements for the degree of
Doctor of Philosophy
College of Marine Science
University of South Florida

Major Professor: Frank E. Muller-Karger, Ph.D.
Don Chambers, Ph.D.
Holly Greening, M.S.
Mark Luther, Ph.D.
J.M. Smoak, Ph.D.

Date of Approval:
November 6, 2017

Keywords: Water quality, wetlands, mangroves, Gulf of Mexico, WorldView-2, VIS/NIR satellite imagery

DEDICATION

This dissertation is dedicated to my parents, Kevin McCarthy, Karelisa Hartigan, and Cynthia Wetzel. Thank you for the years of support, love, guidance and inspiration. Thanks also to my wife, Jennifer Granneman, for encouraging me as we pursued our doctoral dreams together.

ACKNOWLEDGMENTS

I must first thank my advisor, Dr. Frank Muller-Karger, for the support, encouragement and mentorship offered throughout my time at USF. His guidance allowed me to explore multiple elements of marine science and remote sensing research with a solid foundation in scientific principles. I also thank the members of my dissertation committee - Dr. Mark Luther, Dr. Don Chambers, Dr. J.M. Smoak, and Ms. Holly Greening - for guiding me through the research development, statistical analyses, and implication discussions of this research. I must likewise thank my coauthors from the University of South Florida, University of Puerto Rico, and Florida Fish and Wildlife Research Institute, for helping me publish some of this research before defending.

As noted in the dedication, I am deeply grateful for the love and support of my wife, Jennifer Granneman, whom I met at orientation for this doctoral program. I could not have asked for a more thoughtful, brilliant and considerate partner with whom to pursue this academic endeavor. My colleagues in the Institute for Marine Remote Sensing lab over the past five years have been wonderful to work with and learn from, and I appreciate the sense of community and belonging that they inspired in me from my first day.

This research would not have been possible without the financial support from the Environmental Protection Agency Science to Achieve Results Program, and 2016 USF Gulf Oceanographic Charitable Trust Foundation Endowed Fellowship in Marine Science.

TABLE OF CONTENTS

LIST OF TABLES

LIST OF FIGURES

ABSTRACT

Water quality and wetlands represent two vital elements of a healthy coastal ecosystem. Both experienced substantial declines in the U.S. during the 20th century. Overall coastal wetland cover decreased over 50% in the 20th century due to coastal development and water pollution. Management and legislative efforts have successfully addressed some of the problems and threats, but recent research indicates that the diffuse impacts of climate change and non-point source pollution may be the primary drivers of current and future water-quality and wetland stress. In order to respond to these pervasive threats, traditional management approaches need to adopt modern technological tools for more synoptic, frequent and fine-scale monitoring and assessment. In this dissertation, I explored some of the applications possible with new, commercial satellite imagery to better assess the status of coastal ecosystems.

Large-scale land-cover change influences the quality of adjacent coastal water. Satellite imagery has been used to derive land-cover maps since the 1960's. It provides multiple data points with which to evaluate the effects of land-cover change on water quality. The objective of the first chapter of this research was to determine how 40 years of land-cover change in the Tampa Bay watershed (6,500 km^2) may have affected turbidity and chlorophyll concentration – two proxies for coastal water quality. Land cover classes were evaluated along with precipitation and wind stress as explanatory variables. Results varied between analyses for the entire estuary and those of segments within the bay. Changes in developed land percent cover best explained the turbidity and chlorophyll-concentration time series for the entire bay ($R^2 > 0.75$, $p < 0.02$).

The paucity of official land-cover maps (i.e. five maps) restricted the temporal resolution of the assessments. Furthermore, most estuaries along the Gulf of Mexico do not have forty years of water-quality time series with which to perform evaluations against land-cover change. Ocean-color satellite imagery was used to derive proxies for coastal water with near-daily satellite observations since 2000. The goal of chapter two was to identify drivers of turbidity variability for 11 National Estuary Program water bodies along the Gulf of Mexico. Land cover assessments could not be used as an explanatory variable because of the low temporal resolution (i.e. approximately one map per five-year period). Ocean color metrics were evaluated against atmospheric, meteorological, and oceanographic variables including precipitation, wind speed, U and V wind vectors, river discharge, and water level over weekly, monthly, seasonal and annual time steps. Climate indices like the North Atlantic Oscillation and El Niño Southern Oscillation index were also examined as possible drivers of long-term changes. Extreme turbidity events were defined by the 90^{th} and 95^{th} percentile observations over each time step. Wind speed, river discharge and El Niño best explained variability in turbidity time-series and extreme events ($R^2 > 0.2$, $p < 0.05$), but this varied substantially between time steps and estuaries.

The background land cover analyses conducted for coastal water quality studies showed that there are substantial discrepancies between the wetland extent estimates mapped by local, state and federal agencies. The third chapter of my research sought to examine these differences and evaluate the accuracy and precision of wetland maps using high spatial-resolution (i.e. two-meter) WorldView-2 satellite imagery. Ground validation data showed that wetlands mapped at two study sites in Tampa Bay were more accurately identified by WorldView-2 than by Landsat imagery (30-meter resolution). When compared to maps produced separately by the National Oceanic and Atmospheric Administration, Southwest Florida Water Management District, and

National Wetland Inventory, we found that these historical land cover products overestimated by 2-10 times the actual extent of wetlands as identified in the WorldView-2 maps.

We could find no study that had utilized more than six of these commercial images for a given project. Part of the problem is cost of the images, but there is also the cost of processing the images, which is typically done one at a time and with substantial human interaction. Chapter four explains an approach to automate the preprocessing and classification of imagery to detect wetlands within the Tampa Bay watershed (6,500 km^2). Software scripts in Python, Matlab and Linux were used to ingest 130 WorldView-2 images and to generate maps that included wetlands, uplands, water, and bare and developed land. These maps proved to be more accurate at identifying forested wetland (78%) than those by NOAA, SWFWMD, and NWI (45-65%) based on ground validation data. Typical processing methods would have required 4-5 months to complete this work, but this protocol completed the 130 images in under 24 hours.

Chapter five of the dissertation reviews coastal management case studies that have used satellite technologies. The objective was to illustrate the utility of this technology. The management sectors reviewed included coral reefs, wetlands, water quality, public health, and fisheries and aquaculture.

CHAPTER ONE:

IMPACTS OF 40 YEARS OF LAND COVER CHANGE ON WATER QUALITY IN TAMPA BAY, FLORIDA

1. Research Overview

Estuarine water-quality is a foundational element of coastal-ecosystem health. It may be affected by both natural and anthropogenic phenomena. Managing water quality requires comprehensive knowledge of the factors that drive local water-quality variability. Four decades of turbidity and chlorophyll-concentration measurements in Tampa Bay, Florida, were evaluated for statistical relationships with adjacent land cover change, precipitation, and wind stress. The spatial extent of analyses included the entire estuary and the three individual bay segments within the estuary that have heterogeneous characteristics. Land cover classes were selected based on consistency between mapped products used to cover the study period, and were each included as unique, independent variables for analysis. Results showed that decreased turbidity and chlorophyll-concentrations for the estuary as a whole were best explained by increased developed land fraction. Results for individual bay segments, however, found that developed, agricultural, and bare land, as well as wind stress, explained variability to different degrees depending on the bay segment and time of year.

Note to Reader

This chapter was submitted to the peer-reviewed journal *Cogent Environmental Science* and is included here in Appendix B. The full citation is: McCarthy, M.J., Muller-Karger,

F.E., Otis, D.B., and Méndez-Lázaro, P. Impacts of 40 years of land cover change on water quality in Tampa Bay, Florida. *Cogent Environmental Science*, submitted September 2017.

CHAPTER TWO:

WATER QUALITY DRIVERS IN 11 GULF OF MEXICO ESTUARIES

Abstract

Coastal water-quality is both a primary driver and also a consequence of coastal ecosystem health. Turbidity, a measure of dissolved and particulate water-quality matter, varies daily and can also have large interannual fluctuations. Water quality is influenced by a variety of factors. Identifying which factors drive trends and extreme events in turbidity in an estuary helps environmental managers and decision makers plan for and mitigate against water-quality issues. Efforts to do so on large spatial scales have been hampered due to limitations of turbidity data, including coarse and irregular temporal resolution and poor spatial coverage. We addressed these issues by deriving a proxy for turbidity using ocean color satellite products for 11 Gulf of Mexico estuaries from 2000-2014 on weekly, monthly, seasonal and annual time-steps. Turbidity variability was best explained ($R^2 > 0.2$, $p < 0.05$) by wind speed over short time scales (weekly to monthly), while occurrence of extreme turbidity events was closely related ($R^2 > 0.2$, $p < 0.05$) to El Niño-Southern Oscillation cycles in six estuaries over long time frames (months to seasons). As expected, river discharge drove both seasonal as well as event-scale variability in turbidity across estuaries.

1. Introduction

The quality of estuarine and other coastal waters is a complex function of hydrological, meteorological, oceanographic, and human drivers **(**Schmidt et al., 2004; Eleveld et al., 2014;

Yin et al., 2005; Moreno Madriñán et al., 2012). The relative influence of these processes affects water-quality trends, variability, and the occurrence of extreme events. Identifying the primary drivers of such events can be useful for management and mitigation purposes. For example, a state of emergency was declared in two Florida counties in 2016 as a result of thick algal mats growing along highly populated coastal waterways in the St. Lucie and Caloosahatchee estuaries, causing massive fish kills. A commentary published by Michalak (2016) called for targeted research to determine which environmental conditions, and in what combination, increase the likelihood of extreme water-quality issues.

According to the 2012 Environmental Protection Agency (EPA) National Coastal Condition Report, the overall rating of Gulf coast waters was 2.4 out of 5, or "fair" (EPA, 2012). Approximately 10% of the coastal waters were rated "poor", and 53% were rated "fair" for water quality index. More specifically, water clarity was rated poor for 21% of the area. In Tampa Bay, Florida, water quality measured by turbidity and average chlorophyll concentration has improved since the 1970's (Janicki et al., 2001; Moreno Madriñán et al., 2012). This is primarily attributed to the upgrade of waste water treatment plants to tertiary level starting in 1979. This reduced point-source pollution to the bay. Greening et al. (2014) found that nitrogen contributions of point and nonpoint sources to Tampa Bay were 60.3% and 23.9%, respectively, of the total nitrogen loadings in the 1970's. By the 2000's, the total pollution was reduced by about half, but relative contributions were inverted, with point sources contributing about 19.5% and nonpoint 57.4% to nitrogen discharges into the bay. Other Gulf of Mexico estuaries have seen similar trends in water quality in recent decades. In order to continue improving water-quality management in these estuaries, we must better understand the drivers of nonpoint-source water-quality degradation, and constrain their relative effects on long-term trends as well as extreme

events in the bays. Doing so requires long time-series of water quality with sufficient spatial and temporal resolution to characterize variability and enable management actions.

Turbidity is an index of water quality used by the U.S. Environmental Protection Agency (EPA) that measures light transparency in aquatic environments. Turbidity may be modulated by changes in the concentration of colored dissolved organic matter and suspended particulates including sediment and phytoplankton, which are affected by changes in hydrological, meteorological, and oceanographic phenomena (Eleveld et al., 2014; Chen et al., 2007a; Miller et al., 2011).

Precipitation within a drainage basin influences water quality through increased nutrient and sediment discharge into rivers (Al-Taani, 2014; Jordan et al., 2012; Miller et al., 2011). Wind also influences water quality through sediment resuspension in coastal areas (Chen et al. 2007b; Chen et al. 2007c; Hu et al. 2004). Schoen et al. (2014) modeled circulation in an estuarine lake and found that circulation patterns were highly influenced by diurnal wind speed and direction variability, driving significant intermittent mixing. Dixon et al. (2014) studied seasonal colored dissolved organic matter (CDOM) sources within a North Carolina estuary, and found that CDOM was controlled by wind speed, wind direction, and river discharge.

River discharge increases nutrient and sediment loads to coastal waters, thereby increasing turbidity with suspended sediments, CDOM, and phytoplankton blooms (Stoker, et al. 1996; Fernandez-Novoa et al. 2014). Dorado et al. (2015) evaluated the effects of freshwater inflow on phytoplankton in Galveston Bay, Texas, and found that a combination of nutrient loading and hydraulic displacement drove phytoplankton biomass and community composition throughout the bay.

In addition to wind and freshwater-inflow variability, other forces that affect water level drive estuarine water quality by influencing circulation, sediment suspension, and coastal erosion. Over hourly to daily periods, tidal circulation can impact estuarine phytoplankton and suspended sediment concentrations (Chen et al., 2010). Over longer periods, the sea-level cycle of the Gulf coast has changed such that lower winter and higher summer levels are now observed (Wahl et al. 2014). While long-term water level is not typically investigated for effects on water quality, we include it here to account for apparent changes in this fundamental element of estuarine composition.

While each of these environmental variables has been shown or hypothesized to influence local water quality parameters, broader climatic variability may explain long-term patterns in regional water quality. Scarsbrook et al. (2003) studied the effects of El Niño-Southern Oscillation (ENSO) patterns on New Zealand riverine water quality and found significant relationships between them, even after accounting for river flow variability. Their results suggested that ENSO significantly impacted water quality, independent of indirect effects through known precipitation variability caused by ENSO patterns. Schmidt et al. (2001) evaluated the effects of ENSO patterns on precipitation and river discharge throughout Florida's watersheds. They found a complex pattern of spatially variable, seasonal relationships, including statistically significant relationships between extreme ENSO events and winter precipitation and river discharge patterns in the Tampa Bay area.

The North Atlantic Oscillation (NAO) also drives seasonal wind and precipitation patterns in the Southeast (Hurrel et al., 2003). The NAO is defined as a meridional alternation of atmospheric mass between the subtropical and arctic North Atlantic. NAO phases may vary from one year to the next, and are greatest in amplitude during November to April (Stenseth et al.,

2003). Kenyon and Hegerl (2010) quantified the impact of the NAO on global precipitation extremes and found that, while more closely connected with European precipitation, statistically significant responses were found in some North American precipitation stations, including those along the Gulf of Mexico coast.

To identify how any of these variables drive bay-wide turbidity patterns, we need time series of turbidity observations collected simultaneously throughout an estuary. Data from individual stations may reflect localized phenomena. For large estuaries spanning several tens of kilometers in length and width, traditional ocean color satellite imagery can improve spatial and temporal sampling of water quality by providing data for the entire estuary in a single observation, often near daily (Sokoletsky et al., 2011). Chen et al. (2010) employed in-situ sensors and satellite data to determine the mechanisms responsible for observed variability in phytoplankton and sediment in Tampa Bay over a two-month period. They identified three strong wind events, which generated critical bottom shear stress and suspended bottom sediments that were observed in concurrent MODIS imagery. They concluded that collecting a single monthly grid of samples with one water sample per station per month can lead to variability of -50% to 200% of particular samples relative to the monthly mean of chlorophyll or sediment. Fernandez-Novoa et al. (2014) used imagery from the Moderate Resolution Imaging Spectroradiometer (MODIS) to study turbidity plumes from the Ebro River over the period 2003-2011. There was sufficient coverage to isolate specific environmental conditions coinciding with satellite overpasses, including specific river discharge conditions and wind patterns. With this dataset they were able to identify the direction and extent of river plume events into the Mediterranean, and conclude that wind direction was the dominant driver of turbidity magnitude.

Eleven Gulf of Mexico estuaries from Texas to Florida were selected for this study to provide a synoptic assessment of water-quality drivers throughout the U.S. Gulf coast. These estuaries were chosen, in part, because the surface area of each (Table 1) is large enough to accommodate the 250-meter spatial resolution of MODIS imagery. Additionally, all of these estuaries are adjacent to large population centers, and therefore their health and management may impact more stakeholders than isolated estuaries.

The objective of this study was to determine the meteorological, oceanographic and atmospheric drivers of water quality time-series and extreme events in 11 Gulf of Mexico estuaries between 2000 and 2014 using a satellite-derived proxy for turbidity binned to weekly, monthly, seasonal and annual time steps.

1.1 Study areas

Each of the 11 estuaries studied here is a designated member of the National Estuary Program (NEP; Figure 1). The NEP is an Environmental Protection Agency program created to protect and restore the water quality and ecological integrity of national estuaries.

Charlotte Harbor (CH), Florida, is a water body of 805 km^2 and 2.4 m deep on average that receives water from a watershed extending over 12,000 km^2 of southwestern Florida (Turner et al. 2006). Sarasota Bay (SB), Florida, lies between Charlotte Harbor to the south and Tampa Bay to the north. It drains the smallest watershed (1,100 km^2) of those evaluated in this study, and covers the smallest surface water area at just over 100 km^2 (https://sarasotabay.org/). Tampa Bay (TB), Florida covers over 1,000 km^2 with an average depth of 3.4 m, and drains a watershed of over 6,500 km^2 (Dixon et al., 2009). Six counties and the cities of Tampa, Clearwater, and Saint Petersburg intersect the watershed, making it the second largest metropolitan area in Florida.

Mobile Bay (MB) is located along the northern Gulf Coast in the state of Alabama. With an inflow of 1755 cubic meters of water per second it receives 20% of the freshwater supply in the US and is the fourth largest estuary in the country draining a watershed of 113,084 km^2 (Roman et al. 2011).

The Barataria (BTB) and Terrebonne (TBB) estuaries are distinct bodies of water with separate watersheds, but are managed as a single NEP. They are located between the Mississippi and Atchafalaya Rivers in southern Louisiana. Freshwater input was effectively cut off by the flood protection levees erected along the Mississippi River such that rainwater constitutes the primary source of it. These bays are bounded to the south by barrier islands that are expected to decline in size from 1,800 acres to 400 acres by 2045 due to erosion, resulting in greater tidal mixing (https://www.lacoast.gov).

Galveston Bay (GB), Texas, is the seventh largest estuary in the country with over 1,500 km^2 of surface water and the fourth most populous metropolitan area in the country. The estuary has experienced substantial environmental degradation, losing over 95% of submerged vegetation from the 1950's to 1970's due in part to poor water clarity caused by increased erosion (Pulich, 2007).

The Coastal Bend Bays NEP includes the Aransas (ARB), San Antonio (SAB), Corpus Christi (CCB) and Matagorda (MGB) Bays. These four water bodies combined cover over 1,300 km^2 and drain the second largest watershed of those studied here at 32,580 km^2 (Table 1).

Table 1. National Estuary Programs studied here and relevant characteristics.

National Estuary Program	Surface Water Area (km^2)	Watershed Area (km^2)	Average Depth (m)	Year Designated
Barataria-Terrebonne	415/1090	16,500	2	1990
Charlotte Harbor	805	12,200	2.4	1995
Coastal Bend Bays	1330	32,580	3	1994
Galveston Bay	1550	12,500	2.1	1988
Mobile Bay	1059	113,084	3.048	1995
Sarasota Bay	106	1,100	1.98	1988
Tampa Bay	1000	6,800	3.6	1990

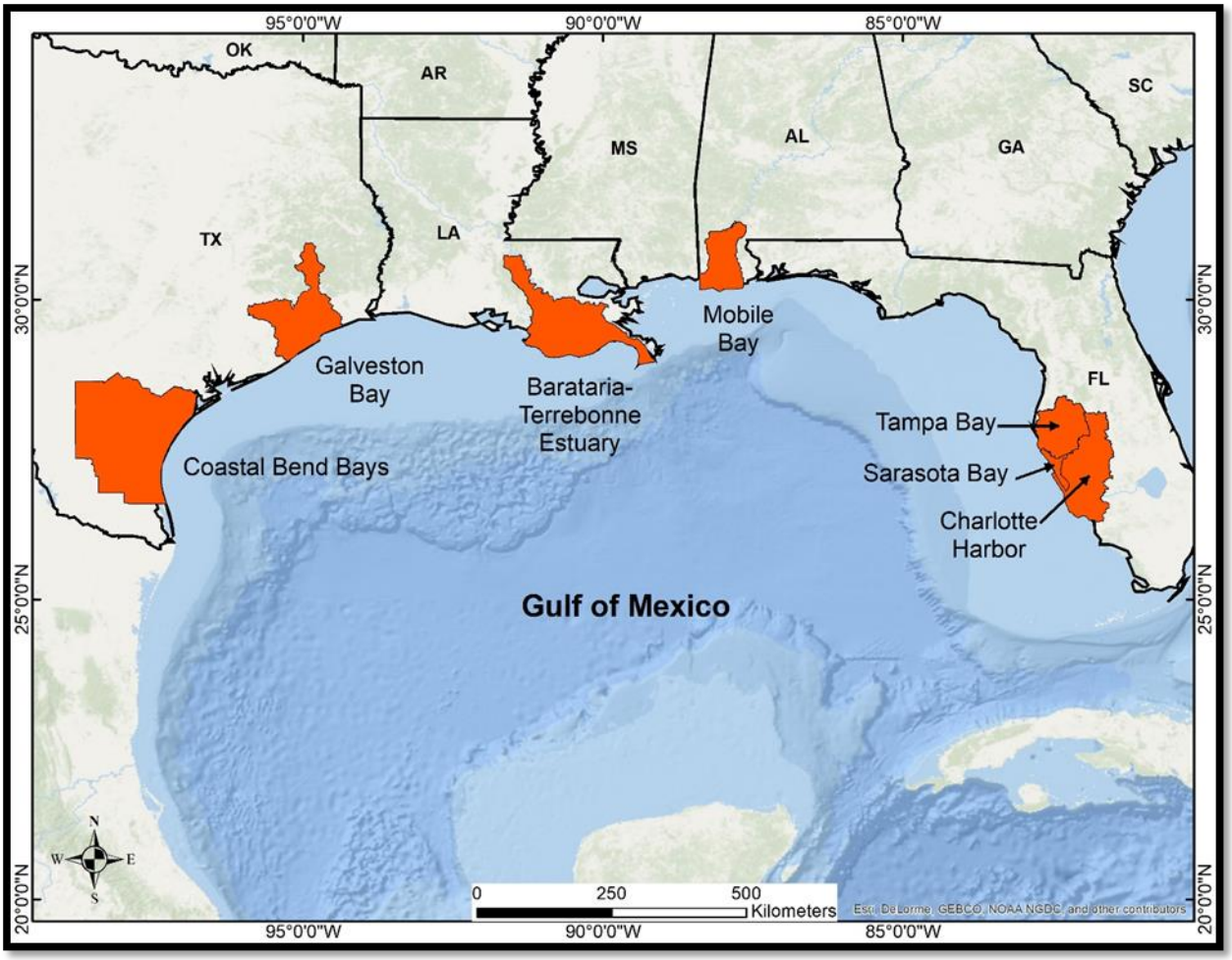

Figure 1. National Estuary Programs of the Gulf of Mexico studied here.

2. Materials and Methods

All independent-variable data preprocessing and statistical analyses were conducted using Matlab^{TM} and the Fathom toolbox.

2.1 Turbidity Data

We used satellite data from the NASA Moderate Resolution Imaging Spectroradiometer (MODIS) sensor flown on the Terra satellite to derive a proxy for turbidity. MODIS Terra has provided a time-series of remote sensing observations at relatively high temporal resolution (near-weekly or better at the latitudes of Gulf estuaries) and high spatial resolution (250 m pixels and coarser) since 2000. Specifically, we generated time-series of water quality indices using remote-sensing reflectance measurements at 645nm using MODIS Band 1 as a proxy. The basic assumption is that sediments suspended near the water surface provide a signal in this red band. In general, we assumed that MODIS Band 1 observations have minimal contributions from light reflected from the sea bottom in estuarine waters deeper than about 2.8 m due to the strong absorption of red light by water (Chen et al. 2010). This approach has been used several times in the past, with mixed success, in different estuaries and coastal waters around the world (Miller and McKee, 2004; Zawada et al. 2007; Chen et al. 2007a,b,c; Lahet and Stramski 2010; Chen et al. 2010; Moreno et al. 2010; Aurin et al. 2013; and others). Other bio-optical measurements that use blue, green, or yellow bands to estimate variables such as chlorophyll-a concentration are usually heavily affected by reflectance from the ocean bottom in shallow areas and give erroneous values.

We derived remote sensing reflectance at 645 nm (Rrs_{645}) starting from MODIS Terra Level-1A files. Rrs_{645} represents the normalized water-leaving radiance (Gordon and Clark, 1981) at 645 nm divided by the extraterrestrial solar irradiance at 645 nm. MODIS images were

downloaded from the NASA Goddard Space Flight Center Ocean Color data portal. Images were processed using the SeaWiFS Data Analysis System (SeaDAS) software package, version 7.1. Processing to Level-2 used the near infrared/short-wave infrared (NIR/SWIR) switching atmospheric correction approach of Wang and Shi (2007). All data were mapped to an equidistant cylindrical projection with a nominal pixel size of 262 m. Using the SeaDAS l2gen module, masks were applied for clouds, straylight, and sunglint. A custom filter file was used to mask stray light using a 1x1 pixel filter, as opposed to the default 3x3 pixel filter. The cloud mask was applied using data at 2130 nm with a threshold of 0.018 (Aurin et al. 2013). Individual scenes with high cloud cover (>85%) and sunglint contamination were removed by visual inspection of each individual image. To minimize the effects of negative Rrs_{645} retrievals, the median value of all negative Rrs_{645} values was calculated and applied as a bias to each MODIS scene (Aurin et al. 2013). Values of this bias ranged from -0.002 sr^{-1} to zero. All remaining negative pixels were excluded from further analyses.

2.2 Meteorological Data

Daily precipitation, wind speed and wind direction data were downloaded from the NOAA National Climate Data Center (NCDC) for the stations listed in Table 2. Stations were selected from all available stations adjacent to each estuary that contained data for each variable covering the 2000-2014 time period. Precipitation data was binned to weekly, monthly, seasonal and annual time steps by summing the data for each interval. We chose to represent precipitation cumulatively for two reasons: occasional downpours characteristic of Gulf coast winter frontal systems and summer convective storms may substantially influence runoff and erosion, but their extreme nature may be muted by averaging with surrounding days or weeks of little or no rain; and consistent rain over days or weeks may synergistically impact drainage by reaching a soil

saturation point beyond which surface runoff may increase. Unfortunately, precipitation data from all stations adjacent to the Barataria-Terrebonne NEP were missing more than 25% of daily observations for this time period, and were therefore excluded from analyses.

Wind speed was binned to the same time steps as precipitation, but using an average for each time step. Coinciding hourly wind speed and direction observations were additionally processed by converting to *u* (east-west) and *v* (north-south) component vectors, and binning each to the same time steps by average.

2.3 River Discharge Data

River discharge was downloaded from the United States Geological Survey website (https://maps.waterdata.usgs.gov/mapper/index.html?state) for every monitored river system that entered into each estuary. Rivers that were regulated with known dams or bypasses, such as Hillsborough River in Tampa Bay, were excluded to eliminate potentially anomalous anthropogenic influence. That is, management of Hillsborough River discharge is likely to primarily affect Hillsborough Bay – a subset of Tampa Bay – and therefore not be resolved by the bay-wide turbidity proxy. When data was available for multiple rivers that discharged into the same estuary, each dataset of daily measurements was compared with daily Rrs_{645} measurements to determine if substantial gaps in discharge data existed. If more than 25% of total daily Rrs_{645} observations were missing from any of the rivers' discharge datasets (i.e. data gaps), that discharge dataset was considered too sparse for evaluation and excluded from further analyses. If, however, multiple rivers for a given estuary were found to be sufficient, their data was combined into one discharge dataset for that estuary by summing daily measurements, and then binning the data to the weekly, monthly, seasonal and annual time steps by average. Table 2

lists the rivers used for each estuary. For both Barataria and Terrebonne Bays, water level data from the Gulf Intracoastal Waterway (GIWW) station at Houma, Louisiana, was used.

2.4 Water Level Data

Hourly water-level data were downloaded from the NOAA website (tidesandcurrents.noaa.gov) for all stations monitored during the time period and located within the estuaries (MLLW datum; Table 2). Verified water-level data was missing more than 25% of daily observations for the study period within the Sarasota Bay, Corpus Christi Bay, Matagorda Bay, or San Antonio Bay estuaries. Data from Tampa Bay was assumed to be a sufficient proxy for Sarasota Bay, as was data from Aransas Bay for the three adjacent Coastal Bend Bays. Datasets were binned to weekly, monthly, seasonal and annual time steps by average.

2.5 NAO Data

Daily NAO index data was downloaded from NOAA (ftp://ftp.cpc.ncep.noaa.gov/cwlinks/norm.daily.nao.index.b500101.current.ascii) and binned to the same time steps.

2.6 ENSO Data

Monthly Niño-3.4 index data was downloaded from NOAA (http://www.cpc.ncep.noaa.gov/products/analysis_monitoring/ensostuff/detrend.nino34.ascii.txt) and binned to seasonal and annual time steps. As weekly data was not available, the ENSO variable was excluded from weekly analyses.

Table 2. Station locations used for meteorological, river discharge, and water level data for each estuary.

Estuary	Meteorological Station	River Discharge	Water Level Stations
Aransas Bay	Corpus Christi, TX	Mission	Rockport, TX
Barataria Bay	Houma, LA	GIWW at Houma	Grand Isle, LA
Corpus Christi Bay	Corpus Christi, TX	Nueces	Rockport, TX
Charlotte Harbor	Punta Gorda, FL	Myakka and Peace	Fort Myers, FL
Galveston Bay	Galveston, TX	Trinity	Eagle Point, TX
Mobile Bay	Mobile, AL	Alabama and Tombigbee	Dauphin Island, AL
Matagorda Bay	Corpus Christi, TX	Lavaca and Palacios	Rockport, TX
San Antonio Bay	Corpus Christi, TX	Guadelupe	Rockport, TX
Sarasota Bay	Sarasota, FL	Walker	Saint Petersburg, FL
Tampa Bay	Tampa, FL	Alafia and Little Manatee	Saint Petersburg, FL
Terrebonne Bay	Houma, LA	GIWW at Houma	Port Fourchon, LA

2.7 Preprocessing

Observations from each dataset for each time step were first matched to the Rrs dataset by identifying coinciding observations. This allowed for a direct comparison of datasets to identify gaps. If any independent variable for a given estuary matched fewer than 75% of Rrs observations, that variable was eliminated from further analyses. A linear trend was then fit to each dataset and removed (detrended). Next, climatologies for each time step were computed for each detrended dataset from the 15-year period of available data. Typically, climatologies are computed using 30-year time periods, but many of the datasets used for this work, including Rrs, did not have 30 years of available data. We chose to restrict climatologies to the 15-year period evaluated here for consistency between datasets. Anomalies were computed by subtracting the climatology values from the coinciding time-series observation. Extreme events were identified as those Rrs observations within the 90^{th} and 95^{th} percentiles of each estuary's dataset. The time-series anomalies, and 90^{th} and 95^{th} percentile extreme-event anomalies (hereafter "XE_{90} and XE_{95}) were then used for statistical analyses.

2.8 Statistical Analyses

Redundancy Analyses with Akaike's Information Criterion (RDA AIC) were used first to identify the independent variables that explained the most variation in the dependent variable. The f_rdaAIC Matlab™ function from the Fathom toolbox standardized all input independent variables and determined the 'best' independent variables through constrained ordination. This assessed how much of the variation in one set of variables explained variation in another set, while accounting for independent-variable multicollinearity (Wollenberg 1977). Akaike (1973) proposed an information criterion to quantify the amount of information and statistically determine the number of parameters for an equation that represents a group of experimental data. The equation with the minimum AIC is considered the best representation of the experimental data (Yamaoka et al. 1978). A null model is created by assigning a value below which the best equation's AIC value must be in order to be considered viable to explain variation in the dependent variable. If no equation explains more variation than a null model, no independent variable is selected.

For any variable(s) identified as 'best' for a given estuary, correlation coefficients were computed with all other variables. If any correlations with 'best' variables exceeded ± 0.7, the correlated variables were recorded for consideration.

Multiple regressions were run on the variable(s) identified as 'best' by the RDA AIC using the f_mregress function. One thousand iterations were run for each regression to compute permutation-based p-values because some of the data were not normally distributed. Adjusted-R^2 coefficients (R^2adj) were recorded, as opposed to R^2 coefficients, because the former accounts for the number of predictors and sample size. Figure 2 summarizes the data on which statistical analyses were performed.

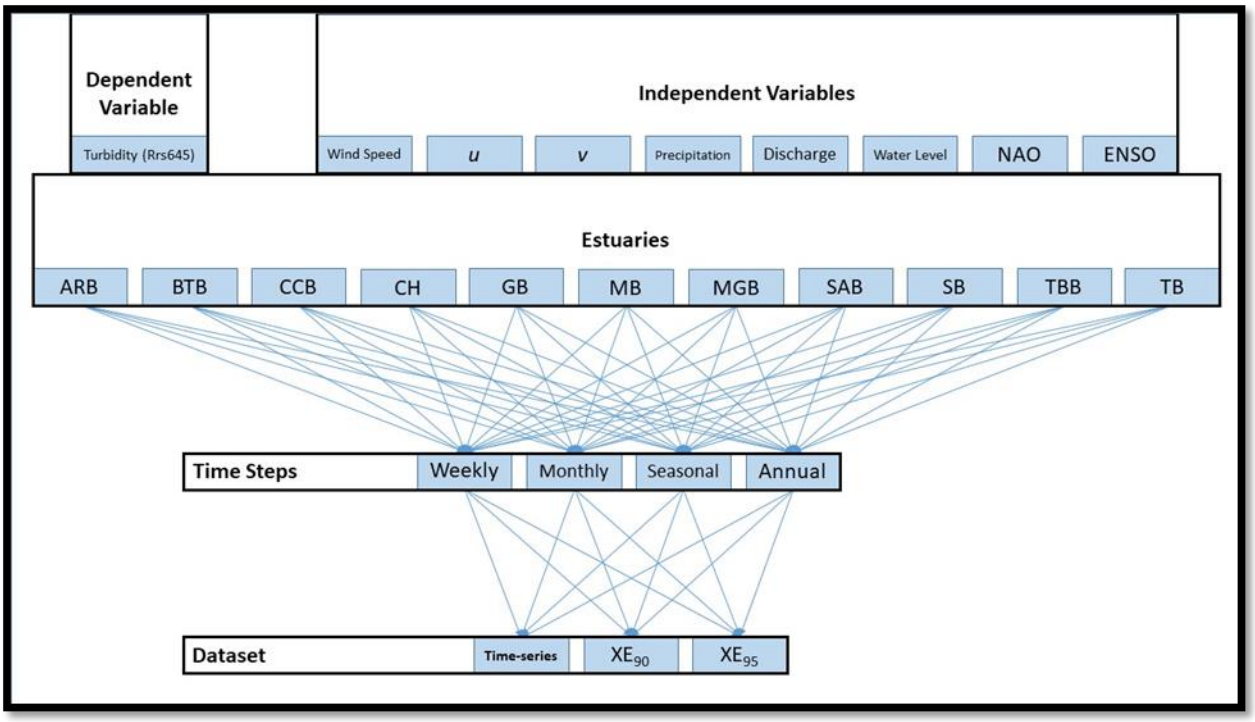

Figure 2. Summary of the variables, estuaries, time steps and datasets used for statistical analyses.

3. Results

To identify the drivers of turbidity across the coastal Gulf of Mexico, we evaluated the results of statistical analyses by estuary, time step, and time series or extreme event dataset. The variable(s) identified as statistically significant drivers of time-series, XE_{90} and XE_{95} turbidity for each estuary over all time steps are indicated in Table 3 by the number of iterations in which they were found to be significant. Additionally, the number of estuaries for which each variable was identified as a statistically significant driver is summarized in the Table 4 by time step.

Table 3. The number of time steps for which each variable was identified as a significant driver (R^2adj > 0.2, p < 0.05) of turbidity time-series, 90th percentile events (in parentheses), and 95th percentile events [in brackets] for each estuary.

	Wind Speed	Wind U	Wind V	Precip	Discharge	Water Level	NAO	ENSO
ARB	1 (0) [0]	1 (0) [0]	0 (0) [0]	0 (0) [0]	0 (0) [0]	0 (0) [0]	0 (0) [0]	0 (1) [0]
BTB	2 (0) [0]	0 (0) [0]	0 (0) [1]	0 (0) [0]	0 (0) [0]	0 (0) [0]	0 (0) [0]	0 (1) [0]
CCB	1 (0) [0]	0 (0) [0]	1 (0) [1]	0 (0) [0]	2 (0) [0]	0 (0) [0]	1 (0) [0]	1 (2) [0]
CH	0 (0) [0]	0 (1) [1]	0 (0) [0]	0 (0) [0]	1 (0) [0]	0 (0) [0]	0 (1) [0]	0 (0) [0]
GB	0 (0) [0]	0 (0) [0]	0 (0) [0]	0 (0) [0]	0 (0) [0]	0 (0) [0]	0 (0) [0]	0 (0) [0]
MB	3 (1) [0]	2 (0) [0]	0 (1) [0]	1 (0) [0]	4 (0) [0]	1 (0) [0]	0 (0) [0]	0 (1) [0]
MGB	1 (0) [0]	0 (1) [0]	0 (0) [0]	0 (0) [0]	2 (1) [0]	0 (0) [0]	0 (0) [0]	0 (0) [0]
SAB	0 (0) [0]	0 (0) [0]	0 (0) [0]	0 (0) [0]	0 (0) [0]	0 (0) [1]	0 (0) [0]	0 (0) [0]
SB	0 (1) [1]	0 (0) [0]	0 (0) [0]	0 (1) [0]	0 (0) [0]	0 (0) [0]	0 (0) [0]	0 (1) [0]
TBB	0 (1) [0]	0 (0) [0]	0 (0) [0]	0 (0) [0]	0 (1) [0]	0 (0) [0]	0 (0) [0]	0 (0) [0]
TB	0 (1) [0]	0 (0) [0]	0 (0) [0]	0 (0) [0]	0 (0) [0]	0 (0) [0]	0 (0) [0]	2 (0) [0]
Total	8 (4) [1]	3 (2) [1]	1 (1) [2]	1 (1) [0]	9 (2) [0]	1 (0) [1]	1 (1) [0]	3 (6) [0]

Table 4. The number of estuaries for which each variable was identified as a significant driver (R^2adj > 0.2, p < 0.05) of turbidity time-series, 90th percentile events (in parentheses), and 95th percentile events [in brackets] for each time step.

	Wind Speed	Wind U	Wind V	Precip	Discharge	Water Level	NAO	ENSO
Weekly	1 (0) [0]	1 (0) [0]	0 (0) [1]	1 (0) [0]	1 (0) [0]	0 (0) [0]	0 (0) [0]	0 (0) [0]
Monthly	2 (2) [1]	0 (2) [1]	0 (1) [1]	0 (1) [0]	1 (0) [0]	1 (0) [1]	0 (1) [0]	1 (2) [0]
Seasonal	3 (2) [0]	0 (0) [0]	1 (0) [0]	0 (0) [0]	4 (2) [0]	0 (0) [0]	0 (0) [0]	1 (4) [0]
Annual	2 (0) [0]	2 (0) [0]	0 (0) [0]	0 (0) [0]	3 (0) [0]	0 (0) [0]	1 (0) [0]	1 (0) [0]

Analyses of time series data identified statistically significant relationships (p < 0.05) between turbidity and at least one independent variable for all time steps (i.e. weekly, monthly, seasonal, and annual) in all estuaries, with the exception of nine iterations. That is, no variables were identified as "best" by the AIC step in four runs, and only five runs identified at least one "best" variable, but the resulting model could not explain turbidity variation significantly. Excluding those results, the variables most often found to explain turbidity variation were wind speed (25 iterations) and discharge (15 iterations). If we exclude those statistically significant relationships that found R^2adj values under 0.2, the variables found to most frequently explain

turbidity variation were discharge (9 times) and wind speed (8 times; Table 3). Discharge data was found to contain too many gaps to be sufficient for weekly or monthly analyses in Galveston Bay. Also, water level was excluded from Terrebonne Bay weekly and monthly analyses for the same reason.

Analyses of 90th percentile extreme events (XE_{90}) found statistically significant relationships between turbidity and at least one independent variable in 20 of the 44 analyses. None of the annual analyses identified a "best" variable, probably due to low sample sizes. For all analyses that identified a significant variable, wind speed (7 times) was identified the most, followed by ENSO (6 times), and discharge (3 times). Excluding significant relationships with R^2adj values under 0.2, the variables found to most frequently explain turbidity variation were ENSO (6 times), and wind speed (4 times; Table 3). Discharge and water level were excluded from Galveston Bay and Terrebonne Bay, respectively, due to insufficient data.

Analyses of 95th percentile extreme events (XE_{95}) found statistically significant relationships between turbidity and at least one independent variable in 7 of the 44 runs. None of the seasonal or annual runs identified a "best" variable, probably due to low sample sizes. For all runs that identified a significant variable, the V vector (3 times), and U vector (2 times) were identified most. Excluding significant relationships with R^2adj values under 0.2, the variable found to most frequently explain turbidity variation was the V vector (2 times; Table 3). Discharge and water level were excluded from Galveston Bay and Terrebonne Bay, respectively, due to insufficient data.

4. Discussion

We will refer to variables that were identified as statistically significantly ($p < 0.05$) correlated to the Rrs turbidity proxy with R^2adj values greater than 0.2 as "significant drivers" of

turbidity. Because RDA AIC and multiple regression analyses may identify more than one variable per iteration, we will discuss the results by noting both the number of estuaries for which an independent variable was identified as a driver, and the number of times a variable was identified as a driver.

For time-series datasets, wind speed and discharge were each found to be a significant driver of turbidity in more estuaries than any other variable (wind: 5 estuaries, and discharge: 4 estuaries). These two variables alone were found to be significantly correlated with turbidity in six of the 11 estuaries. The direction of the relationship between these two variables and turbidity was consistent for wind speed (i.e. positive relationship in all 8 time-series iterations), but not for discharge (i.e. four positive relationships in Mobile Bay, and five negative relationships among three estuaries.). This suggests that increased wind speed consistently increases turbidity, but that discharge has a more dynamic relationship that varies among estuaries and possibly with other factors. Galveston Bay, San Antonio Bay, Sarasota Bay, and Terrebonne Bay turbidity time-series were not significantly driven by any variable.

For extreme-event datasets, ENSO was found to be a significant driver of turbidity in more estuaries than any other variable (5 estuaries), followed by wind speed (4 estuaries). However, the direction of the relationships was inconsistent: 3 estuaries displayed negative turbidity responses to ENSO variability while 2 estuaries were positive.

Analyses of weekly time-series datasets found that significant drivers of turbidity could only be identified for Mobile Bay. Here, turbidity was driven by four variables (wind speed, U vector, precipitation, and discharge). Monthly time-series analyses revealed significant drivers in only two estuaries: Mobile Bay (wind speed, discharge, and water level) and Corpus Christi Bay (wind speed and ENSO). Seasonal analyses of time-series datasets found significant drivers in

seven estuaries, explained most frequently by discharge (4 times) and wind speed (3 times). Annual analyses of time-series datasets found significant drivers in six estuaries, explained most frequently by discharge (3 times), followed by wind speed and the *u* vector (2 times each).

Weekly extreme-event analyses found that no estuaries had a significant turbidity driver of XE_{90} data. However, weekly XE_{95} data for three estuaries (Barataria Bay, Charlotte Harbor, and Matagorda Bay) were driven by the wind vector variables (V twice, and U once). Monthly analyses of XE_{90} (XE_{95}) data found significant drivers in eight (four) estuaries, explained twice (once) each by wind speed, *u* vector, and ENSO (wind speed, *u*, *v*, water level). Monthly analyses of XE_{95} data found significant drivers in four estuaries, explained once each by wind speed, *u*, *v*, and water level. Seasonal XE_{95} sample sizes were too small to detect any significant relationships, but seasonal XE_{90} analyses revealed significant drivers in seven estuaries with ENSO (4 times) driving turbidity more than any other variable, followed by wind speed and discharge (twice each).

Evaluating the results by time step reveals that turbidity time-series variability across the Gulf of Mexico can be more frequently explained by these independent variables for seasonal and annual steps (7 estuaries and 6 estuaries, respectively) than weekly and monthly variability (1 and 2 estuaries, respectively). Similarly, extreme-event variability can be more frequently explained on monthly and seasonal periods (7 estuaries each for XE_{90}; 4 estuaries for monthly XE_{95}), than on weekly scales (none for XE_{90}; once for XE_{95}; note that XE_{95} seasonal, and both XE annual data sample sizes were too small for analyses). This may indicate that short-term turbidity responses lag behind environmental phenomena. Schmidt et al. (2001) found that river discharge in Florida watersheds lagged an ENSO index by several months, depending on season.

Lagged relationships between independent variables and turbidity were not included in this study. We decided that lag estimates could not be constrained well enough for all estuaries at all time-scales to facilitate accurate comparisons, but that the identification and evaluation of lagged effects of these variables on turbidity is a possible area of valuable future research for these estuaries. Further, Eleveld et al. (2014) compared satellite-derived water quality products with modelled water quality and found that sun-synchronous satellites alias tidal patterns and are also biased by acquiring usable data under cloud-free conditions. These constraints led to biases in satellite-derived water quality products (Eleveld et al. 2014), and may have limited our ability to resolve water quality in this study. Further, Zheng et al. (2017) reviewed satellite-derived ocean color products and concluded that, while coastal turbidity proxies tend to be relatively accurate in the 2-7 NTU range, they also tend to lose sensitivity beyond 7 NTU depending largely on colored dissolved organic matter concentration and atmospheric correction techniques. This relatively narrow range of turbidity values that tend to be accurately identified by satellite data may explain the paucity of significant relationships and prevalence of low R^2adj values for many of these analyses, especially regarding extreme events (i.e. high-turbidity observations). Nonetheless, the consistent identification of wind speed and ENSO as drivers of turbidity variability across estuaries in agreement with past work leads us to believe that our product is sufficient to identify broad patterns in water-quality drivers.

We were able to synoptically assess environmental drivers of water-quality variation in all Gulf of Mexico National Estuary Programs over multiple time steps (weekly, monthly, seasonal and annual data bins), including extreme events (90^{th} and 95^{th} percentile observations) and identify statistically significant drivers for some estuaries. In doing so, we spatially and

temporally scale up what are typically short-term, local evaluations of water-quality variability to identify drivers across the basin.

5. Conclusions

Fifteen years of satellite-derived turbidity data for 11 Gulf of Mexico estuaries revealed statistically significant relationships with several environmental variables. Wind speed was found to be the most consistent driver of turbidity time-series variability across estuaries, while ENSO was the primary driver of extreme turbidity events. River discharge was also found to drive turbidity variability, increasing turbidity in Mobile Bay, but decreasing it in three other estuaries (Corpus Christi Bay, Charlotte Harbor, and Matagorda Bay).

The explanatory variables investigated here were found to have stronger statistical relationships with turbidity when the data were binned over longer time steps (i.e. monthly to annual). This may be due to lags, which were not evaluated here and should be considered for future work, or may indicate that the turbidity proxy used contained a low signal-to-noise ratio for weekly binned data. Longer bins averaged more data points, which may have improved the accuracy of the monthly, seasonal and annual products over weekly data.

While these results find a consistent relationship between high winds and increased turbidity, they also reveal varied dynamics between turbidity and environmental phenomena between estuaries. Muller-Karger et al. (2015) found substantial changes in Gulf of Mexico wind speed from the 1980s to 2012. As climate change modulates future patterns in wind, precipitation, discharge, sea level, and climate oscillations, local water-quality managers should consider the dynamics of their local estuarine water-quality responses to environmental forcings to prepare for future water-quality trends and extreme events.

6. References

Akaike, H. Information theory and an extension of maximum likelihood principle. In B. N. Petrov and F. Csaki (eds), Second International Symposium on Information Theory, Akademiai Kiado, Budapest, 1973, pp. 267-281.

Al-Taani, A.A. (2014). Trend analysis in water quality of Al-Wehda Dam, north of Jordan. *Environmental Monitoring and Assessment,* doi:10.1007/s10661-014-3850-2.
Aurin et al. 2013

Chen, Z., Hu, C., Conmy, R.N., Muller-Karger, F., and Swarzenski, P. (2007a). Colored dissolved organic matter in Tampa Bay, Florida. *Marine Chemistry, 104*, 98-109.

Chen, Z., Hu, C., and Muller-Karger, F. (2007b). Monitoring turbidity in Tampa Bay using MODIS/Aqua 250-m imagery. *Remote Sensing of Environment, 109*, 207-220.

Chen, Z., Muller-Karger, F., and Hu, C. (2007c). Remote sensing of water clarity in Tampa Bay. *Remote Sensing of Environment, 109*, 249-259.

Chen, Z., Hu, C., Muller-Karger, F., and Luther, M.E. (2010). Short-term variability of suspended sediment and phytoplankton in Tampa Bay, Florida: Observations from a coastal oceanographic tower and ocean color satellites. *Estuarine, Coastal and Shelf Science, 89*, 62-72.

Dixon, L.K., Vargo, G.A., Johansson, J.O.R., Montgomery, R.T., and Neely, M.B. (2009). Trends and explanatory variables for the major phytoplankton groups of two southwestern Florida estuaries, USA. *Journal of Sea Research, 61*, 95-102.

Dixon, J.L., Osburn, C.L., Paerl, H.W., and Peierls, B.L. (2014). Seasonal changes in estuarine dissolved organic matter due to variable flushing time and wind-driven mixing events. *Estuarine, Coastal and Shelf Science, 151*, 210-220.

Dorado, S., Booe, T., Steichen, J., McInnes, A.S., Windham, R., Shepard, A., Lucchese, A.E.B., Preischel, H., Pinckney, J.L., Davis, S.E., Roelke, D.L., and Quigg, A. (2015). Towards an understanding of the interactions between freshwater inflows and phytoplankton communities in a subtropical estuary in the Gulf of Mexico. *PLoS ONE, 10*: doi:10.1371/journal.pone.0130931

Eleveld, M.A., van der Wal, D., and van Kessel, T. (2014). Estuarine suspended particulate matter concentrations from sun-synchronous satellite remote sensing: Tidal and meteorological effects and biases. *Remote Sensing of Environment, 143*, 204-215.

Environmental Protection Agency, 2012. National Coastal Condition Report IV. EPA/842-R-10-003 U.S. Environmental Protection Agency, Office of Research and Development and Office of Water, Washington, DC.

Fernandez-Novoa, D., Mendes, R., deCastro, M., Dias, J.M., Sanchez-Arcilla, A., and Gomez-Gesteria, M. (2014). Analysis of the influence of river discharge and wind on the Ebro turbid plume using MODIS- Aqua and MODIS-Terra data. *Journal of Marine Systems,* doi:10.1016/j.jmarsys.2014.09.009.

Gordon, H.R., and Clark, D.K. (1981). Clear water radiances for atmospheric correction of coastal zone color scanner imagery. *Applied Optics, 20,* 4175-4180.

Greening, H., Janicki, A., Sherwood, E.T., Pribble, R., and Johansson, J.O.R. (2014). Ecosystem responses to long-term nutrient management in an urban estuary: Tampa Bay, Florida, USA. *Estuarine, Coastal and Shelf Science, 151*, A1-A16.

Hu, C., Chen, Z., Clayton, T.D., Swarzenski, P., Brock, J.C., and Muller-Karger, F. (2004). Assessment of estuarine water-quality indicators using MODIS medium-resolution bands: Initial results from Tampa Bay, FL. *Remote Sensing of Environment, 93,* 423-441.

Hurrell, J.W., Kushnir, Y., Ottersen, G. and Visbeck, M. (2003). An Overview of the North Atlantic Oscillation, in The North Atlantic Oscillation: Climatic Significance and Environmental Impact (eds J. W. Hurrell, Y. Kushnir, G. Ottersen and M. Visbeck), American Geophysical Union, Washington, D. C.. doi: 10.1029/134GM01

Janicki, A., Pribble, R., Janicki, S., and Winowitch, M. (2001). An analysis of long-term trends in Tampa Bay water quality. Technical Report. Available at: http://www.tbeptech.org/TBEP_TECH_PUBS/2001/TBEP_04_01WQTrends.pdf. Accessed 2 Aug 2014.

Jordan, Y.C., Ghulam, A., and Herrmann, R.B. (2012). Floodplain ecosystem response to climate variability and land-cover and land-use change in Lower Missouri River basin. *Landscape Ecology, 27,* 843-857.

Kenyon, J., and Hegerl, G.C. (2010). Influence of modes of climate variability on global precipitation extremes. *Journal of Climate, 23*, 6248-6262.

Lahet, F., and Stramski, D. (2010). MODIS imagery of turbid plumes in San Diego coastal waters during rainstorm events. *Remote Sensing of Environment, 114,* 332-344.

Le, C., Hu, C., English, D., Cannizzaro, J., and Kovach, C. (2013). Climate-driven chlorophyll-a changes in a turbid estuary: Observations from satellites and implications for management. *Remote Sensing of Environment, 130,* 11-24.

Michalak, A.M. (2016) Comment: Study role of climate change in extreme threats to water quality. *Nature, 535,* 349-350.

Miller, R.L., and McKee, B.A. (2004). Using MODIS Terra 250 m imagery to map concentrations of total suspended matter in coastal waters. *Remote Sensing of Environment, 93,* 259-266.

Miller, R.L., Liu, C., B., C.J., and Wu, A. (2011). A multi-sensor approach to examining the distribution of total suspended matter (TSM) in the Albemarle-Pamlico estuarine system, NC, USA. *Remote Sensing, 3*, 962-974.

Moreno Madriñán, M.J., Al-Hamdan, M.Z., Rickman, D.L., and Muller-Karger, F.E. (2010). Using the surface reflectance MODIS Terra product to estimate turbidity in Tampa Bay, Florida. *Remote Sensing, 2*, 2713-2728.

Moreno Madriñán, M.J., Al-Hamdan, M.Z., Rickman, D.L., and Ye, J. (2012). Relationship between watershed land-cover/land-use change and water turbidity status of Tampa Bay major tributaries, Florida, USA. *Water, Air & Soil Pollution, 223*, 2093-2109.

Muller-Karger, F.E., Smith, J.P., Werner, S., Chen, R., Roffer, M., Liu, Y., Muhling, B., Lindo-Atichati, D., Lamkin, J., Cerdeira-Estrada, S., and Enfield, D.B. (2015). Natural variability of surface oceanographic conditions in the offshore Gulf of Mexico. *Progress in Oceanography, 134*, 54-76.

Pulich, W. (2007). Texas Coastal Bend, in: Handley, L., Altsman, D. and DeMay, R. (Eds.), Seagrass status and trends in the northern Gulf of Mexico: 1940-2002. U.S. Geological Survey Scientific Investigations Report 2006-5287 and U.S. Environmental Protection Agency 855-R-04-003, pp. 41-59.

Roman, C.B., Estes, M.G., and Al-Hamdan, M.Z. (2011). Impacts of land use and climate change on hydrologic processes in shallow aquatic ecosystems. Oceans, 2011 IEEE, Santander, Spain, June 6-9, 2011.

Scarsbrook, M.R., McBride, C.G., McBride, G.B., and Bryers, G.G. (2003). Effects of climate variability on rivers: Consequences for long term water quality analyses. *Journal of the American Water Resources Association, 39*, 1435-1447.

Schmidt, N., Lipp, E.K., Rose, J.B, and Luther, M.E. (2001). ENSO influences on seasonal rainfall and river discharge in Florida. *Journal of Climate, 14*, 615-628.

Schmidt, N., Luther, M.E., and Johns, R. (2004). Climate variability and estuarine water resources: A case study from Tampa Bay, Florida. *Coastal Management, 32*, 101-116.

Schoen, J., Stretch, D., Tirok, K., Wind-driven circulation patterns in a shallow estuarine lake: St Lucia, South Africa, *Estuarine, Coastal and Shelf Science* (2014), doi:10.1016/j.ecss.2014.05.007.

Sokoletsky, L.G., Lunetta, R.S., Wetz, M.S., and Paerl, H.W. (2011). MERIS retrieval of water quality conditions in the turbid Albermarle-Pamlico Sound estuary, USA. *Remote Sensing, 3*, 684-707.

Stenseth, N.C., Ottersen, G., Hurrel, J.W., Mysterud, A., Lima, M., Chan, K., Yoccoz, N.G., and Adlandsvik, B. (2003). Studying climate effects on ecology through the use of climate indices; the North Atlantic Oscillation, El Nino Southern Oscillation and beyond. *Proceedings of the Royal Society of London B, 270*, 2087-2096.

Stoker, Y.E., Levesque, V.A., and Woodham, W.M. (1996). The effect of discharge and water quality of the Alafia River, Hillsborough River, and the Tampa Bypass Canal on nutrient loading to Hillsborough Bay, Florida. U.S. Geological Survey Water-Resources Investigations Report 95-4107.

Turner, R.E., Rabalais, N.N., Fry, B., Atilla, N., Milan, C.S., Lee, J.M., Normadeau, C., Oswald, T.A., Swenson, E.M., and Tomasko, D.A. (2006). Paleo-indicators and water quality change in the Charlotte Harbor estuary (Florida). *Limnology and Oceanography, 51*, 518-533.

Wahl, T., Calafat, F.M., and Luther, M.E. (2014). Rapid changes in the seasonal sea level cycle along the US Gulf Coast from the late 20th century. *Geophysical Research Letters, 41*, 491-498.

Wang, M., and Shi, W. (2007). The NIR-SWIR combined atmospheric correction approach for MODIS ocean color data processing. *Optics Express*, *15*, 15722-15733.

Wollenberg, A.L. van den (1977). Redundancy analysis: An alternative for canonical correlation analysis. *Psychometrika*, *42*(2), 207-219.

Yamaoka, K., Nakagawa, T., and Uno, T. (1978). Application of Akaike's Information Criteria (AIC) in the evaluation of linear pharmacokinetic equations. *Journal of Pharmacokinetics and Biopharmaceutics, 6*(2), 165-175.

Yin, Z., Walcott, S., Kaplan, B., Cao, J., Lin, W., Chen, M., Liu, D., and Ning, Y. (2005). An analysis of the relationship between spatial patterns of water quality and urban development in Shanghai, China. *Computers, Environment and Urban Systems, 29*, 197-221.

Zawada, D.G., Hu, C., Clayton, T., Chen, Z., Brock, J.C., and Muller-Karger, F.E. (2007). Remote sensing of particle backscattering in Chesapeake Bay: A 6-year SeaWiFS retrospective view. *Estuarine, Coastal and Shelf Science, 73*, 792-806.

Zheng, G., and DiGiacomo, P.M. (2017). Uncertainties and applications of satellite-derived coastal water quality products. *Progress in Oceanography* doi: http://dx.doi.org/10.1016/j.pocean.2017.08.007

CHAPTER THREE:

IMPROVED COASTAL WETLAND MAPPING USING VERY-HIGH 2-METER SPATIAL RESOLUTION IMAGERY

1. Research Overview

Wetlands provide valuable ecosystem services that contribute to both human and ecological health, yet they have declined in extent by over 50% in the U.S. during the 20th century. Restoration efforts have successfully mitigated losses in recent years with the help of synoptic wetland coverage surveys. Unfortunately, existing maps produced by local, state and federal agencies show substantially inconsistent wetland extent due, in part, to the discrepancies in their mapping data and methods.

Satellite images allow land cover classes, including wetlands, to be mapped efficiently using objective methods of identification that have been shown to improve on photo interpretations of aerial imagery. The spatial resolution of the digital satellite data typically used, however, is relatively coarse, and may cause inaccurate wetland extent estimations in areas of mixed wetland and upland vegetation. For this research, wetlands were initially mapped using Landsat imagery (30 m resolution) and WorldView-2 imagery (2 m resolution) for two study sites in Tampa Bay, Florida. Ground-validation points found that WorldView-2 produced more accurate maps than Landsat (82% vs. 46%). To further improve classification accuracy by distinguishing wetland from upland vegetation, a Decision Tree classification system was developed and applied to the WorldView-2 images. The resulting maps accurately identified wetlands to 82% and

90%, and uplands to 94% and 83%, at Fort De Soto State Park and Weedon Island Preserve, respectively. When compared to existing wetland maps, these results showed that published maps overestimate wetland surface cover by factors of 2-10 in these study areas.

Note to Reader

This chapter was published in the peer-reviewed Elsevier journal *International Journal of Applied Earth Observation and Geoinformation* and is included here in Appendix B. The full citation is: McCarthy, M.J., Merton, E.J., & Muller-Karger, F.E. (2015). Improved coastal wetland mapping using very-high 2-meter spatial resolution imagery. *International Journal of Applied Earth Observation and Geoinformation*, 40, 11–18.

CHAPTER FOUR:

ENABLING EFFICIENT, LARGE-SCALE HIGH-SPATIAL RESOLUTION WETLAND MAPPING USING SATELLITES

1. Research Overview

The Decision Tree approach developed in the previous chapter successfully improved wetland-mapping accuracy using an objective, pixel-based method. Similar algorithms have produced accurate results in previous work, but none had been applied to large-scale wetland mapping due, in part, to processing inefficiencies. That is, preprocessing and classifying a single high-resolution image on a standard computer would take about one day to complete. Given that a single image covers approximately 270 km^2, water-shed scale maps (i.e. 5,000 km^2 or more) would require weeks of dedicated processing. Additionally, images often contain substantial cloud-cover, thereby restricting the view of the ground and requiring multiple, typically offset images to complete the ground coverage.

The goal of this chapter was to develop a protocol to efficiently map large-scale wetland coverage by automating the preprocessing and classification schemes executed with programming languages run over the USF supercomputer. Using this approach, 130 2-meter spatial resolution WorldView-2 images mapped wetland, upland, water, and bare and developed land for the entire 6,500 km^2 Tampa Bay watershed in under 24 hours. The classified images were mosaicked into a single map, and compared with existing maps of the watershed for accuracy based on ground validation data. The WorldView-2 map more accurately identified coastal and freshwater wetland (78%) and upland (64%)

than the existing maps (45-65% and 49-53%, respectively). An algorithm was also developed that identified wetlands using a scene-specific index, as opposed to a static threshold, which may allow this approach to be applied to similar watersheds without retraining the classification scheme. This work has high potential for large-scale wetland mapping and change detection at 2-meter resolution.

Note to Reader

This chapter was submitted to the peer-reviewed journal *Remote Sensing of Environment* and is included here in Appendix B. The full citation is: McCarthy, M.J., Radabaugh, K.R., Moyer, R.P., and Muller-Karger, F.E. (2017) Enabling efficient, large-scale, high-spatial resolution wetland mapping using satellites. *Remote Sensing of Environment*. (Major Revision following Reviewer/Editorial comments).

CHAPTER FIVE:

SATELLITE REMOTE SENSING FOR COASTAL MANAGEMENT: A REVIEW OF SUCCESSFUL APPLICATIONS

1. Research Overview

Traditional coastal ecosystem management approaches will require strategies to address the compounding challenges of climate change and a growing global population. Satellite technology has been used in limited applications to supplement management efforts, but concerns over its accuracy, utility and efficacy have restricted wider adoption. The goal of this chapter was to encourage managers to embrace satellite technology by reviewing examples of its use in coastal ecosystems to successfully contribute to management. A background of remote sensing specifications is provided, along with a comprehensive table of existing satellite data that is available for use in a variety of coastal management sectors. Literature reviewed covers the sectors of coral reefs, wetland, water quality, public health, and fisheries and aquaculture.

Note to Reader

This chapter was published in the peer-reviewed journal *Environmental Management* and is included here in Appendix B. The full citation is: McCarthy, M.J., Colna, K.E., El-Mezayen, M.M., Laureano-Rosario, A.E., Méndez-Lázaro, P., Otis, D.B., Toro-Farmer, G., Vega-Rodriguez, M., and Muller-Karger, F.E. (2017). Satellite remote sensing for coastal management: A review of successful applications. *Environmental Management*, doi: 10.1007/s00267-017-0880-x

APPENDIX A:

AUTHOR CONTRIBUTIONS AND COPYRIGHT PERMISSIONS

1. Impacts of 40 years of land cover change on water quality in Tampa Bay, Florida

M.J. McCarthy conceived the research design, led the data acquisition, processing and statistical analysis, and wrote the paper.

F.E. Muller-Karger secured funding, assisted with the research design, and edited the manuscript.

D.B. Otis assisted with data acquisition and preprocessing and edited the manuscript.

P. Méndez-Lázaro assisted with statistical analyses and edited the manuscript.

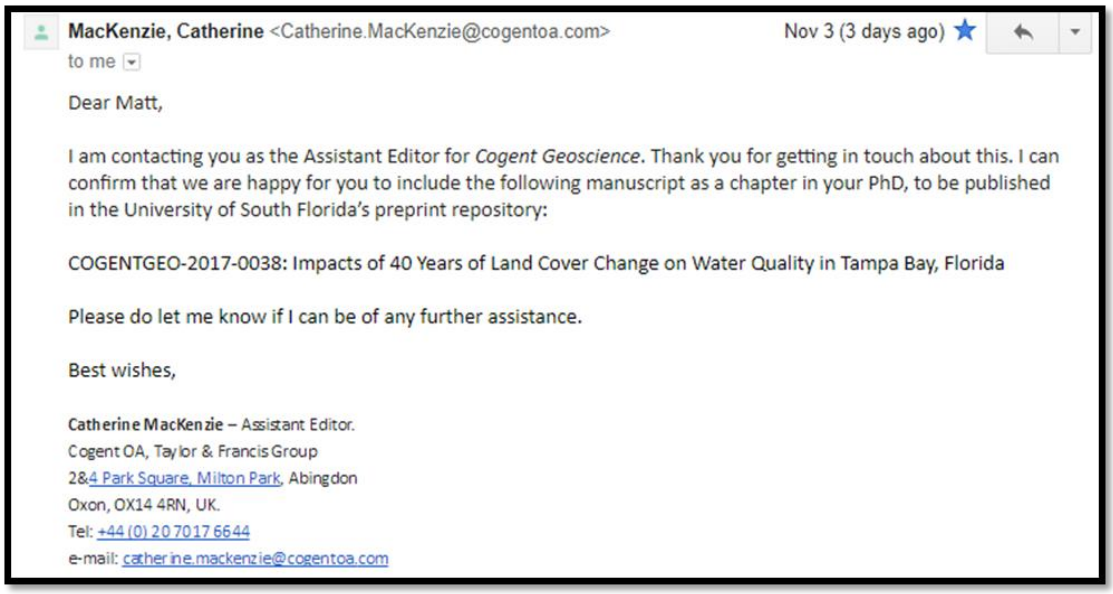

MacKenzie, Catherine <Catherine.MacKenzie@cogentoa.com> Nov 3 (3 days ago)

to me

Dear Matt,

I am contacting you as the Assistant Editor for *Cogent Geoscience*. Thank you for getting in touch about this. I can confirm that we are happy for you to include the following manuscript as a chapter in your PhD, to be published in the University of South Florida's preprint repository:

COGENTGEO-2017-0038: Impacts of 40 Years of Land Cover Change on Water Quality in Tampa Bay, Florida

Please do let me know if I can be of any further assistance.

Best wishes,

Catherine MacKenzie – Assistant Editor.
Cogent OA, Taylor & Francis Group
2&4 Park Square, Milton Park, Abingdon
Oxon, OX14 4RN, UK.
Tel: +44 (0) 20 7017 6644
e-mail: catherine.mackenzie@cogentoa.com

2. Improved coastal wetland mapping using very-high 2-meter spatial resolution imagery

M.J. McCarthy conceived the research question, performed field work and data analysis, and wrote the paper.

E.J. Merton assisted with field work and data analysis, and edited the manuscript.

F.E. Muller-Karger secured funding, assisted with data preprocessing and edited the manuscript.

The final publication is available at: https://doi.org/10.1016/j.jag.2015.03.011

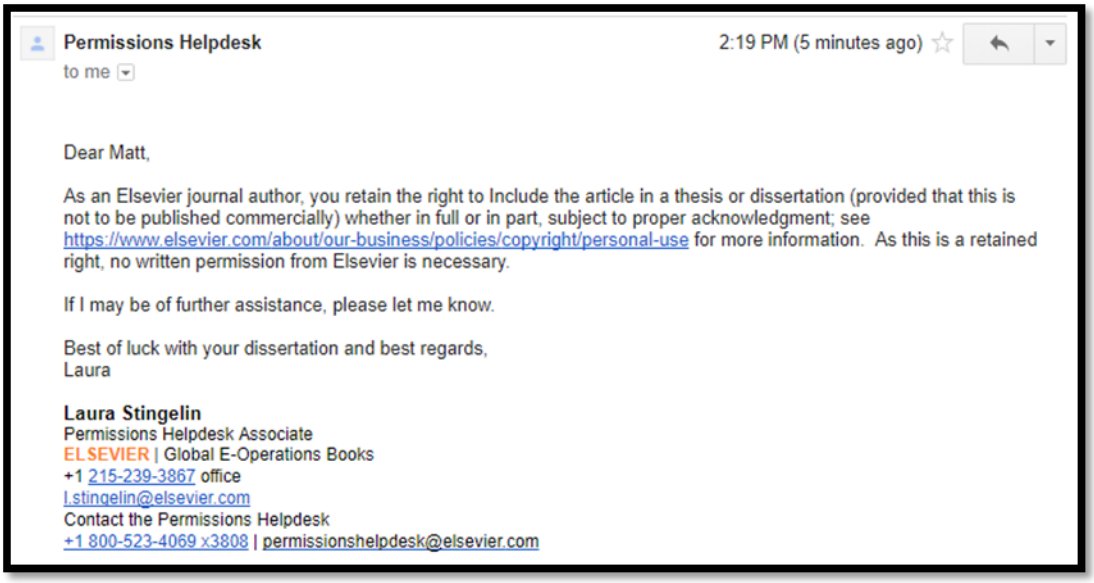

Permissions Helpdesk 2:19 PM (5 minutes ago)

to me

Dear Matt,

As an Elsevier journal author, you retain the right to Include the article in a thesis or dissertation (provided that this is not to be published commercially) whether in full or in part, subject to proper acknowledgment; see https://www.elsevier.com/about/our-business/policies/copyright/personal-use for more information. As this is a retained right, no written permission from Elsevier is necessary.

If I may be of further assistance, please let me know.

Best of luck with your dissertation and best regards,
Laura

Laura Stingelin
Permissions Helpdesk Associate
ELSEVIER | Global E-Operations Books
+1 215-239-3867 office
l.stingelin@elsevier.com
Contact the Permissions Helpdesk
+1 800-523-4069 x3808 | permissionshelpdesk@elsevier.com

3. Enabling efficient, large-scale, high-spatial resolution wetland mapping using satellites

M.J. McCarthy conceived the research question, developed the methodology, led the data processing and analysis, and wrote the paper.

K.R. Radabaugh performed the field work, provided spatial analysis guidance and edited the manuscript.

R.P. Moyer secured funding, performed the field work, and edited the manuscript.

F.E. Muller-Karger secured funding, assisted in the data processing approach, and edited the manuscript.

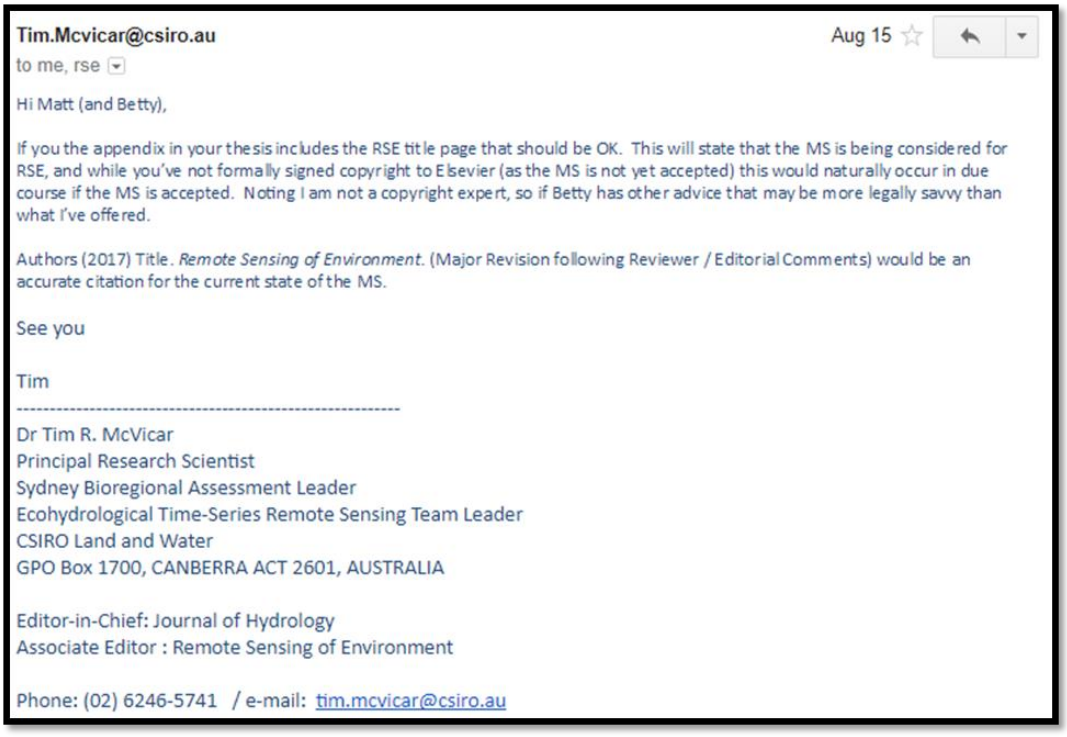

Tim.Mcvicar@csiro.au Aug 15

to me, rse

Hi Matt (and Betty),

If you the appendix in your thesis includes the RSE title page that should be OK. This will state that the MS is being considered for RSE, and while you've not formally signed copyright to Elsevier (as the MS is not yet accepted) this would naturally occur in due course if the MS is accepted. Noting I am not a copyright expert, so if Betty has other advice that may be more legally savvy than what I've offered.

Authors (2017) Title. *Remote Sensing of Environment*. (Major Revision following Reviewer / Editorial Comments) would be an accurate citation for the current state of the MS.

See you

Tim

Dr Tim R. McVicar
Principal Research Scientist
Sydney Bioregional Assessment Leader
Ecohydrological Time-Series Remote Sensing Team Leader
CSIRO Land and Water
GPO Box 1700, CANBERRA ACT 2601, AUSTRALIA

Editor-in-Chief: Journal of Hydrology
Associate Editor : Remote Sensing of Environment

Phone: (02) 6246-5741 / e-mail: tim.mcvicar@csiro.au

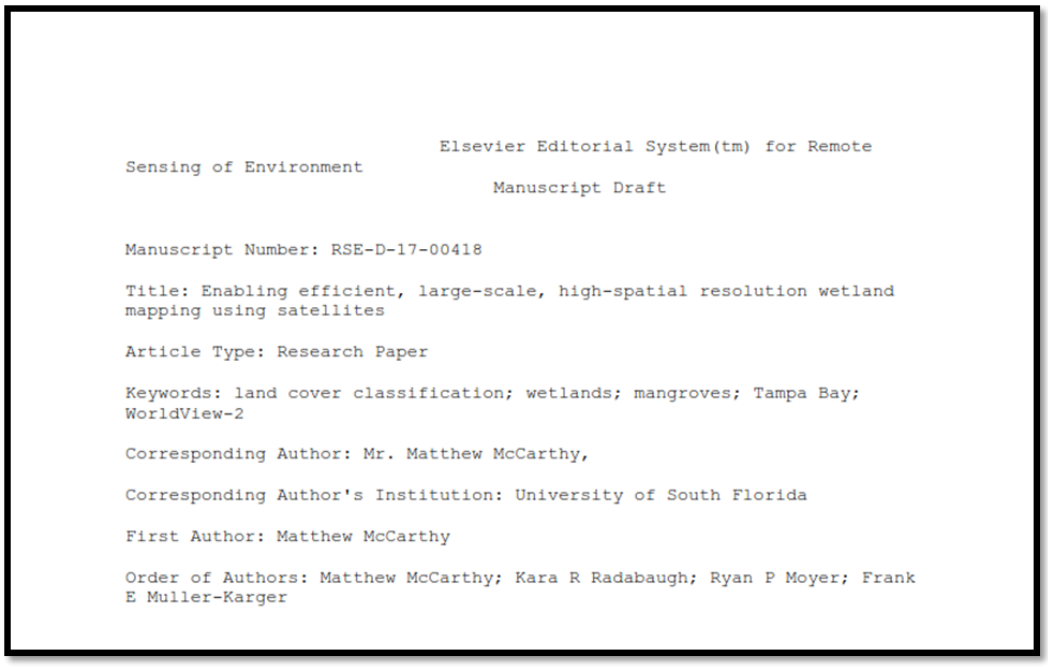

Elsevier Editorial System(tm) for Remote Sensing of Environment

Manuscript Draft

Manuscript Number: RSE-D-17-00418

Title: Enabling efficient, large-scale, high-spatial resolution wetland mapping using satellites

Article Type: Research Paper

Keywords: land cover classification; wetlands; mangroves; Tampa Bay; WorldView-2

Corresponding Author: Mr. Matthew McCarthy,

Corresponding Author's Institution: University of South Florida

First Author: Matthew McCarthy

Order of Authors: Matthew McCarthy; Kara R Radabaugh; Ryan P Moyer; Frank E Muller-Karger

4. Satellite remote sensing for coastal management: A review of successful applications

M.J. McCarthy conceived the research question, wrote the Introduction, Wetlands, Challenges, and Conclusions sections, and compiled and edited the manuscript.
K.E. Colna wrote part of the Fisheries and Aquaculture section and edited the manuscript.
M.M. El-Mezayen wrote part of the Fisheries and Aquaculture section and edited the manuscript.
A.E. Laureano-Rosario wrote part of the Public Health section and edited the manuscript.
P. Méndez-Lázaro wrote part of the Public Health section and edited the manuscript.
D.B. Otis wrote the Water Quality section and edited the manuscript.
G. Toro-Farmer wrote part of the Coral Reefs section and edited the manuscript.
M. Vega-Rodriguez wrote part of the Coral Reefs section and edited the manuscript.
F.E. Muller-Karger secured funding, wrote part of the Introduction and Conclusions sections, and edited the manuscript.

The final publication is available at Springer via http://dx.doi.org/10.1007/s00267-017-0880-x.

APPENDIX B:

PUBLISHED AND SUBMITTED CHAPTERS

Impacts of 40 Years of Land Cover Change on Water Quality in Tampa Bay, Florida

Matthew J. McCarthy[a]*, Frank E. Muller-Karger[a], Daniel B. Otis[a], and Pablo Méndez-Lázaro[b]

[a] Institute for Marine Remote Sensing, College of Marine Science, University of South Florida, 140 7th Ave. South, St. Petersburg, Fl 33701; E-Mails: mjm8@mail.usf.edu, carib@usf.edu; dotis@mail.usf.edu

[b] Environmental Health Department, Graduate School of Public Health, University of Puerto Rico, Medical Sciences Campus, PO Box 365067, San Juan Puerto Rico 00936-5067; Email: pablo.mendez1@upr.edu

* Author to whom correspondence should be addressed; E-Mail: mjm8@mail.usf.edu Tel.: +1-727-553-1186; Fax: +1-727-553-1103.

Abstract

Land cover changes in the Tampa Bay watershed (Florida) over the past four decades were examined along with precipitation and wind observations to help understand causes of long-term changes in turbidity and chlorophyll concentration within the Tampa Bay estuary. Water quality showed a statistically significant relationship to land cover fraction in the watershed compared to long-term precipitation or wind stress. Redundancy Analyses with Akaike's Information Criterion and non-parametric multiple regressions determined that turbidity and chlorophyll concentration decreased bay-wide from 1974-2012 with increased developed land fraction ($R^2 > 0.75$, p-value < 0.05). Various segments of the estuary showed different significant responses to developed land ($R^2 > 0.75$, p-value < 0.05), agricultural land ($R^2 > 0.93$, p-value < 0.02), bare land ($R^2 = 0.77$, p-value $= 0.001$), and wind stress ($R^2 = 0.91$, p-value $= 0.04$) at different times of year.

Keywords: land cover, land use change, water quality, Tampa Bay estuary

1. Introduction

The quality of estuarine and other coastal waters is a complex function of hydrological, meteorological, oceanographic, and human drivers **(**Chen et al., 2010; Schmidt et al., 2004; Eleveld et al., 2014; Yin et al., 2005; Moreno Madriñán et al., 2012). The interplay between these different processes may lead to different water quality outcomes over time. In Tampa Bay, Florida, turbidity and average chlorophyll concentration have decreased since the 1970's (Janicki et al. 2001; Moreno Madriñán et al. 2012). This is a result of the upgrade of waste water treatment plants to tertiary level starting in 1979 and other voluntary and regulated reductions in point-source pollution. Nonpoint sources have not been managed as effectively. Greening et al. (2014) found that nitrogen contributions of point and nonpoint sources to Tampa Bay were 60.3% and 23.9%, respectively, of the total nitrogen loadings in the 1970's. By the 2000's, the relative contributions were inverted, with point sources contributing about 19.5% and nonpoint 57.4% to nitrogen discharges into the bay. Much of this change may be expected to be related to urbanization and other changes in land use in the Tampa Bay watershed. In this study we evaluate the role of land cover changes, precipitation, and wind stress on turbidity in Tampa Bay between the 1970s and 2010.

Tampa Bay (27.5 – 28.08° N and 82.36 – 82.75° W) is the largest open-water estuary in Florida (Figure 1). It covers over 1,000 km^2 at high tide, with an average depth of 3.4 m. The watershed area covers over 6,500 km^2. Six counties and the city of Tampa, the second largest metropolitan area in Florida, intersect the watershed. An estimated 2.3 million people lived in the Tampa Bay watershed in 2003, with population growth between 1990 and 2003 reaching ~22% (US Census 2007). Approximately 500 new residents moved to counties surrounding Tampa Bay each week during this timeframe.

Turbidity is a measure of light transparency in aquatic environments used by the U.S. Environmental Protection Agency (EPA) as an index of water quality. Turbidity may be influenced by changes in the concentration of colored dissolved matter and suspended particulates including sediment and phytoplankton. These variables are affected by changes in hydrological, meteorological, and oceanographic phenomena (Eleveld et al., 2014; Chen et al., 2007a; Chen et al., 2010; Miller et al., 2011).

Land cover and land use affect downstream water quality through runoff of freshwater, nutrients, sediment, and pollution (Wickham et al. 2005; Bateni et al. 2013; Miller et al. 2011; Jordan et al. 2012). Nelson and Booth (2002) conducted a watershed-scale sediment budget analysis in western Washington state, and found that urban development and subsequent stream-channel erosion has contributed an increase of nearly 50% in the annual sediment yield. However, impervious surfaces (e.g. roads, buildings, parking lots) tend to enhance sediment-free stormwater runoff (Estes et al. 2009; Miller et al. 2011; Moreno Madriñán et al. 2012). Miller et al. (2011) developed regression models for 43 watersheds in Illinois. They found that during base flow conditions, agriculture-dominated watersheds had significantly higher turbidity and total suspended solid concentrations compared with urban watersheds. Turbidity during storm flow conditions was also significantly lower in urban watersheds. Moreno Madriñán et al. (2012) found a negative relationship between the fraction of developed land in each watershed segment and turbidity at the mouths of the rivers entering Tampa Bay.

Precipitation in the watershed affects estuarine water quality through increased nutrient and sediment discharge into rivers (Al-Taani 2014; Estes et al. 2009; Jordan et al. 2012; Miller et al. 2011). Le et al. (2013) used satellite-derived chlorophyll concentration maps of Tampa Bay from 1998-2011 to show that river discharge explains approximately 60% of seasonal variability and

about 90% of interannual variability in chlorophyll in the bay. Interannual variability was strongly influenced by El Niño-Southern Oscillation cycles and tropical cyclones. Le et al. (2013) were not able to detect long-term variations, in part because the satellite data record used was short. Eleveld et al. (2014) compared satellite-derived water quality products with modelled water quality and found that sun-synchronous satellites alias tidal patterns and are also biased by acquiring usable data under cloud-free conditions. These constraints led to biases in satellite-derived water quality products (Eleveld et al. 2014). Schoonard et al. (2014) examined spatial patterns of precipitation in Pinellas County, which forms the western boundary of Tampa Bay, from 2003 to 2007 and found that convective storms related to the seabreeze during the summer wet season were highly spatially variable and heavily influenced by dominant wind direction. This process results in a broad and diffuse discharge into Tampa Bay which cannot be quantified as river discharge. Most of the river discharge enters Tampa Bay from the north and eastern sides of the bay.

Winds also influence sediment load by resuspension in Tampa Bay and in other coastal areas (Chen et al. 2007b; Chen et al. 2007c; Hu et al. 2004; Miller et al. 2004). Wind stress is a well-known driver of sediment resuspension (Demers et al. 1987; Madsen et al. 1993; Schoen et al. 2014; Sheng and Lick 1979). In Tampa Bay, turbidity is directly related to seasonal wind forcing, especially in the lower segment of the estuary (Chen et al., 2007b; Chen et al. 2010).

1.1 Study Area

The Tampa Bay watershed has historically been divided into segments (Janicki et al., 2001; see Figure 1). The landward extent of the watershed for each segment was defined using the level 8 hydrologic units of the Tampa Bay watershed. Each land cover map (described below)

was clipped to match the watershed for each bay segment. The Hillsborough Bay (HB) watershed (3,192 km^2) is dominated by wetland and agricultural land. We limited Old Tampa Bay (OTB) to the area north of a causeway (specifically Gandy Bridge) because this structure limits water exchange with the rest of Tampa Bay (Zhu et al. 2014). Figure 2 shows the gap we created by limiting the coverage of what is formally known as OTB. The OTB watershed (822 km^2) is dominated by developed land and wetland. The Middle Tampa Bay (MTB) watershed (1,073 km^2) is dominated by agricultural land and wetland. Land cover area from each of these segments was combined for an aggregated assessment (hereafter referred to as Bay-Wide or Upper TB). The Lower TB segment was excluded from this study because water quality here is more strongly influenced by oceanographic processes of exchange with the Gulf of Mexico than by the adjacent watershed (Zhu et al. 2014). Thirty-year precipitation and temperature normals based on data during the period 1981-2010 from this station are presented in Table 1.

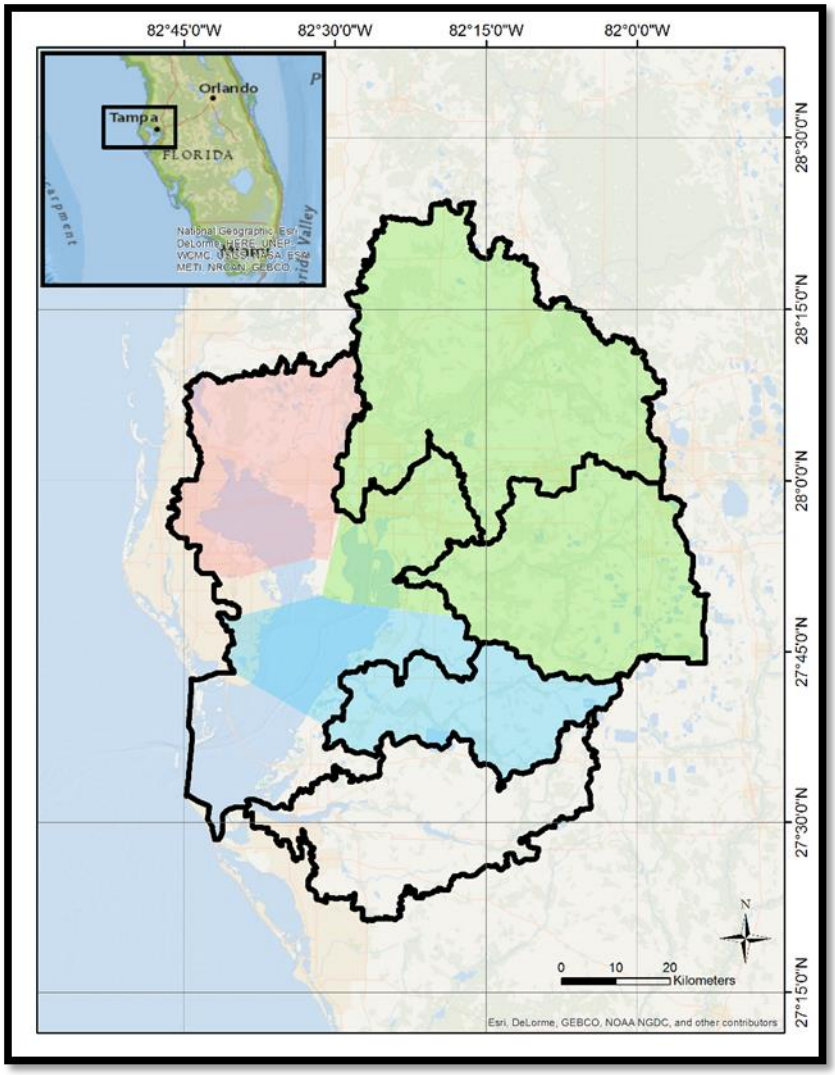

Figure 1. The Tampa Bay watershed study area as defined by the National Estuary Program. The map shows drainage basins (black polygons) as per hydrologic unit code-8 (HUC-8), and watersheds for Old Tampa Bay (red), Hillsborough Bay (green) and Middle Tampa Bay (blue).

Table 1. Annual and seasonal precipitation and temperature normals (1981-2010).

Season	Precip (cm)	Min Tmp (°C)	Avg Tmp (°C)	Max Tmp (°C)
Annual	117.6	18.4	23.0	27.6
DJF	19.1	11.9	16.9	21.9
JJA	54.7	24.2	28.2	32.2
MAM	18.2	17.6	22.6	27.5
SON	25.7	19.8	24.3	28.8

1.2 Hypotheses

The following null hypotheses guided this study:

1. Neither bay-segment nor bay-wide water-quality are significantly related to land cover, precipitation, or wind stress ($p < 0.05$);
2. Neither bay-segment nor bay-wide periods of high turbidity or high chlorophyll concentration are significantly related to land cover, precipitation, or wind stress ($p < 0.05$);
3. Neither bay-segment nor bay-wide periods of low turbidity or low chlorophyll concentration are significantly related to land cover, precipitation or wind stress ($p < 0.05$);

We examined precipitation, wind stress, and historical land use changes as possible drivers of changes in water quality within Tampa Bay over the period 1970s-2010. Turbidity and chlorophyll concentration served as indices of water quality. Analyses focused on possible relationships between water quality within each segment of the bay and changes in the watershed. A similar analysis was done for bay-wide conditions. We examined changes over time since the 1970's, within annual periods as well as during periods of high and low turbidity and chlorophyll concentration separately.

2. Materials and Methods

2.1 Land Cover Data

Land cover maps were downloaded from the United States Geological Survey (USGS) Enhanced Historical Land-Use and Land-Cover Data Sets (http://water.usgs.gov/GIS/dsdl/ds240/index.html) and the National Oceanic and Atmospheric

Administration (NOAA) Coastal-Change Analysis Program (C-CAP; http://csc.noaa.gov/ccapftp/). The former was created using high-altitude aerial photographs of the U.S. collected in 1970-1985. The USGS land cover datasets were created to support the National Water-Quality Assessment Program and other environmental impact assessments (Anderson et al., 1976; Price et al., 2007). The data represent the initial land cover status (1970-1985; Figure 2) and will hereafter be referred to as the 1977 map as the central year of this period. The specific date of each classified region within this period is not documented. The USGS maps were digitized at a scale of 1:250,000. The minimum size of most class polygons is 4 hectares, although for some it is 16 hectares. Seven class groups were identified for this region: urban or built-up land, agricultural land, rangeland, forest land, water, wetland, and barren land.

NOAA C-CAP maps were created from the National Land Cover Database (NLCD). These were derived from 30 meter spatial resolution Landsat satellite images. Each mapped product was based on imagery from multiple years centered on a nominal date, specifically 1996 (1995-1997), 2001 (2000-2002), 2006 (2005-2007), and 2010 (2009-2011) (Figure 2). Multiple years of satellite imagery were required to create the maps to minimize interference from cloud cover. C-CAP maps for this region include class groups similar to those described above from the USGS: developed land, agricultural land, grassland, forest land, scrubland, barren land, palustrine wetland, estuarine wetlands, and water and submerged lands. Based on the definitions of the classes, C-CAP grassland and scrubland classes were merged into one ‘rangeland’ class for consistency with the USGS maps.

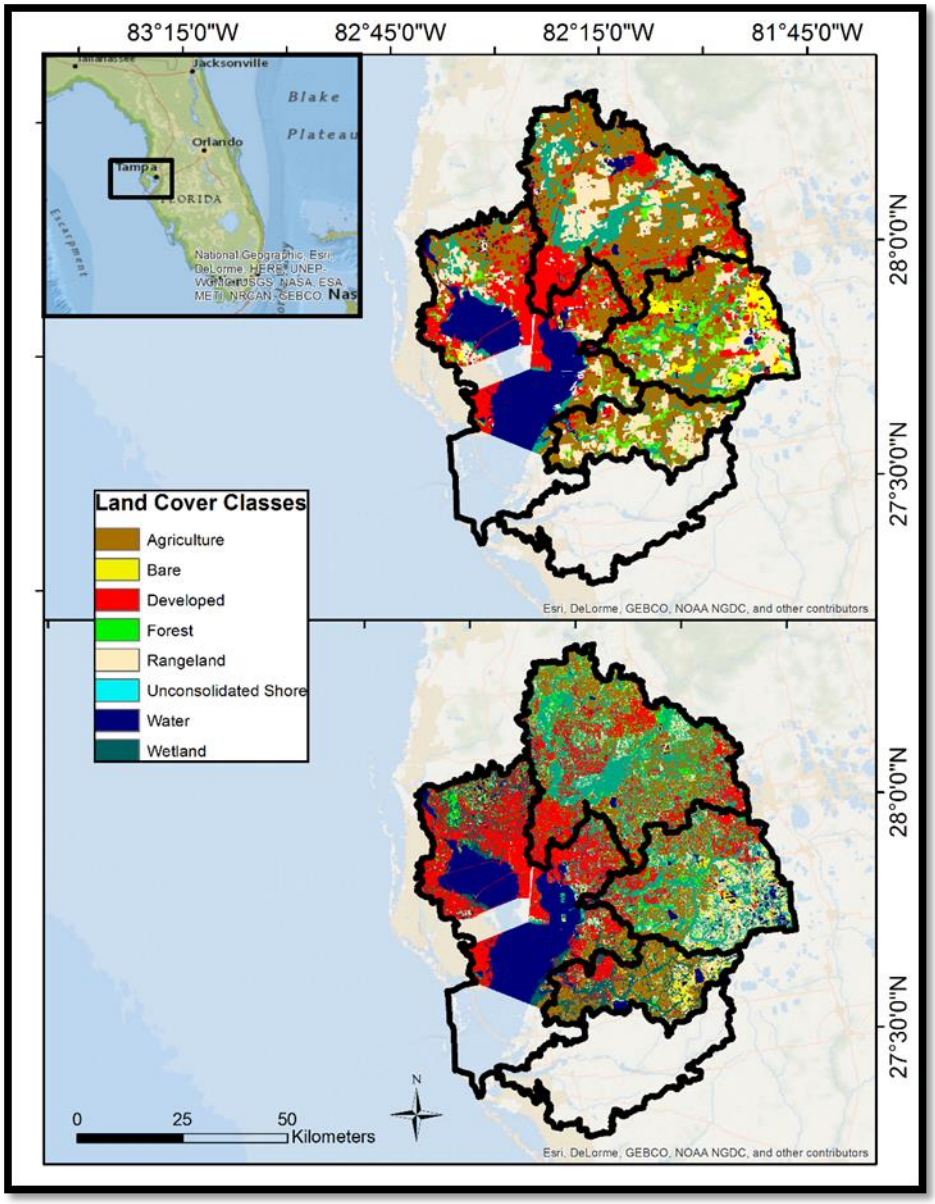

Figure 2. Top panel: USGS map representing land use classes for 1970-1985. Bottom panel: C-CAP map representing land use classes during the three-year period centered on 2010 (2009-2011).

A comparison of the USGS and NOAA land use products with wetland maps produced by the National Wetlands Inventory (NWI) and the Southwest Florida Water Management District (SWFWMD) (Rains et al. 2012) suggested that the USGS and NOAA products substantially overestimate wetland area at the expense of forest area. C-CAP maps show over 2,000 km^2 of

wetlands for 1996, 2001, and 2006. NWI and SWFWMD report approximately 800-900 km^2 in wetlands for the same time periods. A previous C-CAP accuracy assessment indeed reports high errors of omission and of commission (up to 94%) for wetland and forest classes (Assessment Report 2013). To minimize biases in our conclusions, we merged wetland and forest land classes for USGS and C-CAP maps into one forest/wetland class.

2.2 Water Quality Data

In situ water quality data for each segment of the Tampa Bay estuary were obtained from the Environmental Protection Commission of Hillsborough County (EPCHC; the Tampa Bay Water Atlas: http://www.tampabay.wateratlas.usf.edu). Samples were collected monthly at over 60 stations in Tampa Bay. Anomalously high turbidity values (i.e. turbidity >24 NTU) were removed following Chen et al. (2010). Data were averaged over the following epochs to match the land cover map periods: 1976-1978, 1995-1997, 2000-2002, 2005-2007, and 2009-2011. The first epoch (1976-1978) was chosen as the middle three years of the USGS land cover map period, instead of the entire period (1970-1985), to maintain consistency with the other three-year epochs examined.

Monthly water-quality climatologies (averages calculated for each month from every year of available data) were computed based on data from 1974-2011. These climatologies were used to identify periods of higher or lower turbidity, and higher or lower chlorophyll concentration. Periods of reduced and enhanced water-quality were assessed separately to help understand possible interactions between land cover and precipitation-driven runoff on water quality. Separating these seasons as opposed to conducting an analysis that simply aggregates data by

epoch over entire annual periods helped to minimize possible confounding of zero-precipitation periods and the land cover change.

High-turbidity and high-chlorophyll periods were identified as those months in which climatology values exceeded the climatological average plus one standard deviation. Low-turbidity and low-chlorophyll periods were identified simply as those months in which climatology values fell below the climatological mean. High-turbidity and low-turbidity months were examined separately from high-chlorophyll and low-chlorophyll months. Low turbidity and low chlorophyll months represent "background" water quality conditions. Averages for each of those periods, and annual overall averages, were computed for all epochs. These were used as the "response variable" in analyses over the corresponding epochs.

2.3 Meteorological Data

Daily precipitation and wind speed data for Tampa International Airport (1893-2012) were downloaded from the National Climate Data Center (NCDC; http://www.ncdc.noaa.gov/). These data were binned to monthly values using Matlab™. Precipitation was assumed to have a cumulative effect and was therefore binned monthly by summing daily data. Daily East-West (u) and North-South (v) wind components were averaged separately before recombining to compute average daily wind speed and direction (see method of Gilhousen 1987). Wind stress was computed from the daily wind speed data (Equation 1), and binned as monthly averages (Wu 1969).

Equation 1: $$\tau = C_D \rho_{air} U^2$$

where C_D is a drag coefficient (1.2×10^{-3}), ρ_{air} is the density of air (1.22 kg/m^3), and U is wind velocity.

Averages of monthly precipitation and wind stress were computed for annual, high, and low water-quality periods. Both meteorological variables (precipitation and wind stress) were used as explanatory variables.

2.4 Statistical Analyses

Standard normal homogeneity tests (SNHT) were run on all variables (wind speed was used to represent wind stress) to find breaks in the datasets which may indicate changes in sampling technique or location. Significance values were computed using 10,000 Monte Carlo simulations. Mann-Kendall Trend Tests (MK) were run on each time series of monthly values to evaluate possible trends (Mei et al. 2014).

Multiple regressions alone would be insufficient for this study because of the high ratio of explanatory variables to sample size (9:5). Therefore, Redundancy Analyses with Akaike's Information Criterion (RDA AIC) were used first to identify those explanatory variables that explained the most variation in the response variable. These analyses were conducted using Matlab^{TM}. The RDA AIC function standardized all input explanatory variables and determined the best explanatory variables through constrained ordination. This assessed how much of the variation in one set of variables explained variation in another set, while accounting for explanatory variable multicollinearity (Wollenberg 1977). Akaike (1973) proposed an information criterion to quantify the amount of information and statistically determine the number of parameters for an equation that represents a group of experimental data. The equation with the minimum AIC is considered the best representation of the experimental data (Yamaoka et al. 1978). A null model is created by assigning a value below which the best equation's AIC

value must be in order to be considered viable to explain variation in the dependent variable. If no equation explains more variation than a null model, no independent variable is selected.

Multiple regressions were run on the variable(s) identified as 'best' by the RDA AIC. One thousand iterations were run for each regression to compute permutation-based p-values because much of the data were not normally distributed. Finally, an outlier test was run on all significant relationships because any one outlier could have significantly influenced results sice we only have five sample epochs. For each observation, an outlying value was identified as exceeding 'N' divided by the sum of squared differences, normalized by subtracting the median and dividing by the median absolute deviation (i.e. median of absolute value of each sample minus the median of the array). Breiman and Cutler (2003) suggested that values >10 be considered outliers when using this method.

3. Results

Percent of watershed area that was covered by each class for each map epoch are shown in Tables 2-5. Total percent is shown at the bottom of each table. This number is <100 for each 1970s map because these used an additional class called "transitional areas". "Transitional areas" were defined "by the lack of remote sensor information which could enable the interpreter to predict reliably the future use or discern the past use" (Anderson et al. 1976). Because land of this class could not be accurately described, and it could not be reconciled with any C-CAP class, it was excluded from this analysis. Percent cover of each class for each bay segment is shown in Tables 2-5.

Turbidity and chlorophyll averages for each segment and respective segment area are presented in Table 6. Upper Tampa Bay turbidity and chlorophyll, and Tampa International

Airport precipitation, wind speed time series, and climatologies are shown in Figure 3. Monthly turbidity and chlorophyll climatologies for each bay segment and Upper Tampa Bay are shown in Figures 4 and 5. Table 7 lists the months that were identified for each bay segment as "high" and "low" for turbidity and chlorophyll.

SNHT evaluations found significant changes in wind speed, chlorophyll concentration, and turbidity time series. The time series of wind speed shows a significant decrease in values starting in May 1993. The mean of the data before May 1993 was 3.45 m/s and average wind speed decreased gradually over time through December 2012, to give an average of 3.02 m/s for this period following the break (Figure 6a). Bay-wide chlorophyll concentration showed a change in December of 1983. The mean of the data prior to December 1983 was 16.1 mg/m^3, and 9.6 mg/m^3afterward (Figure 6b). This change corresponds to the period of intensive wastewater treatment plant improvements, but it also marks a period of substantial increase in turbidity in Tampa Bay. Bay-wide turbidity showed marked variability over time. Turbidity was about 5 NTU on average before 1989. Turbidity was anomalously high between 1990 and 1993. The mean of the data after this period was about 3.4 NTU (Figure 6c). Precipitation data tested as homogenous (i.e. no apparent mid-series breaks; Figure 6d).

Table 2. Hillsborough Bay land cover class as percent of watershed.

	1970s	**1996**	**2001**	**2006**	**2010**
Developed	17.5	16.6	18.9	19.2	18.2
Agriculture	39.1	22.0	21.4	20.9	23.5
Forest/Wetland	17.7	43.9	43.5	42.7	38.3
Unconsolidated Shore	0.0	0.0	0.0	0.0	0.0
Bare	4.3	1.5	1.7	2.3	2.0
Water	5.1	4.8	4.7	5.4	5.5
Range	15.6	11.2	9.8	9.6	12.6
Total	99.4	100.0	100.0	100.0	100.0

Table 3. Old Tampa Bay land cover class as percent of watershed.

	1970s	1996	2001	2006	2010
Developed	27.0	34.8	38.1	38.2	36.0
Agriculture	24.3	7.3	6.6	6.5	10.1
Forest/Wetland	10.4	28.7	27.7	27.6	25.5
Unconsolidated Shore	0.0	0.0	0.0	0.0	0.0
Bare	0.3	0.5	0.1	0.2	0.1
Water	25.7	24.6	24.6	24.7	24.8
Range	10.9	4.0	2.9	2.8	3.5
Total	98.7	100.0	100.0	100.0	100.0

Table 4. Middle Tampa Bay land cover class as percent of watershed.

	1970s	1996	2001	2006	2010
Developed	7.2	9.5	10.2	10.6	10.6
Agriculture	33.5	31.7	30.0	28.1	27.2
Forest/Wetland	12.0	26.5	26.3	25.3	22.8
Unconsolidated Shore	0.0	0.0	0.0	0.0	0.1
Bare	0.0	1.0	2.8	3.7	3.4
Water	25.4	26.2	26.1	27.4	27.7
Range	20.9	5.2	4.6	4.9	8.3
Total	99.0	100.0	100.0	100.0	100.0

Table 5. Upper Tampa Bay land cover class as percent of watershed.

	1970s	1996	2001	2006	2010
Developed	16.9	18.0	20.2	20.5	19.5
Agriculture	35.5	21.7	20.8	20.1	22.1
Forest/Wetland	15.4	37.8	37.3	36.6	32.9
Unconsolidated Shore	0.0	0.0	0.0	0.0	0.0
Bare	2.8	1.2	1.7	2.2	2.0
Water	12.7	12.5	12.4	13.2	13.3
Range	15.9	8.8	7.6	7.5	10.2
Total	99.2	100	100	100	100

Table 6. Average turbidity and chlorophyll concentrations for the study areas with their respective bay and watershed areas (1974-2012).

Region	Avg. Turbidity (NTU)	Avg. Chlorophyll (mg/m^3)	Bay Area (km^2)	Watershed Area (km^2)
Upper TB	3.65	9.92	676	5,088
OTB	3.83	9.77	204	822
HB	4.81	14.56	175	3,192
MTB	3.26	7.38	298	1,073

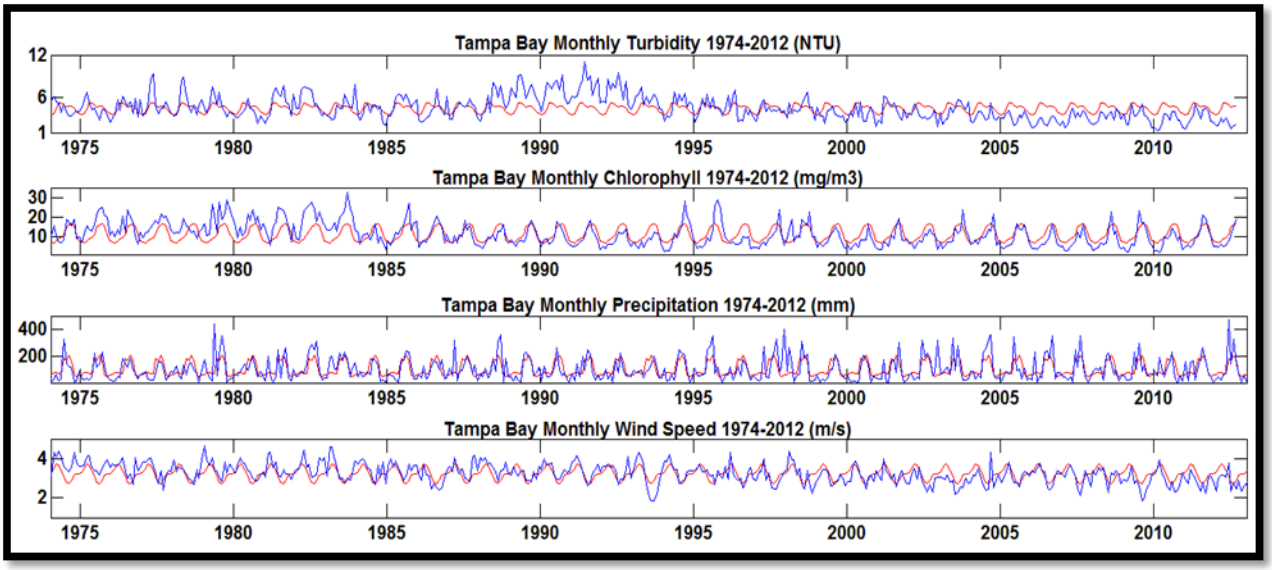

Figure 3. Monthly time series (blue) and mean annual cycle (red) for bay-wide turbidity and chlorophyll, and Tampa International Airport precipitation and wind speed.

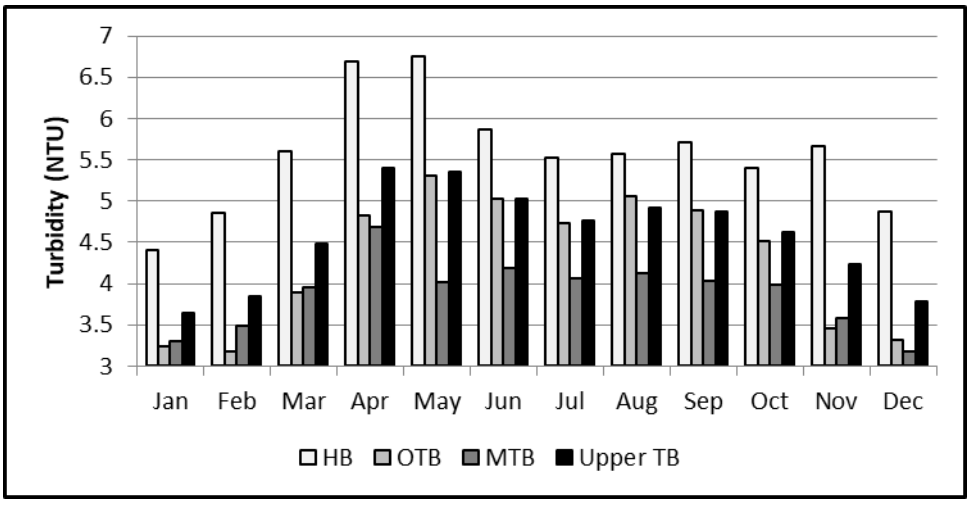

Figure 4. Monthly turbidity climatologies for each bay segment and Upper Tampa Bay.

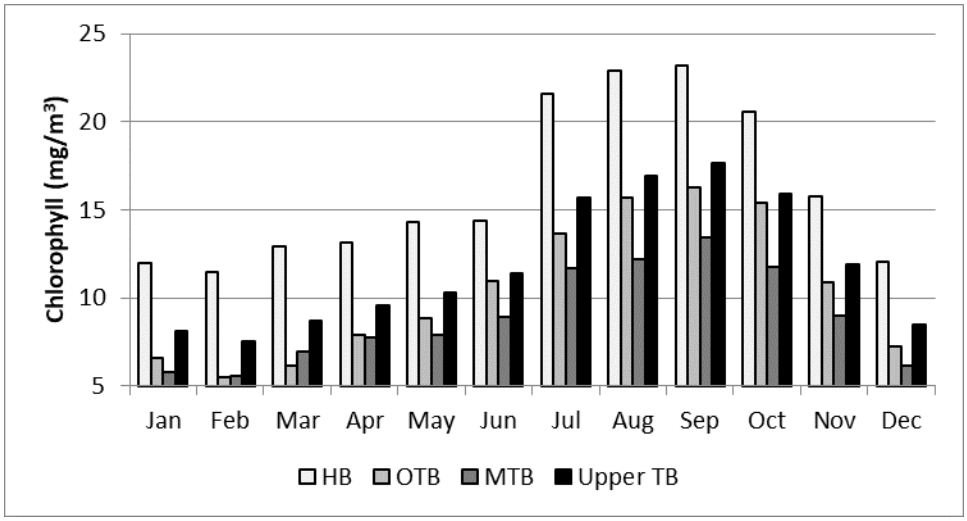

Figure 5. Monthly chlorophyll climatologies for each bay segment and Upper Tampa Bay.

Table 7. Months corresponding to high and low turbidity and chlorophyll for each bay segment.

	High Turbidity Months	**Low Turbidity Months**	**High Chlorophyll Months**	**Low Chlorophyll Months**
Upper TB	Apr, May	Jan, Feb, Mar, Nov, Dec	Aug, Sep, Oct	Jan-Jun, Dec
HB	Apr, May	Jan, Feb, Jul, Aug, Oct, Dec	Jul, Aug, Sep	Jan-Jun, Nov, Dec
OTB	May	Jan, Feb, Mar, Nov, Dec	Aug, Sep, Oct	Jan-May, Dec
MTB	Apr	Jan, Feb, Nov, Dec	Jul-Oct	Jan-May, Dec

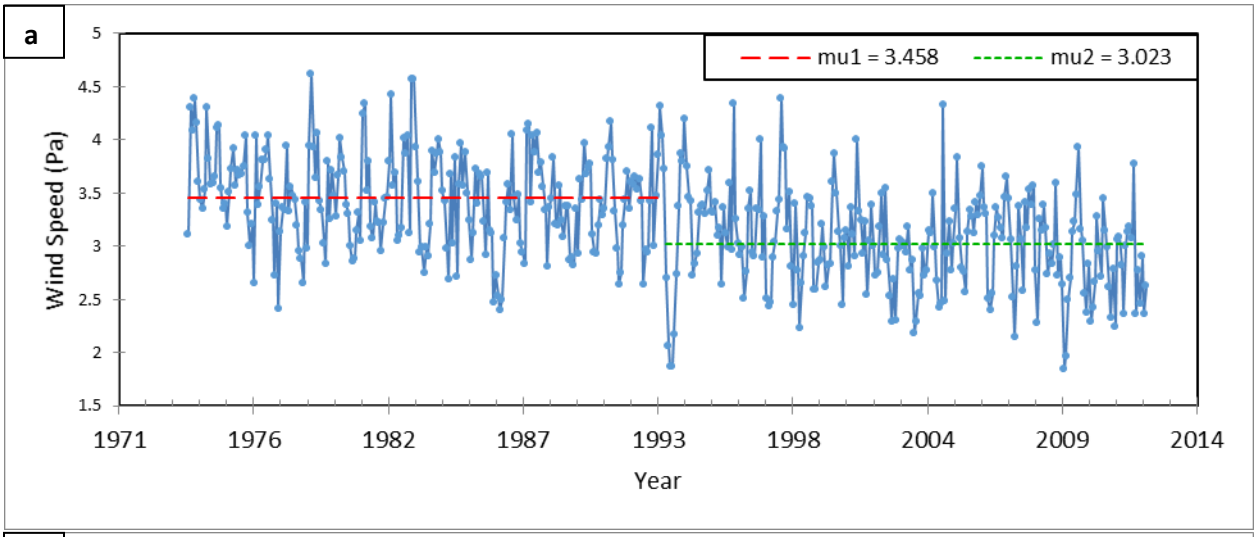
a
mu1 = 3.458
mu2 = 3.023
Wind Speed (Pa)
5
4.5
4
3.5
3
2.5
2
1.5
1971
1976
1982
1987
1993
1998
2004
2009
2014
Year

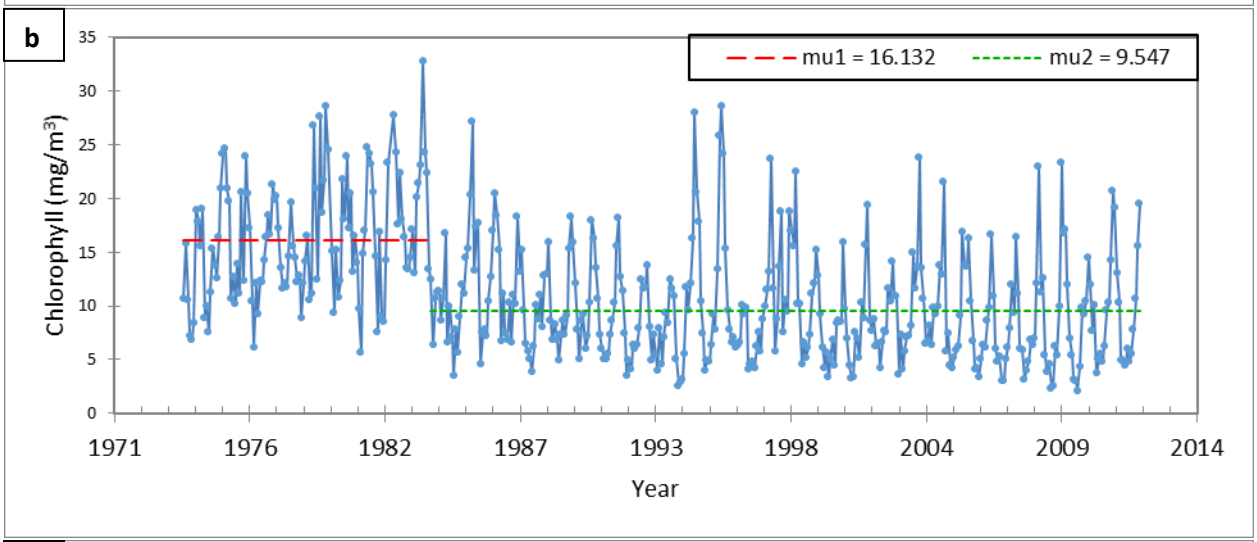
b
mu1 = 16.132
mu2 = 9.547
Chlorophyll (mg/m3)
35
30
25
20
15
10
5
0
1971
1976
1982
1987
1993
1998
2004
2009
2014
Year

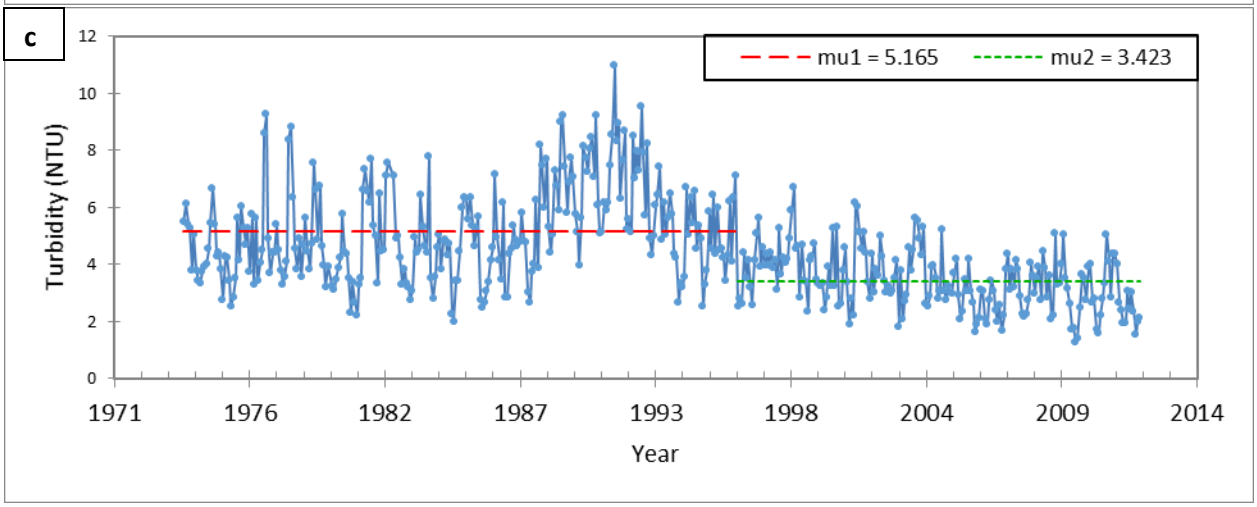
c
mu1 = 5.165
mu2 = 3.423
Turbidity (NTU)
12
10
8
6
4
2
0
1971
1976
1982
1987
1993
1998
2004
2009
2014
Year

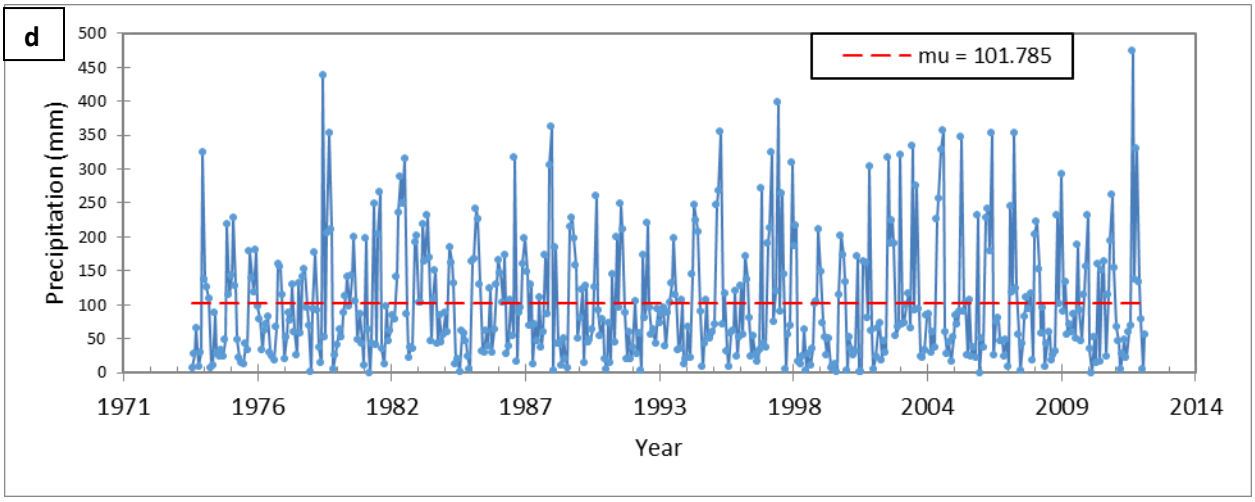

Figure 6. Monthly time series plots of bay-wide wind speed, chlorophyll concentration, turbidity and precipitation with averages (mu) of break periods where applicable as identified by SNHT tests.

SNHT evaluations on monthly turbidity (Figure 7a-c) and chlorophyll concentration (Figure 8a-c) binned within each bay segment also show discontinuities. Turbidity breaks occurred in June of 1997, May of 1996, and June of 2000 for HB, OTB and MTB, respectively. The means of the data before and after the breaks were 6.55 NTU and 4.21 NTU (HB), 5.05 NTU and 3.41 NTU (OTB), and 4.21 NTU and 2.70 NTU (MTB). All three breaks follow a period of high turbidity that was sustained for several years during the early 1990's.

Chlorophyll concentration breaks occurred in December of 1983, January of 1984, and December of 1985 for HB, OTB and MTB, respectively. Again, these changes coincide with the initial indications of the increase in turbidity leading to the turbidity maxima observed in the early 1990's. The means of the data before and after the breaks were 26.48 mg/m^3 and 12.91 mg/m^3 (HB), 13.52 mg/m^3 and 9.50 mg/m^3 (OTB), and 12.78 mg/m^3 and 7.14 mg/m^3 (MTB).

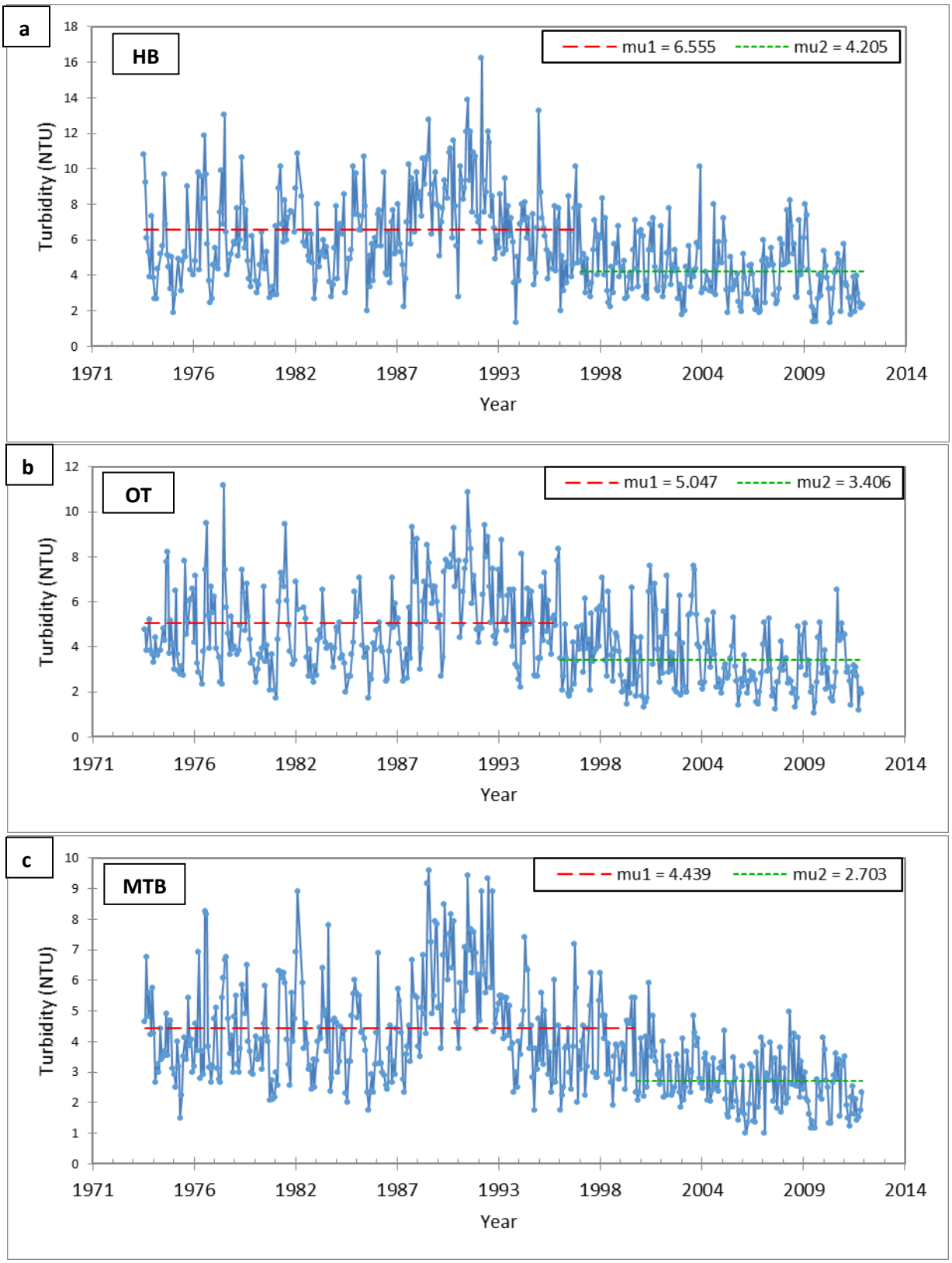

Figure 7. Monthly time series plots of turbidity for HB (a), OTB (b) and MTB (c) with averages (mu) of break periods, where applicable, as identified by SNHT tests.

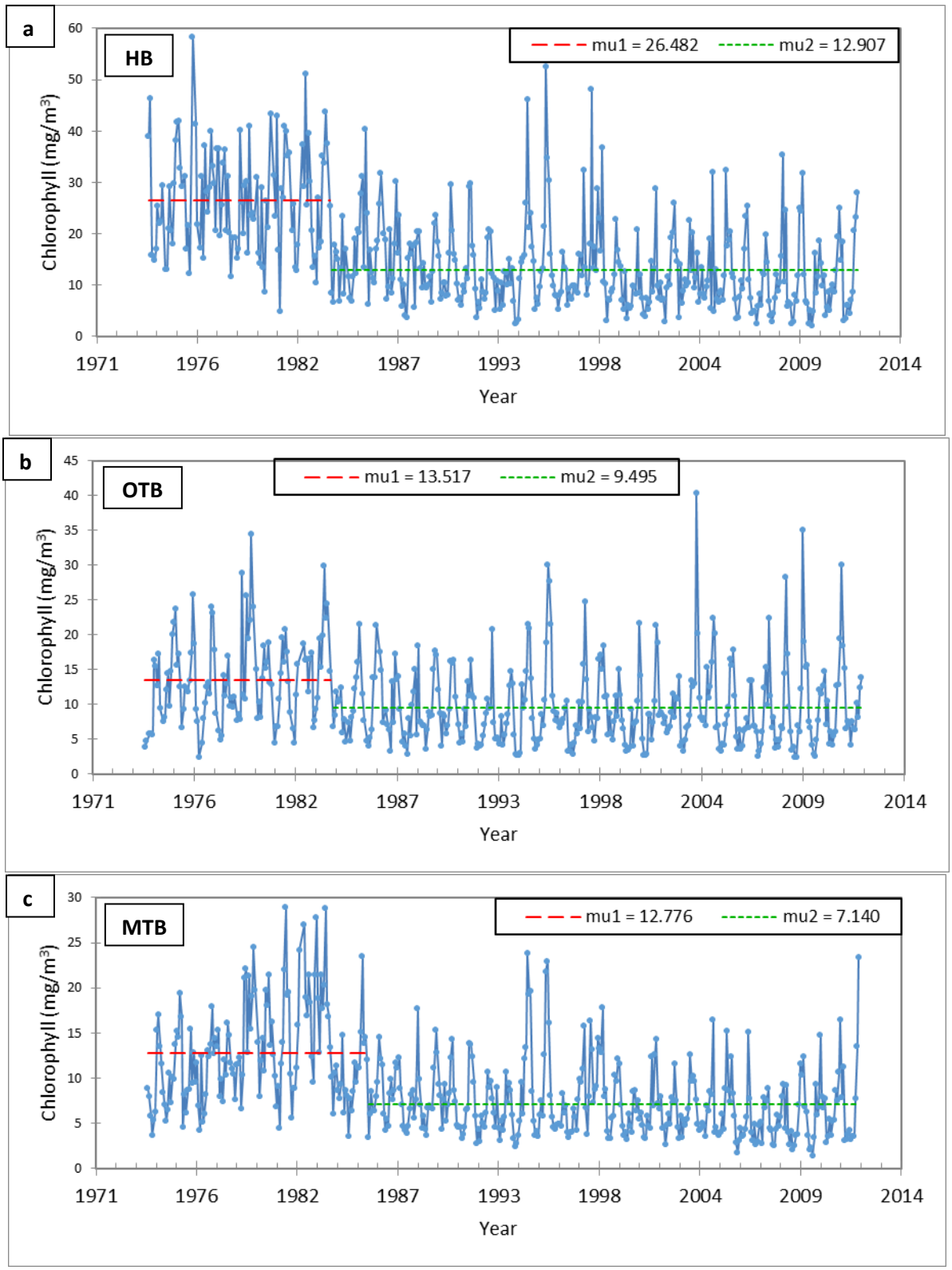

Figure 8. Monthly time series plots of chlorophyll concentration for HB (a), OTB (b) and MTB (c) with averages (mu) of break periods where applicable as identified by SNHT tests.

MK tests found that monthly wind speed and stress decreased significantly ($p < 0.017$) every month during this 39-year period. No trends were found in monthly precipitation with the exception of marginally significant increases in April and decreases in May ($p = 0.02$ and $p = 0.068$, respectively). Bay-wide chlorophyll concentration decreased significantly every month ($p < 0.022$) except for September and October, during which it showed no change ($p > 0.1$). On average, bay-wide turbidity also decreased every month ($p < 0.05$) except for August and September, which again showed no change ($p > 0.1$). The months with no trend in turbidity coincided with the months showing peak chlorophyll concentration.

Variables identified as 'best' by RDA AIC analyses are presented here with the corresponding multiple regression results (Tables 8-9). OTB year-round turbidity was significantly negatively related to developed land percent cover ($R^2 = 0.76$, $p = 0.001$; Figure 9a). MTB year-round turbidity was significantly positively related to agricultural land percent cover ($R^2 = 0.97$, $p = 0.001$; Figure 9b). None of our variables explained HB year-round turbidity patterns over time.

Similar trends were observed for high turbidity months. OTB high-turbidity was significantly negatively related to developed land percent cover ($R^2 = 0.92$, $p = 0.001$; Figure 9c). MTB high-turbidity was significantly positively related to agricultural land percent cover ($R^2 = 0.93$, $p = 0.021$; Figure 9d). No variable explained HB high-turbidity.

During low-turbidity months, MTB turbidity was significantly positively related to agricultural land percent cover ($R^2 = 0.98$, $p = 0.001$; Figure 9e). HB low-turbidity was also significantly positively related to wind stress ($R^2 = 0.91$, $p = 0.041$; Figure 9f). This suggests that, during background turbidity months, increased wind stress led to an increase in turbidity. No variable could explain OTB low-turbidity better than a null model during this period.

HB year-round chlorophyll concentration was significantly positively related to agricultural land percent cover ($R^2 = 0.96$, $p = 0.001$). This relationship was heavily influenced by an outlier in 1977, which, when removed, rendered the relationship insignificant. MTB year-round chlorophyll was significantly negatively related to developed land percent cover ($R^2 = 0.98$, $p = 0.019$; Figure 10a). OTB year-round chlorophyll was negatively related to developed land percent cover, but the relationship was only marginally significant ($R^2 = 0.86$, $p = 0.095$).

During high-chlorophyll months, HB chlorophyll was significantly negatively related to forest/wetland percent cover ($R^2 = 0.91$, $p = 0.001$). Again, this relationship was influenced by an outlier in 1977, which, when removed, rendered the relationship insignificant. MTB high-chlorophyll was found to be significantly negatively related to bare land percent cover ($R^2 = 0.77$, $p = 0.001$; Figure 10b) during this period. No variable could explain OTB high-chlorophyll better than a null model.

During low-chlorophyll months, HB chlorophyll was significantly positively related to agricultural land percent cover ($R^2 = 0.98$, $p = 0.001$), but this relationship was heavily influenced by an outlier in 1977, which, when removed, rendered the relationship insignificant. OTB low chlorophyll was found to be significantly negatively related to developed land percent cover ($R^2 = 0.92$, $p = 0.001$), but this relationship was also heavily influenced by an outlier in 1977, which, when removed, rendered the relationship insignificant. MTB low chlorophyll was found to be significantly negatively related to developed land percent cover ($R^2 = 0.97$, $p = 0.02$; Figure 10c).

Analyses for the entire upper bay found that year-round turbidity was significantly negatively related to developed land percent cover ($R^2 = 0.76$, $p = 0.02$; Figure 11a). Year-round chlorophyll was significantly positively related to agricultural land percent cover ($R^2 = 0.97$, $p =$

0.001). This relationship was influenced by an outlier in 1977, which, when removed, renders the relationship the insignificant. Bay-wide high turbidity was significantly negatively related to developed land percent cover ($R^2 = 0.83$, $p = 0.02$; Figure 11b), but no variable could explain bay-wide low turbidity better than a null model. Bay-wide high chlorophyll was negatively related to developed land percent cover ($R^2 = 0.82$, $p = 0.043$; Figure 11c). An outlier influenced the otherwise significant bay-wide low-chlorophyll relationship with agricultural land percent cover and rendered it insignificant when removed.

Table 8. RDA AIC-identified 'best' variables and multiple regression results for land cover, precipitation, and wind stress vs. turbidity for the Tampa Bay estuary and each segment. "Agr" refers to agricultural land. "Dev" refers to developed land.

	Tampa Bay			**OTB**			**HB**			**MTB**		
Period	**Variable**	**R^2**	**p**	**Variable**	**R^2**	**p**	**Variable**	**R^2**	**p**	**Variable**	**R^2**	**p**
Annual	Dev	0.76	0.02	Dev	0.76	0.001	None	N/A	N/A	Agr	0.97	0.001
HT	Dev	0.83	0.02	Dev	0.92	0.001	None	N/A	N/A	Agr	0.93	0.021
LT	None	N/A	N/A	None	N/A	N/A	Wind Stress	0.91	0.041	Agr	0.98	0.001

Table 9. RDA AIC-identified 'best' variables and multiple regression results for land cover, precipitation, and wind stress vs. chlorophyll for the entire Tampa Bay estuary and for each separate segment (*italics* indicates a relationship that was skewed by an outlier). "Agr" refers to agricultural land. "Dev" refers to developed land. "For/Wet" refers to the combined Forest/Wetland class.

	Tampa Bay			**OTB**			**HB**			**MTB**		
Period	**Variable**	**R^2**	**p**	**Variable**	**R^2**	**p**	**Variable**	**R^2**	**p**	**Variable**	**R^2**	**p**
Annual	*Agr*	*0.97*	*0.001*	Dev	0.86	0.095	*Agr*	*0.96*	*0.001*	Dev	0.98	0.019
HC	Dev	0.82	0.043	None	N/A	N/A	*For/Wet*	*0.91*	*0.001*	Bare	0.77	0.001
LC	*Agr*	*0.98*	*0.001*	*Dev*	*0.92*	*0.001*	*Agr*	*0.98*	*0.001*	Dev	0.97	0.02

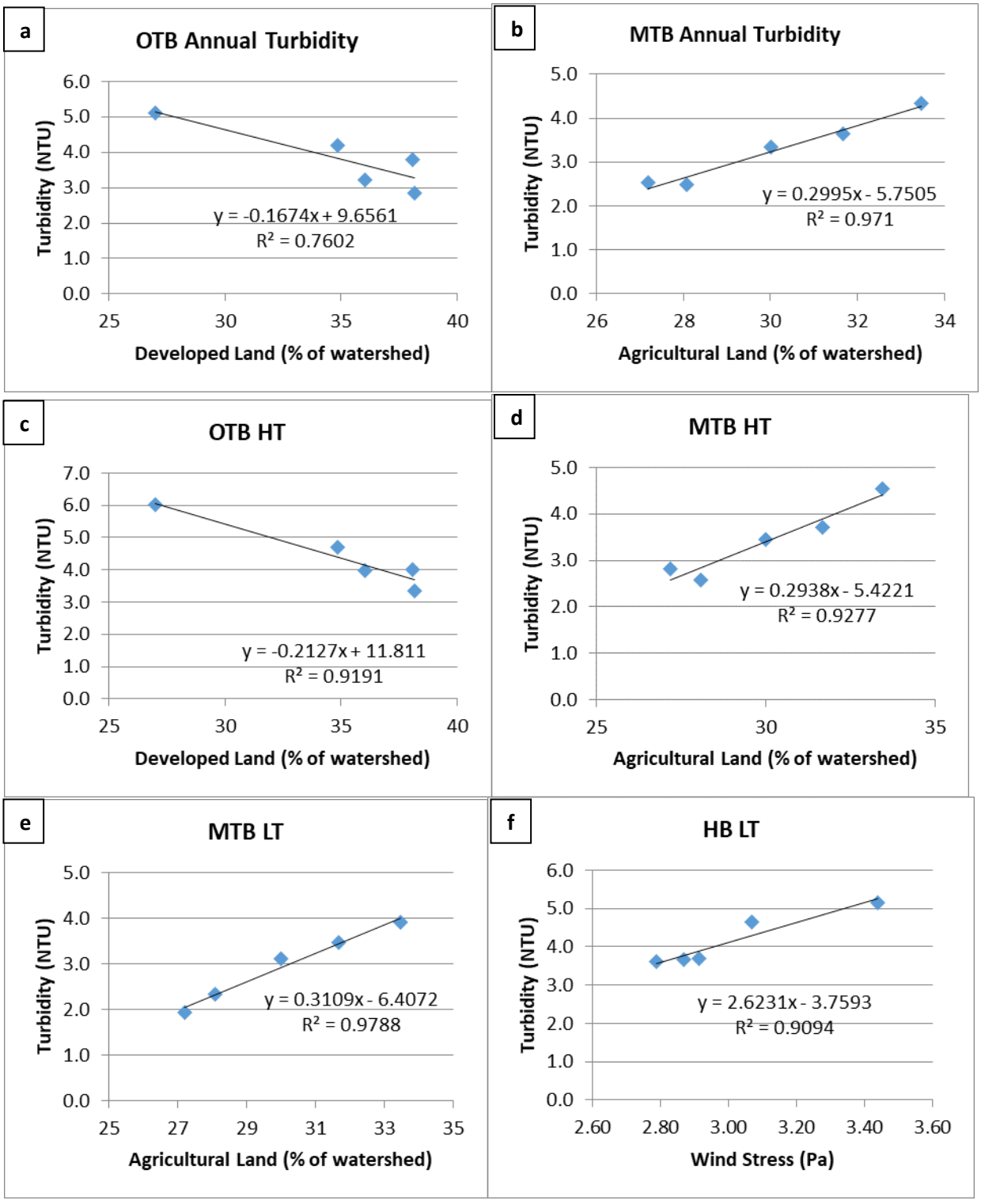

Figure 9. (a) Plot of annual average turbidity in Old Tampa Bay against developed land percent cover. (b) Plot of annual average turbidity in Middle Tampa Bay against agricultural land percent cover. (c) Plot of high-period turbidity in Old Tampa Bay against developed land percent cover. (d) Plot of high-period turbidity in Middle Tampa Bay against agricultural land percent cover. (e)

Plot of low-period turbidity in Middle Tampa Bay against agricultural land percent cover. (f) Plot of low-period turbidity in Hillsborough Bay against wind stress.

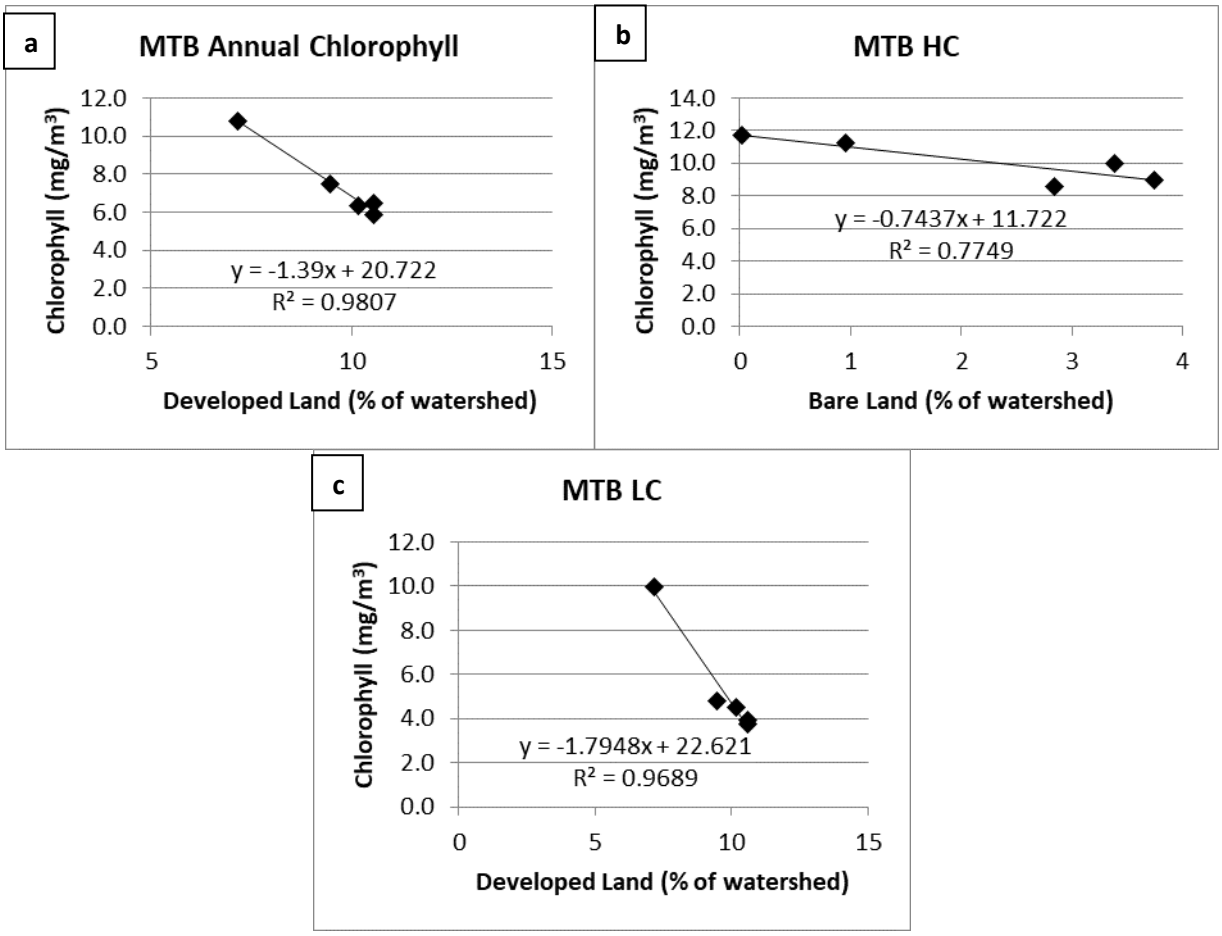

Figure 10. (a) Plot of annual chlorophyll concentration in Middle Tampa Bay against developed land percent cover. (b) Plot of high-period chlorophyll concentration in Middle Tampa Bay against bare land percent cover. (c) Plot of low-period chlorophyll concentration in Middle Tampa Bay against developed land percent cover.

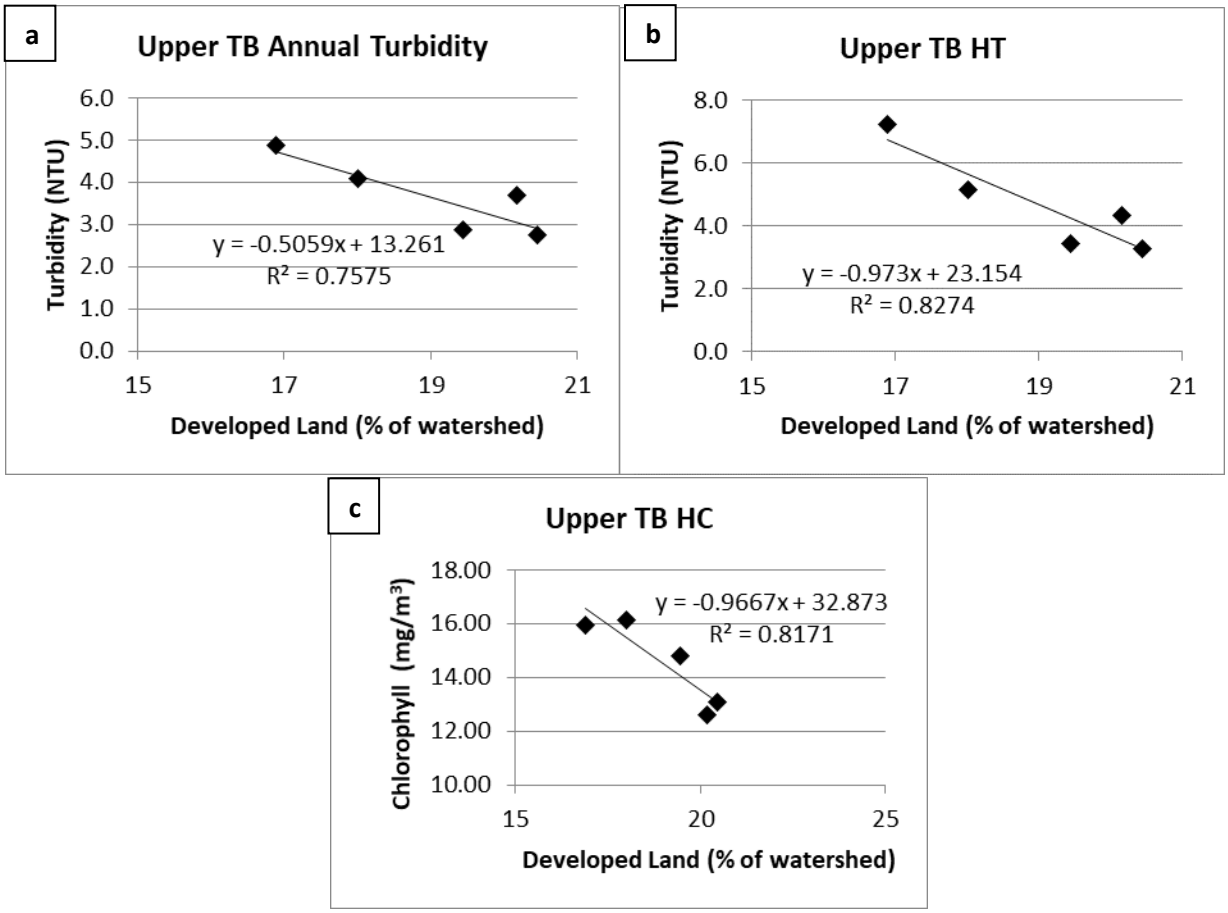

Figure 11. (a) Plot of annual turbidity in Upper TB against developed land percent cover. (b) Plot of high-period turbidity in Upper TB against developed land percent cover. (c) Plot of high-period chlorophyll concentration in Upper TB against developed land percent cover.

4. Discussion

Overall, monthly turbidity and chlorophyll in Tampa Bay show decreasing trends for all months from 1974 to 2011 ($p < 0.05$) except for August, September, and October, for which they show no significant trend. These three months correspond to the annual chlorophyll concentration peaks (Table 7), which follow summer precipitation maxima for the region (Figure 12). The lack of a significant trend in summer chlorophyll concentration over the study period suggests that variables or policies that have effected improved water quality for the rest of the year have had minimal impact on peak chlorophyll each year.

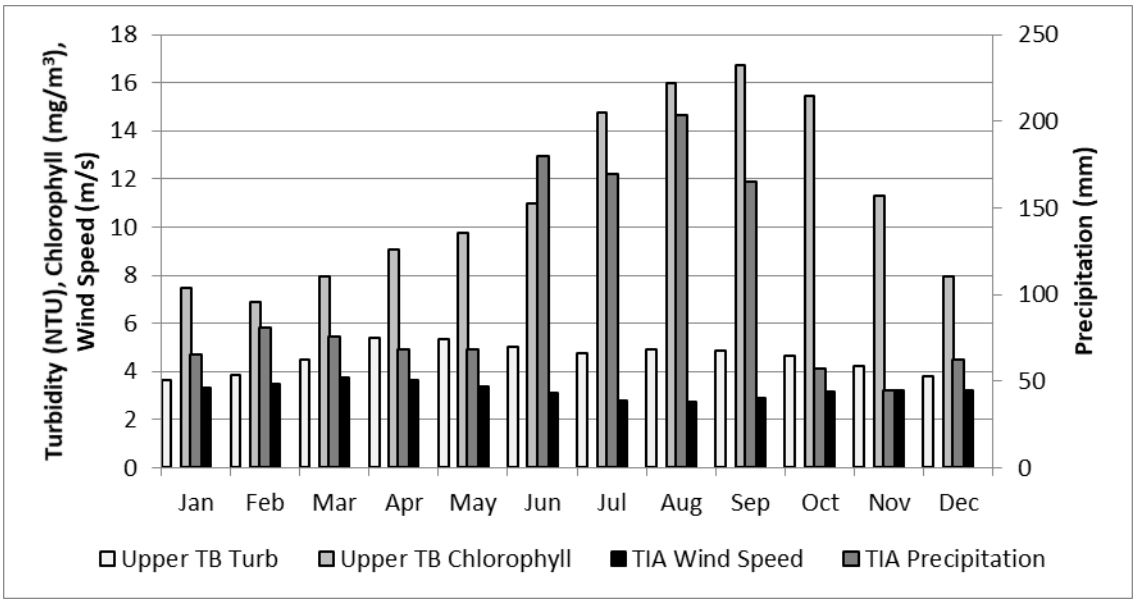

Figure 12. Monthly climatologies of bay-wide turbidity and chlorophyll, and Tampa International Airport precipitation and wind speed.

Increasing urbanization led to a three-fold increase in developed-land within the Tampa Bay watershed from 1991-2002. Developed land replaced other land cover classes. This has led to a significant increase in impervious land surface in the watershed and resulted in increased surface rainfall runoff in a watershed dominated by karst geology that otherwise would allow percolation (Xian and Crane 2005). Developed land percent cover showed a significant inverse relationship with both annual and high turbidity periods, as well as high chlorophyll concentration periods. As developed land area increased, turbidity and chlorophyll concentration decreased, especially during the low discharge season. This is consistent with previous research that concluded that increased impervious surfaces associated with developed land cover leads to sediment-free runoff and lower total suspended solid concentrations compared with agricultural watersheds (Estes et al. 2009; Miller et al. 2011; Moreno Madriñán et al. 2012).

Interannual variation in turbidity and chlorophyll in Tampa Bay were strongly affected by land cover changes, but they are also consistent with the long-term weakening of the wind. The changing turbidity and chlorophyll concentrations are otherwise inconsistent with the lack of a

long-term trend in precipitation. Normally, increased precipitation is expected to diminish water quality. In some areas of the bay, such as in MTB, low-turbidity was significantly related to agricultural land percent cover. Agriculture may modulate water quality through irrigation and changes in fertilizer application practices, and thus a connection with precipitation is not always obvious. Overall, turbidity was most clearly and significantly related to wind stress during the low-turbidity months in HB. Wind stress is also an important driver on very short time scales (i.e. hours; see Chen et al. 2010; Demers et al. 1987).

Annual, high, and low turbidity periods were significantly positively related to agricultural land percent cover in MTB. Annual and low chlorophyll concentration periods were also significantly related to agricultural land percent cover in HB and the entire upper bay, but these relationships were influenced by outliers. All outliers identified occurred in the 1977 period and appear to be due largely to land cover changes. The period between 1977 and 1996 experienced significant growth and thus may appear as outliers relative to change over the shorter gaps in subsequent land use assessments. In any case, turbidity and chlorophyll in Tampa Bay segments always decreased with decreased agricultural land; similar to what has been found elsewhere (Harding et al. 1999; Schlosser and Karr 2007; Sharpley et al. 1994).

Different segments of Tampa Bay have different, localized water quality drivers. OTB is separated by a peninsula from HB and lacks the large riverine influxes of HB and MTB. OTB is also traversed by three causeways and bridges that impact flushing time (Zhu et al. 2014). The only variable assessed here that had an influence on OTB annual or periodic turbidity or chlorophyll concentration was developed land percent cover.

HB is the smallest of the three bay segments, but it has the largest watershed and the highest average turbidity observed over the study period (Table 2). The only variable found to be

significantly related to turbidity here was wind stress. Higher wind stress led to increased turbidity during low-turbidity periods (Figure 9f). Winds likely led to resuspension of sediments (Demers et al. 1987; Madsen et al. 1993; Schoen et al. 2014; Sheng and Lick 1979). No variables were significantly related to chlorophyll concentration when outliers were removed. HB annual and high turbidity periods were not found to be significantly related to any variable, which may be a reflection of the minimal (0.62%) change in developed land in this watershed from the 1970s to 2010 relative to respective changes in OTB (9.03%) and MTB (3.39%).

The number of sampling observations of this study was limited to the epochs for which land cover maps were available. The analysis spans four decades. One variable, specifically developed land percent cover, was consistently the most strongly and significantly related to water quality (Figure 13). Our results indicate that increased developed land percent cover was strongly associated with continued decrease in turbidity and chlorophyll concentration over time. The effect may be due to both increased low-sediment runoff during precipitation events, as well as to reduced inputs of nutrients and sediments due to reduced agricultural land cover. Other studies that have assessed other water quality parameters (e.g. pollution, nitrate concentration, pH, sulfate concentration) found positive relationships with developed land cover (Burgos-Caraballo et al. 2014; Coulter et al. 2004; Ren et al. 2003). Clearly, "water quality" is a complex concept that must be defined appropriately for the research question being assessed. In any case, given the extensive efforts to improve point-source pollution to Tampa Bay, there is likely a dynamic combination of targeted pollution reduction and non-point source land cover change that has contributed to the general water quality improvement in the bay over the past 40 years. Constraining the contribution of each land cover type is difficult. Greening and Janicki (2014) point out that the substantial decrease of point source pollution to the bay has led to an increase

in the relative contribution of non-point source pollution. Therefore, identifying substantial non-point sources and evaluating their trends and impacts on Tampa Bay are essential for continued water quality improvement.

Tampa Bay has also undergone substantial changes as a result of concerted efforts to restore wetland and seagrass coverage to historic levels, and reduce point- and non-point-source pollution. Starting in 1992, almost 1,000 individual projects designed to restore seagrass and reduce pollution may have also contributed to improved long-term water-quality conditions (https://apdb.tbeptech.org/). Efforts like these should be considered by managers for their relevance to addressing water-quality issues, but were beyond the scope of this work. There was also a period of substantially elevated turbidity (Figure 3) spanning the late-1980's to early-1990's that did not coincide with land cover map years and was therefore not evaluated here, but is worth evaluating further in future research. No independent variables appeared to explain this prolonged deviation, which suggests that additional elements not investigated here (e.g. channel-dredging activities) may substantially influence water quality.

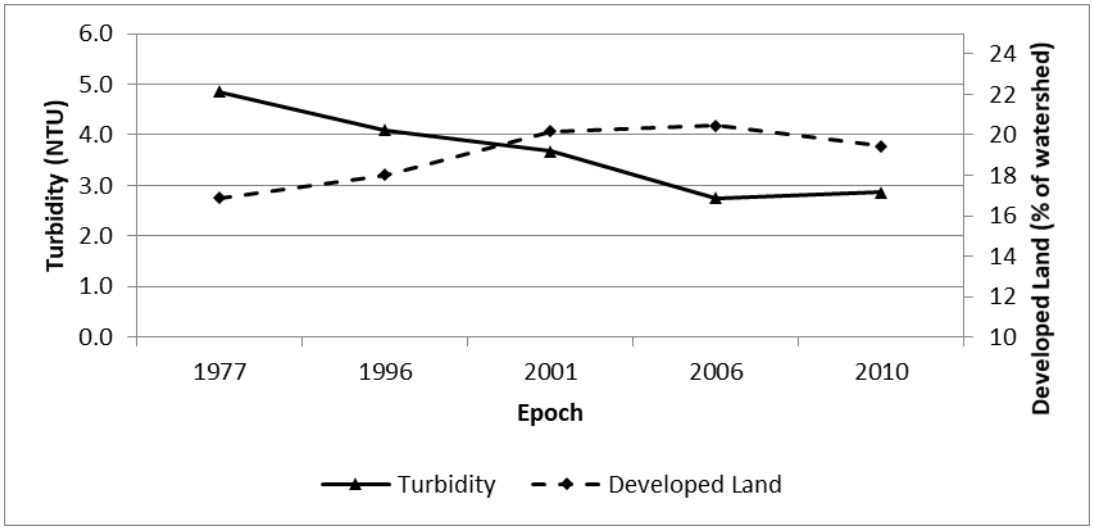

Figure 13. Plot of Tampa Bay-wide turbidity with developed land percent of watershed area for each epoch.

5. Conclusions

Land cover and water quality show a relationship in Tampa Bay from scales spanning local river mouths to the entire estuary. The long-term decrease in turbidity and chlorophyll concentration shows a strong negative correlation with developed land percent cover. There was no clear long-term change in precipitation between the 1970's and the 2000's, but the trend in water quality may have also been in part driven by a small decrease in average annual wind speed over the study period.

Changes in agricultural land cover were significantly related to turbidity only for MTB. Improving water quality in this bay segment seems to have been related to the decrease in agricultural land use in the adjacent watershed. Wind stress was significantly positively related to low-turbidity periods in HB (i.e. higher wind stress was correlated with higher turbidity during these generally low-turbidity months). There was no relationship between precipitation and turbidity or chlorophyll concentration over any spatial scale or period. The increase of impervious cover likely led to increased low-nutrient and low-sediment runoff, which helped improve water quality. Future research should focus on higher temporal resolution data and extreme events to identify drivers of short-term water quality events that may have greater impact on the bay's overall health as inter-annual water quality continues to improve.

Acknowledgements

Support for this study was provided by EPA Star grant RD835193010 to FMK. The study benefitted from discussions with L. Cross and H. Greening from the Tampa Bay National Estuary Program.

References

Akaike, H. Information theory and an extension of maximum likelihood principle. In B. N. Petrov and F. Csaki (eds), Second International Symposium on Information Theory, Akademiai Kiado, Budapest, 1973, pp. 267-281.

Al-Taani, A.A. (2014). Trend analysis in water quality of Al-Wehda Dam, north of Jordan. *Environmental Monitoring and Assessment,* doi:10.1007/s10661-014-3850-2.

Anderson, J.R., Hardy, E.E., Roach J.T., and Witmer R.E., 1976, A land use and land cover classification system for use with remote sensor data: U.S. Geological Survey Professional Paper 964, 28 p., http://pubs.er.usgs.gov/pubs/pp/pp964

Assessment report of wetland mapping improvement to NOAA's Coastal Change Analysis Program (C-CAP) land cover in western Washington State (2013). State of Washington Department of Ecology. Available in http://www.ecy.wa.gov/programs/sea/wetlands/pdf/C-CAPWetlandAssessmentReport.pdf. Accessed on 20 April 2014.

Bateni, F., Fakheran, S., and Soffianian, A. (2013). Assessment of land cover changes & water quality changes in the Zayandehroud River Basin between 1997-2008. *Environmental Monitoring and Assessment,* doi:10.1007/s10661-013-3348-3.

Breiman, L., & Culter, A. (2003). Manual on setting up, using, and understanding Random Forests v4.0. Technical Report.

Burgos-Caraballa, S., Cantrell, S.A., and Ramirez, A. (2014). Diversity of benthic biofilms along a land use gradient in tropical headwater streams, Puerto Rico. *Microbial Ecology,* doi: 10.1007/s00248-014-0401-x.

Chen, Z., Hu, C., Conmy, R.N., Muller-Karger, F., and Swarzenski, P. (2007a). Colored dissolved organic matter in Tampa Bay, Florida. *Marine Chemistry, 104*, 98-109.

Chen, Z., Hu, C., and Muller-Karger, F. (2007b). Monitoring turbidity in Tampa Bay using MODIS/Aqua 250-m imagery. *Remote Sensing of Environment, 109*, 207-220.

Chen, Z., Muller-Karger, F., and Hu, C. (2007c). Remote sensing of water clarity in Tampa Bay. *Remote Sensing of Environment, 109*, 249-259.

Chen, Z., Hu, C., Muller-Karger, F., and Luther, M.E. (2010). Short-term variability of suspended sediment and phytoplankton in Tampa Bay, Florida: Observations from a coastal oceanographic tower and ocean color satellites. *Estuarine, Coastal and Shelf Science, 89*, 62-72.

Coulter, C.B., Kolka, R.K. and Thompson, J.A. (2004). Water quality in agricultural, urban, and mixed land use watersheds. *Journal of the American Water Resources Association, 40*(6), 1593-1601.

Demers, S., Therriault, J., Bourget, E., and Bah, A. (1987). Resuspension in the shallow sublittoral zone of a macrotidal estuarine environment: Wind influence. *Limnology and Oceanography, 32*(2), 327-339.

Eleveld, M.A., van der Wal, D., and van Kessel, T. (2014). Estuarine suspended particulate matter concentrations from sun-synchronous satellite remote sensing: Tidal and meteorological effects and biases. *Remote Sensing of Environment, 143*, 204-215.

Estes, M.G. Jr., Al-Hamdan, M., Thom, R., Quattrochi, D., Woodruff, D., Judd, C., Ellis, J., Watson, B., Rodriguez, H., and Johnson, H. (2009). "Watershed and hydrodynamic modeling for evaluating the impact of land use change on submerged aquatic vegetation and seagrasses in Mobile Bay." OCEANS IEEE. Biloxi, MS. Oct. 26-29, 2009.

Gilhousen, D.B., 1987: A field evaluation of NDBC moored buoy winds. *Journal of Atmospheric and Oceanic Technology*,**4**, 94-104.

Greening, H., Janicki, A., Sherwood, E.T., Pribble, R., and Johansson, J.O.R. (2014). Ecosystem responses to long-term nutrient management in an urban estuary: Tampa Bay, Florida, USA. *Estuarine, Coastal and Shelf Science, 151*, A1-A16.

Harding, J. S., Young, R. G., Hayes, J. W., Shearer, K. A., & Stark, J. D. (1999). Changes in agricultural intensity and river health along a river continuum. *Freshwater Biology, 42*, 345-357.

Hu, C., Chen, Z., Clayton, T.D., Swarzenski, P., Brock, J.C., and Muller-Karger, F. (2004). Assessment of estuarine water-quality indicators using MODIS medium-resolution bands: Initial results from Tampa Bay, FL. *Remote Sensing of Environment, 93*, 423-441.

Janicki, A., Pribble, R., Janicki, S., and Winowitch, M. (2001). An analysis of long-term trends in Tampa Bay water quality. Technical Report. Available at: http://www.tbeptech.org/TBEP_TECH_PUBS/2001/TBEP_04_01WQTrends.pdf. Accessed 2 Aug 2014.

Jordan, Y.C., Ghulam, A., and Herrmann, R.B. (2012). Floodplain ecosystem response to climate variability and land-cover and land-use change in Lower Missouri River basin. *Landscape Ecology, 27*, 843-857.

Le, C., Hu, C., English, D., Cannizzaro, J., and Kovach, C. (2013). Climate-driven chlorophyll-a changes in a turbid estuary: Observations from satellites and implications for management. *Remote Sensing of Environment, 130*, 11-24.

Madsen, O. S., Wright, L. D., Boon, J. D., & Chisholm, T. A. (1993). Wind stress, bed roughness and sediment resuspension on the inner shelf during an extreme storm event. *Continental Shelf Research, 13*(11), 1303-1324.

Mei, K., Liao, L., Zhu, Y., Lu, P., Wang, Z., Dahlgren, R.A., and Zhang, M. (2014). Evaluation of spatial-temporal variations and trends in surface water quality across a rural-suburban-urban interface. *Environmental Science and Pollution Research,* doi:10.1007/s11356-014-2716-z.

Miller, R.L., and McKee, B.A. (2004). Using MODIS Terra 250 m imagery to map concentrations of total suspended matter in coastal waters. *Remote Sensing of Environment, 93,* 259-266.

Miller, R.L., Liu, C., B., C.J., and Wu, A. (2011). A multi-sensor approach to examining the distribution of total suspended matter (TSM) in the Albemarle-Pamlico estuarine system, NC, USA. *Remote Sensing, 3,* 962-974.

Moreno Madriñán, M.J., Al-Hamdan, M.Z., Rickman, D.L., and Ye, J. (2012). Relationship between watershed land-cover/land-use change and water turbidity status of Tampa Bay major tributaries, Florida, USA. *Water, Air & Soil Pollution, 223,* 2093-2109.

Nelson, E.J. and Booth, D.B. (2002). Sediment sources in an urbanizing, mixed land-use watershed. *Journal of Hydrology, 264,* 51-68.

Price, Curtis V., Naomi Nakagaki, Kerie J. Hitt, and Rick M. Clawges. 2007. Enhanced Historical Land-Use and Land-Cover Data Sets of the U.S. Geological Survey. U.S. Department of the Interior. U.S. Geological Survey. Data Series 240. http://pubs.usgs.gov/ds/2006/240/

Rains, M., Landry, S., Seidel, V., Crisman, T. (2012). Prioritizing habitat restoration goals in the Tampa Bay watershed. Technical report to the Tampa Bay Estuary Program # 10-12. Available at: http://www.tbeptech.org/TBEP_TECH_PUBS/2012/TBEP_10_12_USF_Prioritizing_Habitat_Restoration_Goals_2012_04.pdf. Accessed 26 Apr 2014.

Ren, W., Zhong, Y., Meligrana, J., Anderson, B., Watt, W.E., Chen, J., and Leung, H. (2003). Urbanization, land use, and water quality in Shanghai 1947-1996. *Environment International, 29*, 649-659.

Schlosser, I. J., & Karr, J. R. (2007). Water quality in agricultural watersheds: impact of riparian vegetation during base flow. *Journal of the American Water Resources Association, 17*(2), 233-240.

Schmidt, N., Luther, M.E., and Johns, R. (2004). Climate variability and estuarine water resources: A case study from Tampa Bay, Florida. *Coastal Management, 32,* 101-116.

Schoen, J., Stretch, D., Tirok, K., Wind-driven circulation patterns in a shallow estuarine lake: St Lucia, South Africa, *Estuarine, Coastal and Shelf Science* (2014), doi:10.1016/j.ecss.2014.05.007.

Schoonard, C.M., Collins, J., Paxton, C., and Meindl, C. (2014). Explaining the spatial variability of summer rainfall in Pinellas County, Florida using ArcGIS. *Physical Geography*. Available at http://dx.doi.org/10.1080/02723646.2014.895893.

Sharpley, A. N, Chapra, S. C., Wedelpohl, R., & Sims, J. T. (1994). Managing agricultural phosphorous for protection of surface waters: issues and options. *Journal of Environmental Quality, 23,* 437-451.

Sheng, Y. P., and W. Lick (1979), The transport and resuspension of sediments in a shallow lake. *J. Geophys. Res.*, *84*(C4), 1809–1826, doi:10.1029/JC084iC04p01809.

US Census (2007). US Census Bureau, annual estimates of the population of metropolitan and micropolitan statistical areas: April 1, 1990 to July 1, 2003. (5 April 2007). Available at http://www.census.gov/prod/2005pubs/p25-1134.pdf. Accessed 26 Sept 2014.

Wickham, J.D., Riiters, K.H., Wade, T.G., and Jones, K.B. (2005). Evaluating the relative roles of ecological regions and land-cover composition for guiding establishment of nutrient criteria. *Landscape Ecology, 20*, 791-798.

Wollenberg, A.L. van den (1977). Redundancy analysis: An alternative for canonical correlation analysis. *Psychometrika*, *42*(2), 207-219.

Wu, J. (1969). Froude number scaling of wind-stress coefficients. *Journal of Atmospheric Sciences, 26*, 408-413.

Xian, G., & Crane, M. (2005). Assessments of urban growth in the Tampa Bay watershed using remote sensing data. *Remote Sensing of Environment, 97*, 203-215.

Yamaoka, K., Nakagawa, T., and Uno, T. (1978). Application of Akaike's Information Criteria (AIC) in the evaluation of linear pharmacokinetic equations. *Journal of Pharmacokinetics and Biopharmaceutics, 6*(2), 165-175.

Yin, Z., Walcott, S., Kaplan, B., Cao, J., Lin, W., Chen, M., Liu, D., and Ning, Y. (2005). An analysis of the relationship between spatial patterns of water quality and urban development in Shanghai, China. *Computers, Environment and Urban Systems, 29*, 197-221.

Zhu, J., Weisberg, R.H., Zheng, L., and Han, S. (2014). On the flushing of Tampa Bay. *Estuaries and Coasts,* doi:10.1007/s12237-014-9793-6.

Enabling efficient, large-scale high-spatial resolution wetland mapping using satellites

Matthew J. McCarthy[ab*], Kara R. Radabaugh[b], Ryan P. Moyer[b], Frank E. Muller-Karger[a]

[a]Institute for Marine Remote Sensing, College of Marine Science, University of South Florida 140 7th Avenue South, St. Petersburg, FL 33701, USA
[b]Florida Fish and Wildlife Conservation Commission, Fish and Wildlife Research Institute, 100 8th Avenue SE, St. Petersburg, FL, 33701, USA

*****Author to whom correspondence should be addressed; E-Mail: mjm8@mail.usf.edu
Tel.: +1-727-553-1186; Fax: +1-727-553-1103.

Abstract

Global coastal and freshwater wetlands provide ecosystem services valued at over $200,000 USD per hectare per year. Despite their value, wetlands continue to be lost at alarming rates worldwide, with as much as 71% of global wetland extent being converted to other land-cover types since 1900. Targeted conservation and restoration efforts, however, have proven successful, particularly in Europe and North America. Such efforts require accurate protocols to identify, assess, and map wetlands repeatedly to enable detection of change. High-resolution (i.e. 2-meter pixel) satellite imagery has proven effective to map wetlands at higher accuracies than historical 30-meter or coarser satellite data. We describe a method to process and classify high volumes of multispectral high-resolution satellite data to update land cover and land use maps. We show the results of a study conducted with 130 2-meter resolution WorldView-2 satellite images to map forested wetland, upland, water, bare land, and developed lands in a 6,500 km^2 watershed. The processing of the land cover map was completed in under 24 hours and was more accurate at identifying forested wetland (78%) and upland (64%) than three previous, widely used maps of the same area (45–65%, and 49–53%, respectively). This method offers high potential for monitoring change in coastal areas and adjacent watersheds over large geographic scales.

Keywords: land cover classification, wetlands, mangroves, Tampa Bay, WorldView-2

1. Introduction

Wetlands provide a host of essential ecosystem services including nutrient removal, carbon sequestration, shoreline stabilization, flood prevention, and provision of habitat for numerous species of protected or commercially and recreationally important fish, birds, and invertebrates (Barbier, 2015; Barbier et al., 2011; Lewis et al., 1985; Martin et al., 2016; Mcleod et al., 2011). De Groot et al. (2012) estimated the value of tidal and freshwater wetlands at $193,845 and $25,682 USD per hectare per year, respectively – second only to coral reefs in terms of global ecosystem value. Despite increasing recognition of the importance of their

ecosystem services, wetlands continue to be lost at unprecedented rates worldwide. Globally, tidal wetland cover is expected to decline at a rate of 0.7 – 3.0% per year, with freshwater wetlands disappearing at about 1% per year (Davidson, 2014; Mcleod et al., 2011). Local losses within smaller geographic areas, including individual watersheds and estuaries may be significantly higher than the global average (Davidson 2014). Prior to the 1850s, Florida is estimated to have contained 8.2 million hectares of wetlands. Today, roughly half of these swamps and marshes have been lost to draining, flooding, and human development (Dahl 2005). Coastal wetlands in Florida, which include mangrove, salt marsh, and salt barren habitats, have suffered extensive losses to human development in the early- and mid-1900's as a result of concentrated human development along the coast (Lewis et al., 1985; Sherwood and Greening, 2014).

Management of human activities to conserve and restore wetland resources and services requires accurate and up-to-date mapping of these critical ecosystems. Yet wetland cover has been historically difficult to assess. These areas are typically difficult to access, and mapping using field efforts is time-intensive, even for relatively small areas. Remote sensing has served as a valuable tool to evaluate land cover and wetland habitat extent since the 1960's (see references in Tiner et al., 2015). Common remote sensing tools to map wetlands include aerial photography and videography, hyperspectral sensors, radar and LiDAR, and high- and medium-resolution multispectral and radar satellite images (Klemas, 2009; Kuenzer et al., 2011; McCarthy et al., 2015). Aerial photographs are useful for location-specific projects as they provide excellent spatial resolution that can be used to create detailed maps at a relatively low cost (Tiner, 1997). However, the cost of aerial imagery increases with spatial and repeat coverage.

Satellite data offers a cost-effective option for large-scale projects with spatially continuous coverage (Green et al., 1998; Keunzer et al., 2011; Tiner et al., 2015). Additionally, digital data from satellite imagery enable efficient and rapid classifications through automated methods that have been shown to improve accuracy over aerial photo interpretations (Tiner et al., 2015). Medium-resolution imagery from the series of Landsat and SPOT satellite sensors have been used since the 1980's for the classification of land cover types and change detection over large scales, at a spatial resolution of 10–30 m pixels. Higher resolution satellite imagery (i.e., meter-scale pixels) enables study of details such as plant species, damage following severe weather, or fine-scale habitat mapping (Klemas, 2009; Keunzer et al., 2011; McCarthy et al., 2015). The accuracy of habitat maps depends both upon the spatial and spectral resolutions of the data, the preprocessing methods applied, and the accuracy of the algorithm to discern the spectral signature of the target habitats (Green et al., 1998; Hestir et al., 2015; Klemas, 2014; Klemas, 2013a, b; Turpie et al., 2015; Turpie, 2013).

Mapping mangroves and other forested wetlands is complicated by the variety of substrates, species, and adjacent habitats associated with these complex ecosystems. Many mangroves are intermixed with other salt marsh or upland vegetation that grows in pockets of higher elevation. For example, in Florida, mangrove landscapes are also often interrupted by mosquito ditching and adjacent spoil piles, which are then vegetated by invasive non-wetland species such as Brazilian pepper (*Schinus terebinthifolius*) (Smith et al., 2007). Mangroves in the oligohaline reaches of estuaries are often intermixed with transitional upland and freshwater vegetation. The spectral signature of mangroves also varies with species, physiology and health, age, and season (Blasco et al., 1998; Kuenzer et al., 2011; Wang et al., 2008). Despite this variability among and within wetland habitats, similarities in spectral characteristics enable

differentiation between wetland and upland vegetation through the use of digital classification techniques, including unsupervised and supervised statistical methods, spectral indices, object-based analysis, and more (Carle et al., 2014; Chakravortty, 2013; Gianinetto et al., 2014; Giri et al., 2011; Jia et al., 2014; Kamal and Phinn, 2011; Wang et al., 2004). Ground truthing is used to assess the accuracy of habitat maps, but many mangrove maps lack these assessments due to the difficulty of accessing the wetland (Green et al., 1998).

Recent studies have capitalized on the enhanced spatial resolution of new satellite sensors. These data can provide greater accuracy and precision of land cover maps by reducing spectral mixing caused when coarse-resolution imagery captures multiple habitats in a single pixel (Chen et al. 2015; McCarthy et al., 2015). MacKay et al. (2009) found that high spatial-resolution imagery is more useful for wetland mapping than medium spatial-resolution imagery, even if the latter also contains greater spectral resolution. Turpie et al. (2015) also finds that the ability to evaluate wetland cover decreases rapidly as spatial resolution decreases (i.e. becomes coarser).

The primary goal of the work presented here was to improve the accuracy and precision of coastal wetland cover maps, by automating the processing and classification of 2-meter resolution satellite imagery collected with the WorldView-2 sensor from DigitalGlobe^{TM}. We describe an approach to automate the preprocessing, classification, and post-classification of large numbers of images of the Tampa Bay watershed in Florida. The strategy addresses large data volumes as well as improved land cover maps.

3. Materials and Methods

3.1 Study area

The study focused on the Tampa Bay watershed, located in a subtropical climate zone on the west-central coast of the State of Florida (Figure 1). The watershed spans over 6,500 km^2 and contains the second-largest metropolitan area in Florida, including the cities of Tampa, St. Petersburg, and Clearwater. Vegetation in the watershed includes mangroves, salt marshes, freshwater swamps, palm hammocks, hardwoods, and grass lands. Mangroves comprise approximately 74% of coastal wetland habitats in Tampa Bay, while salt marshes and salt barrens make up about 24% and 2%, respectively (Sherwood and Greening, 2014). Mangrove forests include three prevalent mangrove species (*Rhizophora mangle, Avicennia germinans,* and *Laguncularia racemosa*), and the mangrove associate buttonwood (*Conocarpus erectus*). The majority (70%) of freshwater wetlands within the Tampa Bay watershed are dominated by woody vegetation (SWFWMD, 2011). Common palustrine swamp species include cypress trees (*Taxodium* spp.), tupelo trees (*Nyssa* spp.), and an assortment of bottomland hardwood trees (FDOT 1999). Upland habitats contain live oaks (*Quercus* spp.), cabbage palms (*Sabal palmetto*), saw palmetto (*Serenoa repens*), and slash pine (*Pinus elliotti*).

Figure 1. Tampa Bay watershed study area. The watershed boundary, as defined by the U.S. Environmental Protection Agency's National Estuary Program, is outlined in red.

3.2 Satellite imagery

We used 130 WorldView-2 satellite images acquired in 2010 (33), 2011 (20), 2012 (21), 2013 (16), and 2014 (40) to cover the study area. The WorldView-2 satellite sensor, operated by DigitalGlobe™, was launched in 2009. It collects data in eight multispectral bands of the visible and near-infrared (NIR; Table 1), at a nominal resolution of two meters, from an altitude of 770 km in a sun-synchronous orbit, and a revisit time of ~1.1 days. It is capable of covering about 1 million km^2 of land area per day (DigitalGlobe™, 2009). The four new spectral bands (coastal,

yellow, red edge, and near-infrared II; see Table 1) improve overall accuracy of land cover classifications over similar high-resolution satellite sensors with fewer spectral bands (Carle et al., 2014; McCarthy and Halls, 2014; Puetz et al., 2009). Images were obtained through a partnership with the Polar Geospatial Center (PGC, University of Minnesota), in Level-1B National Imagery Transmission Format (NITF) along with corresponding metadata.

Table 1. WorldView-2 sensor specifications (NIR stands for Near-Infrared).

Band Name	Band Number	Center Wavelength (nm)	Band Coverage (nm)	Effective Bandwidth (nm)
Coastal	B1	427	396–458	47.3
Blue	B2	478	442–515	54.3
Green	B3	546	506–586	63.0
Yellow	B4	608	584–632	37.4
Red	B5	659	624–694	57.4
Red Edge	B6	724	699–749	39.3
NIR I	B7	833	765–901	98.9
NIR II	B8	949	856–1043	99.6

3.3 Preprocessing

Preprocessing of the imagery was done with Python code (pgc_ortho.py, available from the PGC, University of Minnesota) to convert the Level-1B NITF images to Level 2A GeoTIFFs and mapping the image to a pre-defined map projection (European Petroleum Survey Group/EPSG code 32617 for UTM zone 17 North and WGS84 datum). The Python code allows georectification using ground-control points or rational polynomial coefficients that may accompany a raw image, but neither option produced satisfactory results and were not used. The standard geolocation accuracy of 3–5 meters for raw WorldView-2 imagery was acceptable for the scope of this work. The optional ortho-rectification using a digital elevation model (DEM)

was not used as the study area comprised a coastal-plain watershed with minimal topographic change. This avoided unnecessary resampling of the digital images.

3.4 Radiometric adjustment and image classification

Further preparation and thematic classification of the WorldView-2 GeoTIFFs was completed using Matlab^{TM} software. This included: radiometric calibration, atmospheric correction, remote sensing reflectance (Rrs) computation, classification, smoothing, and output of a classified GeoTIFF and its complementary Rrs GeoTIFF.

3.4.1 Radiometric calibration

WorldView-2 GeoTIFFs were converted to top-of-atmosphere spectral radiance according to Updike and Comp (2010; Eq. 1) using metadata supplied with each image.

$$\text{(Eq. 1):}\quad L_i = K_i * q_i/\lambda_i$$

Here, L_i is the top-of-atmosphere spectral radiance per band (W m^{-2} sr^{-1} μm^{-1}), K_i is the absolute radiometric calibration factor (W m^{-2} sr^{-1} $count^{-1}$) for a given band, q_i are radiometrically corrected data (counts), and λ_i is the effective bandwidth (μm), defined as the width of the radiation at half of its maximum throughput, for a given band (Table 1). Values for K and λ were extracted from the metadata file accompanying each image.

3.4.2 Atmospheric correction

The attenuation of radiation due to atmospheric scattering must be accounted for to estimate the radiance reflected by the Earth's surface, which is used for the spectral classification. We accounted for scattering due to atmospheric gas molecules (Rayleigh scattering) using

methods outlined by Dash et al. (2012) and Chandrasekhar (1960). This considered sun-sensor geometries (i.e. solar azimuth, sensor azimuth, solar elevation, and sensor elevation angles), band-averaged solar spectral irradiance, and Earth-Sun distance. The latter is derived from scene-specific acquisition dates using equations from Updike and Comp (2010). For Rayleigh optical thickness estimates, we assumed standard atmospheric pressure for all images. The Rayleigh scattering phase function equation (Eq. 2) of Chandrasekhar (1960) was substituted for the more simplified equation used in Dash et al. (2012). The former better accounts for molecular anisotropy affecting the angular distribution of Rayleigh-scattered light (Bucholtz, 1995).

(Eq. 2): $P_{ray}(\Theta)_i = (3/4*(1+2\gamma_i)*[(1+3\gamma_i) + (1-\gamma_i)*\cos^2(\Theta)]$

where P_{ray} represents the Rayleigh phase function per band, γ_i (from Table 1 of Bucholtz, 1995) considers the band-specific depolarization factor, and Θ is the scattering angle.

3.4.3 Remote Sensing Reflectance (Rrs)

Scene-specific, Rayleigh-scattered radiances were subtracted from radiometrically calibrated pixels using Eq. (3). This yields surface-reflected radiance. Dividing by solar irradiance (E_i) in that band gives remote sensing reflectance (Rrs). Solar irradiance was adjusted for Earth-Sun distance (ESd), which varies with time of year, and for atmospheric transmittance in the solar path (TZ) and view path (TV). TZ is estimated based on the solar zenith angle, and TV is estimated from the satellite view angle (Eq. 3 and Eq. 4; Chavez, 1996; Wu et al., 2005). Rrs (sr^{-1}) was calculated according to (Eq. 5; Schowengerdt, 1997; Updike and Comp, 2010).

(Eq. 3): $TZ = \cos(\Theta_{sun})$ where Θ_{sun} is the solar zenith angle.

(Eq. 4): $TV = \cos(\Theta_{sat})$ where Θ_{sat} is the satellite view angle.

(Eq. 5): $Rrs_i = (\pi*(L_i - L_{Rayi})*ESd^2)/(E_i*TZ*TV)$

3.4 Decision Tree classification

The image classification strategy used a Decision Tree. This is a multi-stage classifier tool that uses a series of binary decisions to assign a thematic class to each image pixel. This approach identifies specific classes based on spectral signatures of the target land-cover type.

The Decision Tree was built to identify five thematic classes: forested wetland (including mangroves and freshwater swamps), upland, marsh, bare and developed land, and water. The primary goal was to distinguish between wetland and upland vegetation. The forested wetland class was merged with the marsh class to create a single “wetland” class. Initial spectral analyses were conducted using WorldView-2 images covering the Charlotte Harbor watershed, independent from this study area but adjacent to it. The classification was trained using the Land Use/Land Cover map from 2009. The data were obtained from the Water Atlas portal for the Charlotte Harbor National Estuary Program (http://maps.wateratlas.usf.edu/chnep/).

The first node of the Decision Tree identified "No Data" pixels and excluded them from the remainder of the classification. The second node used a Normalized Difference Vegetation Index (NDVI) to isolate pixels containing vegetation. Specifically, the WorldView Improved Vegetative Index (WV-VI) was used (Eq. 6; Wolf, 2010). Some pixels containing vegetation also contained shadows cast by canopy cover and other structures. These pixels were identified with an *ad hoc* shadow filter (Eq. 7). These pixels were assigned a value of zero (0), but could be reclassified based on surrounding classified pixels using a post-classification moving filter.

$$(B8 - B5)/(B8 + B5) > 0.3 \quad \text{(Eq. 6)}$$

$$(B7 - B2)/(B7 + B2) < 0.2 \text{ AND } (B7 - B8)/(B7 + B8) > 0.01 \quad \text{(Eq. 7)}$$

Wetlands were distinguished from uplands using a robust yet simple approach. Numerous algorithms that have been successfully used and published in wetland-mapping literature, including NDVI variants and other band ratios (see Table 2 of Heenkenda et al., 2016 for a summary), were tested on 20 WorldView-2 images, ranging from coastal to inland scenes and collected throughout the year. However, no wetland index consistently distinguished between wetland and upland vegetation across the scenes based on visual analysis relative to existing wetland maps. This could be due to discrepancies in imagery processing between studies, or due to the combination of diverse ecosystems imaged under varying sun and sensor geometries throughout the year. This may be a novel issue inherent with high-resolution images that had not been reported because these images just recently started being processed in massive batches. We could find no peer-reviewed publications that used more than six such images for land-cover mapping, and none that spanned coastal to inland habitats.

A consistent pattern within and across scenes was that wetland vegetation pixels showed substantially lower reflectance in bands 3, 4 and 5 than upland vegetation pixels. Kamal et al. (2015) show this pattern in comparing spectral reflectance of mangroves and upland vegetation types from a WorldView-2 image, and note that bands 3 and 5 yield optimal spectral separation between these vegetation types. Kuenzer et al. (2011) note that spectral discrepancies are related to the internal leaf structure of mangroves, as well as their biophysical and chemical properties (e.g. water, cellulose, lignin and protein content, and leaf pigments chlorophyll a and b and carotenoids).

This pattern was exploited early in the Decision Tree process. Pixels containing vegetation were identified using Eq. 6 with a threshold of 0.6 sr^{-1}, which captured scrub and forested vegetation to the exclusion of grass. Shadows were again excluded using Eq. 7. Rrs

values in bands 3–5 for all shadowless vegetated pixels were summed, and an average "vegetation value" was computed for the image. Grassland pixels were excluded because they tended to have very high Rrs values in bands 3–5, thereby raising the average vegetation value for the scene and potentially causing overestimates of wetland by incorporating more forested upland in the wetland classification. This approach avoided the need to identify a threshold common to all scenes. Rather, a scene-specific metric was thus developed to distinguish between wetland and upland vegetation.

Using this average vegetation value in the Decision Tree, upland vegetation was identified if the sum of Rrs values in bands 3–5 for a given pixel was greater than the average vegetation value. The pixel was then assigned a classification value of four (4), representing upland. Remaining vegetation pixels tended to contain either forested wetland, marsh, or agricultural crops. Crops tended to exhibit relatively high Rrs values in band 2, and were identified as upland using Eq. 8.

$$(\text{Eq. 8}): (B2 - B5)/(B2 + B5) > 0.4$$

Marsh was identified in the remaining pixels if the Rrs value in band 7 was greater than the sum of the values in band 1 and band 5 (Eq. 9), and assigned a value of five (5). This *ad hoc* pattern was adapted from Equation 2 of Kamal et al. (2015), and also derived from investigation of multiple scenes in Charlotte Harbor.

$$(\text{Eq. 9}): B7 > (B5 + B1)$$

All remaining vegetated pixels were assigned a value of six (6), representing forested wetland.

Water was identified using a version of the Normalized Difference Water Index (NDWI) combined with a requirement that band 8 have a value less than 0.1 sr^{-1} to exclude dark, bare land

(Eq. 10). Water pixels were assigned a classification value of three (3). All remaining pixels were identified as bare and developed, and assigned a value of two (2).

$$\text{Eq. (10): } (B8 - B2)/(B8 + B2) < 0 \text{ AND } B8 < 0.1$$

3.4.1 Smoothing of the land cover product

Land-cover classifications often use a moving-window filter to smooth the raw map and remove erroneous pixels (Figure 2; Kim et al., 2014; Lv et al., 2016; McCarthy et al., 2015). Our method applies an 11x11-pixel moving-window filter on the initial classification. The filter calculates the mode of the pixels in a roughly 22x22 meter area, and assigns to the central pixel the most common value found in the 11x11-pixel box. Excluded from the mode calculation are any pixels containing a value of zero (shadows). This yields a more homogenous product and allows shadowed vegetation pixels to be reclassified based on the most common pixels adjacent to them for a more accurate identification of otherwise muted spectral signatures. Figure 2 shows an example of the smoothed thematic classification product.

If a pixel in the center of the box was initially classified as wetland (value = 6), all of the pixels in this box that were classified as wetland, upland (value = 4), or bare and developed (value = 2) were counted, and the value assigned to the central pixel was wetland only if at least two-thirds of the pixels in the window were classified as wetland. Otherwise, the central pixel was reclassified as upland. This two-thirds requirement was based on our observation that wetlands tend to be found as clumped stands, as opposed to isolated, individual trees.

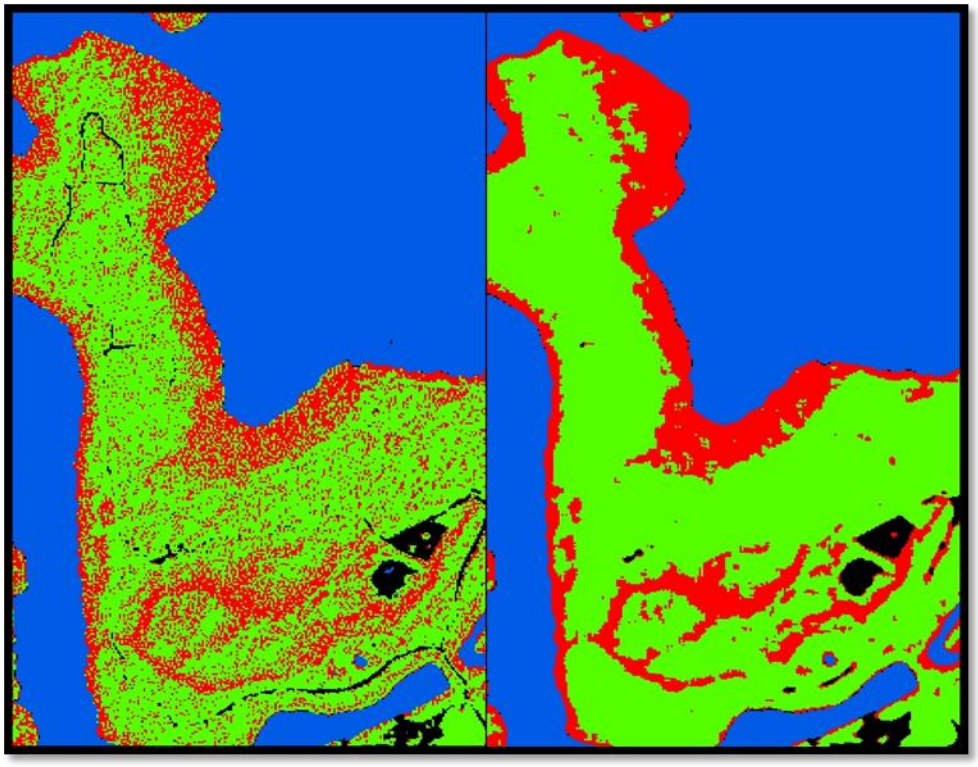

Figure 2. A moving-window filter applied to an initial classified map (left) produces a "smoother" map (right) by using adjacent-pixel information to remove pixilation.

3.5 Supercomputing batch processing

Both the Python and Matlab functions were run on the University of South Florida (USF) supercomputing cluster to increase processing speed. This supercomputer is comprised of over 4,000 processors with 2.5 terabytes of memory. While the Python and Matlab codes can each be run on a standard computer, using the cluster allowed us to process up to 20 images at a time (the actual number processed at any one time was limited by assignment by the supercomputer management center).

Traditional methods to preprocess and classify these images, including radiometric calibration, atmospheric correction and unsupervised classification, took us on average about one full day per image using ENVI software tools on a 64-bit Windows-platform computer.

Processing times per image for the Python and Matlab codes run on the same computer were approximately 10 minutes, and 20 minutes, respectively. Using the filter (recommended) increased the Matlab processing time to about 3 hours. The supercomputer allowed us to classify 20 WorldView-2 images at a time, cutting the total per-image processing down to approximately 17 seconds using the Python code and 1 minute using the Matlab code. The subsequent spatial filter could be completed in under 10 minutes per image using the Matlab code on the supercomputer. In total, the 130 images were processed through both Python and Matlab code, including filtration, in under 20 hours.

3.6 Field validation

Ground reference points (GRPs) were collected throughout the Tampa Bay watershed during surveys conducted from 2014 to 2016. This included surveys reported in McCarthy et al. (2015) using a Trimble GeoExplorer 6000 series GPS unit (horizontal accuracy 2.5 cm). Most of the points were collected during field work for unrelated projects using a Garmin GPS MAP 78SC. Points were primarily collected in vegetated habitats and excluded bare and developed land cover and water. A total of 226 points were collected, including 150 forested wetland and 76 upland (Figure 3).

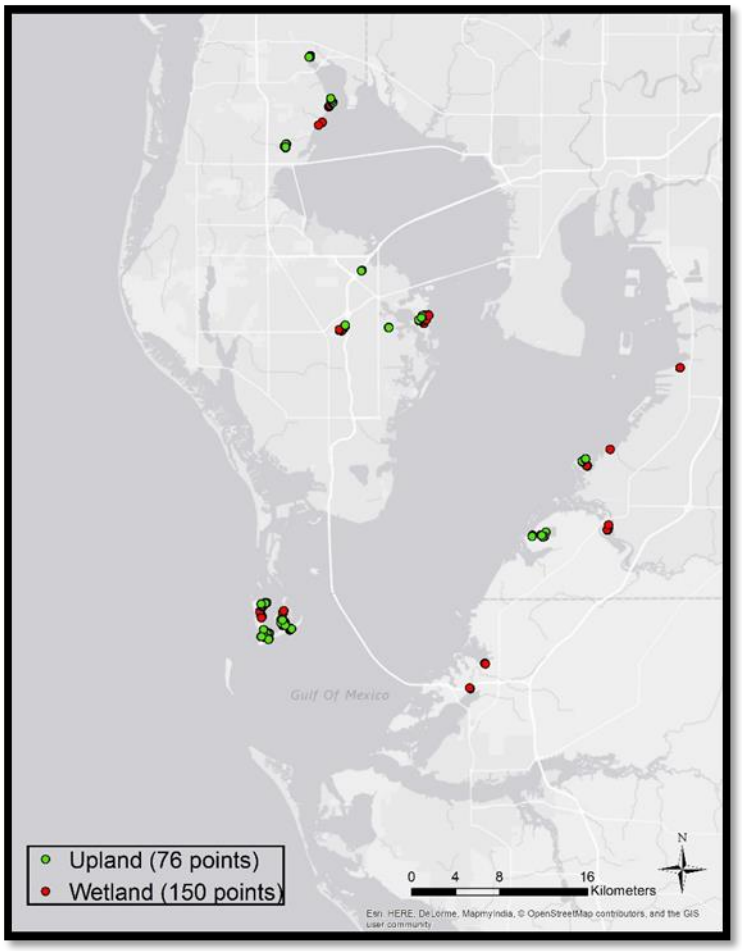

Figure 3. Ground-reference points collected to validate the classified maps.

3.7 Post-processing

All classified GeoTIFF images were evaluated in ArcGIS 10.1 for quality control. Evaluation revealed substantial cloud cover interference in 9 images, which were then discarded from further use. The remaining 121 mapped images were mosaicked using the Mosaic to New Raster tool. To counterbalance the conservative 2/3 wetland-filter requirement (see section 3.4.1), the ArcGIS 10.1 Mosaic tool's Mosaic Operator function was set to "Maximum". When two or more images overlapped, the mosaic would preferentially assign the highest value of any

overlapping pixels to the output class. As wetlands were assigned the highest value (6) in the Decision Tree, wetlands were preferentially assigned to the output.

The mosaicked map was then clipped using the ArcGIS Extract by Mask tool to match the extent of the watershed. This facilitates comparison with other maps of the same extent. The final surface area of the mosaicked map was 2 km^2 smaller than the watershed as a result of data lost due to cloud cover identified during the quality-control process.

3.8 Accuracy assessment

Field survey data were segregated into upland and wetland validation data sets. Accuracy of these classes was determined in ArcMap by intersecting the points with the underlying classified-map pixels and recording the number of pixels that agreed and disagreed with validation data. Percent accuracies were calculated for these two classes and their combined accuracy, and Kappa coefficients were calculated for each map. Kappa coefficients consider overall accuracy and individual class accuracy, and provide a useful, additional measure of classifier agreement.

3.9 Map comparisons

The results of this study were compared to a National Wetlands Inventory (NWI) map published in 2009, a NOAA Coastal Change Analysis Program (CCAP) map from 2010, and a 2011 land use/land cover map from the Southwest Florida Water Management District (SWFWMD).

NWI has been generating detailed wetland maps of the United States since the mid-1970's, following the Cowardin et al. (1979) land cover classification scheme. NWI uses a

variety of methods and data sources, including aerial photography and satellite images, to obtain land cover information (Dahl et al., 2015). NWI classes considered wetland for comparison included all estuarine and palustrine scrub-shrub and forested wetlands (Cowardin et al., 1979). NWI does not identify upland or human-development land-cover classes.

The NOAA CCAP provides information on regional land cover change for the coastal United States. Data for CCAP are based on medium-resolution satellite data and are classified according to a CCAP classification scheme (Dobson et al., 1995). For comparison with this study, CCAP classes considered "wetland" include Palustrine Forested Wetland, Palustrine Scrub/Shrub Wetland, Estuarine Forested Wetland, and Estuarine Scrub/Shrub Wetland. CCAP classes that were considered "upland" included Developed Open Space, Cultivated Crops, Pasture/Hay, Grassland/Herbaceous, Deciduous Forest, Evergreen Forest, Mixed Forest, and Scrub/Shrub. CCAP classes that were considered "bare and developed" included Developed (Low – High Intensity), Unconsolidated Shore, and Bare Land.

Finally, the Florida Water Management Districts develop their own land use and land cover maps within their jurisdictions. Tampa Bay is located within the jurisdiction of SWFWMD. SWFWMD land cover maps are based on aerial photography, which is processed and interpreted following the Florida Land Use, Cover and Forms Classification System (FLUCCS) protocol (FDOT, 1999) to a scale of 1:12,000. Minimum mapping units are 0.5 acres (2,023 m^2) for wetlands and 5 acres (20,234 m^2) for uplands. FLUCCS classes that were considered "wetland" included Bay Swamps, Cypress, Mangrove Swamps, Stream and Lake Swamps (Bottomland), Wetland Coniferous Forests, Wetland Forested Mixed, and Wetland Hardwood Forests. FLUCCS land cover categories considered "upland" were Cropland and Pastureland, Golf Courses, Hardwood Conifer Mixed, Herbaceous, Longleaf Pine - Xeric Oak,

Mixed Rangeland, Nurseries and Vineyards, Open Land, Other Open Lands, Pine Flatwoods, Recreational, Row Crops, Shrub and Brushland, Tree Crops, Tree Plantations, Upland Coniferous Forest, and Upland Hardwood Forests. FLUCCS land cover categories considered "bare and developed" land included Beaches Other Than Swimming Beaches, Commercial and Services, Communications, Disturbed Land, Extractive, Industrial, Institutional, Residential (High, Med and Low Density), Sand Other Than Beaches, Transportation, and Utilities.

4. Results

4.1 Accuracy assessment

Accuracy assessments of our map (hereafter referred to as the “IMaRS” map, referring to the Institute for Marine Remote Sensing) resulted in greater accuracies for forested wetland, upland, and overall, and a greater Kappa coefficient than the maps from CCAP, SWFWMD, and NWI (Table 2). Forested wetlands were classified to 78% accuracy in this work, as compared with 62.7%, 64.7% and 48.7% in CCAP, SWFWMD and NWI maps, respectively. Where the NOAA CCAP map disagreed with forested wetland ground reference points, they were most commonly misclassified as Cultivated Crops, Developed (Low and Medium Intensity), Open Space, and Scrub Shrub. The most common misclassification categories for SWFWMD included Recreational, Saltwater Marshes, and Open Land. Where forested wetlands were misclassified by NWI, categories included Estuarine Emergent Vegetation and upland (i.e. no data). Misclassified forested wetlands in the IMaRS map were primarily classified as upland vegetation.

Table 2. Accuracy assessment results based on 150 wetland and 76 upland ground-reference points. Note that the NWI map does not contain upland classes.

	IMaRS	CCAP	SWFWMD	NWI
Forested wetland (%)	78.0	62.7	64.7	30.7
Upland (%)	64.5	28.9	67.1	N/A
Overall (%)	73.5	51.3	65.5	30.7
Kappa	0.42785	0.11681	0.38160	0.12948

4.2 Area cover estimates

Each of the maps evaluated here from different sources obtained substantially different areal cover or extent of wetland and upland vegetation. Our study identified 1,312, and 3,053 km^2 of wetland and upland vegetation, respectively (Table 3). This wetland estimate falls between the higher CCAP estimate of 1,439 km^2, and the lower estimates of NWI (705 km^2) and SWFWMD (442 km^2). We also found substantially more upland area and less bare and developed area than the CCAP (Figure 4) and SWFWMD maps.

Table 3. Bare and developed, forested wetland, and upland area (km^2) identified by this work (IMaRS; 2010–2014), NOAA CCAP (2009–2011), Southwest Florida Water Management District (2011), and National Wetland Inventory (NWI; 2009). NWI did not map upland vegetation.

	IMaRS	CCAP	SWFWMD	NWI
Bare and Developed	979	1326	1549	N/A
Forested wetland	1312	1439	442	705
Upland	3053	2502	1182	N/A
Total Vegetation	4364	3941	1624	705

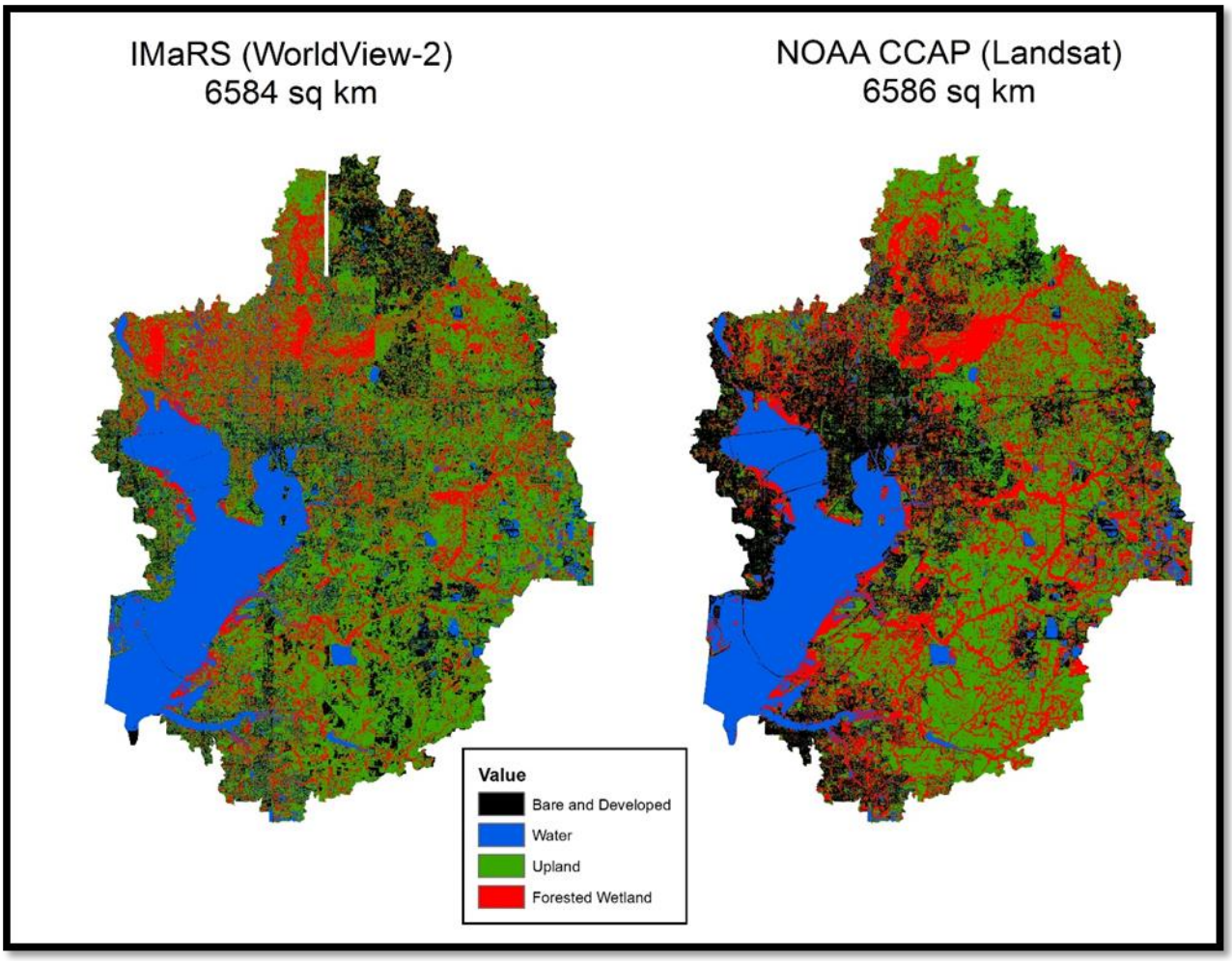

Figure 4. IMaRS (2010–2014) and NOAA CCAP (2010) map comparison.

4. Discussion

The application of two-meter resolution satellite imagery and automated classification and smoothing methods to map wetlands in the 6,500 km^2 Tampa Bay watershed resulted in greater accuracy and precision than existing state- and federal-agency maps. The Decision-Tree technique used for wetland classification combined standard spectral indices with a novel, scene-specific spectral criterion to distinguish between wetland and upland vegetation.

Our results identified both wetland and upland vegetation more accurately than the most recent NOAA CCAP, NWI, and SWFWMD products. We attribute this to the use of high spatial resolution multispectral data. The WorldView-2 pixels mapped 127 fewer square kilometers of wetland and 551 more square kilometers of upland vegetation than the CCAP map. Similarly, we found that bare and developed land comprised approximately 979 km^2 of the 6,500 km^2 of watershed, whereas CCAP identified 1,326 km^2 of bare and developed land.

These discrepancies are likely due in part to the resolution of the imagery used. Coarser pixels cause spectral confusion between habitat types, and spectral diversity within a single habitat type (Chen et al., 2015; McCarthy et al., 2015). Figure 5 highlights the capacity for high-resolution WorldView-2 imagery to distinguish between adjacent wetland and upland vegetation on a finer scale than Landsat imagery. The SWFWMD map identified more bare and developed land than CCAP despite the higher spatial resolution of the aerial photography used to digitize the land cover. This is likely due to SWFWMD definitions of residential and urban areas, which include small areas of vegetation such as private yards.

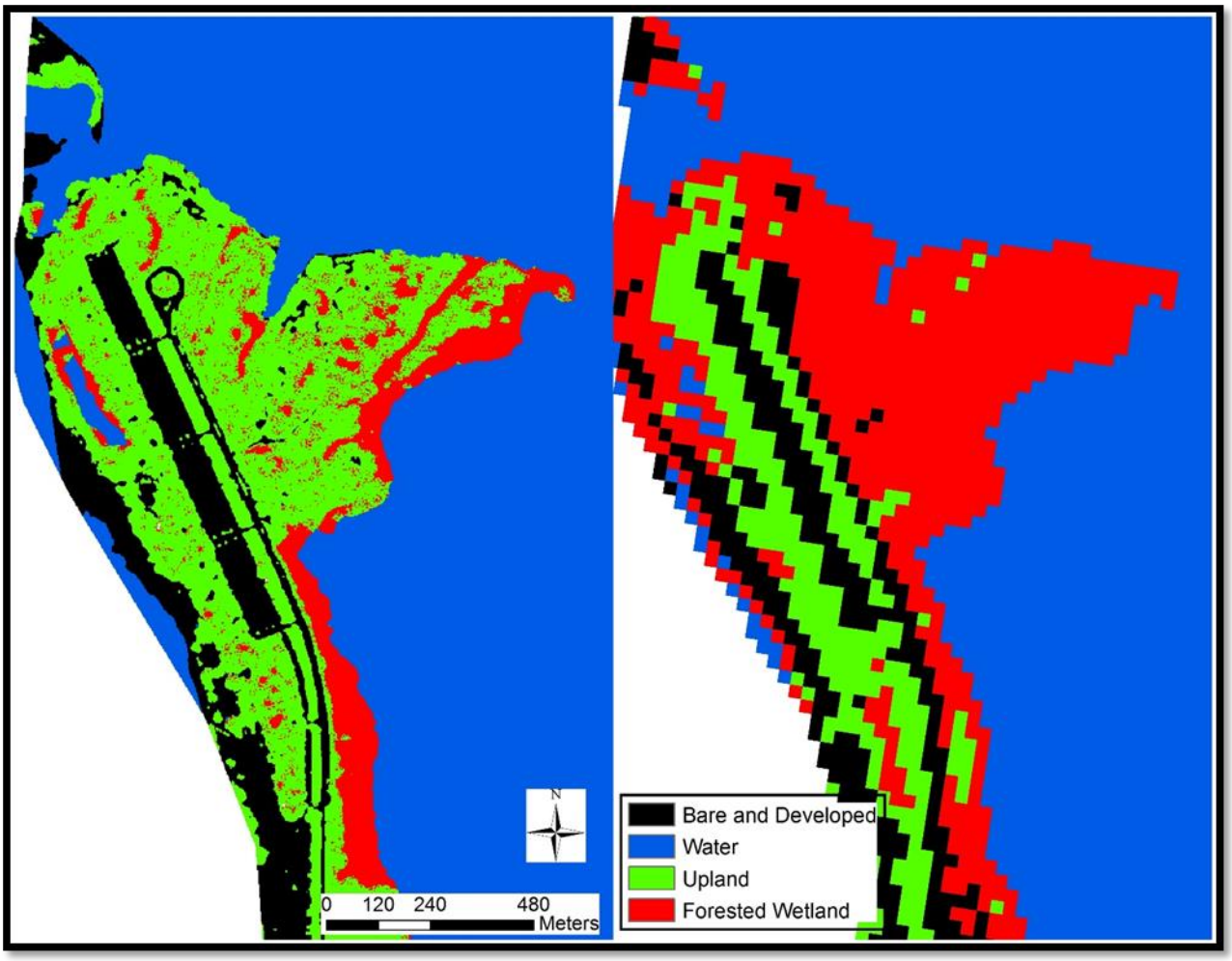

Figure 5. Comparison of IMaRS (left) and NOAA CCAP (right) maps at a scale of 1:10,000 focused on a section of Fort De Soto Park to highlight the effects of spatial resolution on the ability of the land cover classifications to distinguish between fringing mangroves and adjacent upland forest, in addition to parking lots and roads.

Where SWFWMD land cover classes disagree with forested wetland ground reference points, they were most commonly labeled as saltwater marsh, freshwater marsh, salt barrens, or open land. Part of the discrepancy between wetland mapping estimates is likely due to habitat shifts between years when data were collected for the map products. Aerial images from 2010

were used in the 2011 SWFWMD land use maps. The CCAP mapping effort was based upon Landsat images from 2009 to 2011. The NWI mapping effort used aerial images that span several decades. The WorldView-2 imagery used in this effort was collected in 2010–2014, a time span that overlaps with the imagery used for the other mapping efforts, so this dataset may also be impacted by recent habitat shifts. Mangroves are encroaching into salt marsh and salt barren habitats across Tampa Bay as a result of sea-level rise and a lack of recent severe cold events (Raabe et al., 2012; Sherwood and Greening, 2014). Mangrove encroachment can be clearly seen in aerial imagery within a span of 3–5 years, which may account for some of the discrepancies in this study.

Mapping resolution also impacts accuracy. The SWFWMD photo-interpretations included minimum mapping units of 0.5 acres (2,023 m^2) for wetlands, and 5 acres (20,234 m^2) for uplands. These requirements preclude identification of smaller stands of forested wetland, thereby potentially underestimating their extent. The digital classification of individual two-meter pixels may overcome this limitation.

Misclassifications were addressed during post-classification processes. A conservative wetland estimate was made during the filtration process using a conservative requirement that two thirds of the pixels classified as vegetation in an 11x11-pixel box had to be wetland in order for the pixel in the center of the box to be considered wetland. Large upland trees are often found in residential neighborhoods, and were confirmed as upland by using the context of the surrounding roads and houses (i.e. bare and developed land cover) to rule out the likelihood of wetland vegetation. Further, when two images overlapped, the higher pixel value of any overlapping pixels was assigned to the mosaicked pixel. Wetland pixels (value = 6) were assumed to be more accurate than upland pixels (value = 4) based on the increased scrutiny of

wetland pixels during the filtration process. Therefore, preferentially assigning wetlands to the mosaicked map was expected to produce more accurate results.

The identification and reclassification of shadows accounts for a common high-resolution image-mapping issue by reclaiming otherwise unidentifiable surfaces since the filtering process used the context of adjacent pixels to fill missing values (Bhaskaran et al., 2013). A novel spectral pattern was used here for those shadows that met the NDVI criterion, which suggested that the shadow was cast atop vegetated surfaces.

Limitations of this work include the potential for misclassification of vegetation due to seasonal phenology or interannual weather variations (e.g. drought, storm-related destruction, flooding). This is a common problem in aggregating mosaics using sparse remote-sensing data that may be addressed using season-specific imagery. Another potential for error is in the change-detection analysis if there were geographic errors in the IMaRS products, since we did not use a digital elevation model or an automated georectification method.

Our approach was to use a batch process to advance products from level-1B images to surface-radiated remote sensing reflectance, identify five land-cover types through a Decision Tree, and apply a moving-window filter to 130 WorldView-2 8-band multispectral images. Once the process was set up, we were able to run the sequence in under 24 hours. Traditional digital classification tools probably would have completed the same work in approximately four to five months with one workstation. Future work may include the use of parallelization to further enhance processing speed, and additional or improved algorithms to identify more habitat types, including saltwater and freshwater marshes.

The efficiency of this wetland-mapping method will allow coastal managers to generate high-resolution thematic maps more frequently, and thereby better monitor fine-scale wetland

change over shorter periods than current products allow. Florida's coasts are particularly vulnerable to some climate change effects, including accelerated sea-level rise, and tropical-storm intensification. In the past 170 years, Florida has already lost over half of its wetlands to human development (Dahl 2005). While remaining wetlands have been afforded some degree of legal protection, growing populations and urban infrastructure continue to put these valuable habitats at risk. Wetland habitats are also shifting in response to climate change, as mangroves overtake salt marshes in regions where periodic cold events previously kept them at bay. Management policies and conservation efforts depend upon accurate and frequent data to map the status and trends in the extent and health of these dynamic habitats. The results presented here enable such assessments. An important step is to now develop a strategy to conduct such mapping efforts over regional, national and global scales.

Acknowledgements

This manuscript is a contribution to the Marine Biodiversity Observation Network. The work was supported by the Environmental Protection Agency (STAR grant number 835193; PI: FMK) and the 2016 Gulf Oceanographic Charitable Trust Fellowship awarded to MJM. Additional funding was provided to RPM and KRR by the US Fish and Wildlife Service's Florida State Wildlife Grants Program (#F13AF00982) and the National Aeronautics and Space Administration (NASA grant NNX14AP62A to FMK). These funding sources were not directly involved in carrying out this study. Geospatial support and advice for this work was provided by the Polar Geospatial Center under NSF PLR awards 1043681 & 15559691. The services provided by Research Computing at the University of South Florida were essential to conduct this work.

References

Barbier, E.B. (2015) Valuing the storm protection service of estuarine and coastal ecosystems. Ecosystem Services, 11, 32–38. doi:10.1016/j.ecoser.2014.06.010

Barbier, E.B., Hacker, S.D., Kennedy, C., Koch, E.W., Stier, A. C., & Silliman, B.R. (2011). The value of estuarine and coastal ecosystem services. Ecological monographs, 81, 169–193.

Bhaskaran, S., Devi, S., Bhatia, S., Samal, A., & Brown, L. (2013). Mapping shadows in very high-resolution satellite data using HSV and edge detection techniques. Applied Geomatics, 5(4), 299–310.

Blasco, F., Gauquelin, T., Rasolofoharinoro, M., Denis, J., Aizpuru, M., & Caldairou, V. (1998). Recent advances in mangrove studies using remote sensing data. Marine and Freshwater Research, 49, 287–296.

Bucholtz, A. (1995). Rayleigh-scattering calculations for the terrestrial atmosphere. Applied Optics, 34(15), 2765–2773.

Carle, M.V., Wang, L., & Sasser, C.E. (2014). Mapping freshwater marsh species distributions using WorldView-2 high-resolution multispectral satellite imagery. International Journal of Remote Sensing, 35(13), 4698–4716.

Chakravortty, S. (2013). Application of hyperspectral data for Development of spectral library of mangrove species in the Sunderban Delta. International Journal of Geomatics and Geosciences, 4(2), 305–312.

Chandrasekhar, S. (1960). Radiative Transfer. (pp. 49). New York: Dover Publications

Chavez Jr., P.S. (1996). Image-based atmospheric corrections: Revisited and improved. Photogrammetric Engineering and Remote Sensing, 62, 1025–2036.

Chen, J., Chen, J., Liao, A., Cao, X., Chen, X., He, C., Han, G., Peng, S., Lu, M., Zhang, W., Tong, X., & Mills, J. (2015). Global land cover mapping at 30 m resolution: A POK-based operational approach. ISPRS Journal of Photogrammetry and Remote Sensing, 103, 7–27.

Cowardin, L.M., Carter, V., Golet, F.C., & Laroe, E.T. (1979). Classification of Wetlands and Deepwater Habitats of the United States. U.S. Fish and Wildlife Service FWS/OBS-79/31, Washington D.C. 142 p.

Dahl, T.E. (2005). Florida's wetlands: an update on status and trends 1985 to 1996. U.S. Department of the Interior, Fish and Wildlife Service, Washington, D.C . 80 pp.

Dahl, T.E., Dick, J., Swords, J., & Wilen, B.O. (2015). Data Collection Requirements and Procedures for Mapping Wetland, Deepwater and Related Habitats of the United States. Division of Habitat and Resource Conservation (version 2), National Standards and Support Team, Madison, WI. 92 p.

Dash, P., Walker, N., Mishra, D, D'Sa, E., & Ladner, S. (2012). Atmospheric correction and vicarious calibration of Oceansat-1 Ocean Color Monitor (OCM) data in coastal Case 2 waters. Remote Sensing, 4, 1716–1740.

Davidson, N.C. (2014) How much wetland has the world lost? Long-term and recent trends in global wetland area. Marine and Freshwater Research, 65, 934–941.

De Groot, R., Brander, L., van der Ploeg, S., Costanza, R., Bernard, F., Braat, L., Christie, M., Crossman, N., Ghermandi, A., Hein, L., Hussain, S., Kumar, P., McVittie, A., Portela, R., Rodriguez, L.C., ten Brink, P., & van Beukering, P. (2012). Global estimates of the value of ecosystems and their services in monetary units. Ecosystem Services, 1(1) 50–61.

Digital Globe. Radiometric Use of Worldview-2 Imagery; Technical Note; Digital Globe: Westminster, CO, USA, 2009.

Dobson, J.E., Bright, E.A., Ferguson, R.L., Field, D.W., Wood, L.L., Hadded, K.D., Iredale, H. III, Jensen, J.R., Klemas, V.V., Orth, R.J., & Thomas, J.P. (1995). NOAA Coastal Change Analysis Program (C-CAP): Guidance for Regional Implementation. NOAA Technical Report NMFS 123, Seattle, Washington. 104 p.

Florida Department of Transportation. (1999). Florida Land Use, Cover and Forms Classification System, 3rd edition. State Topographic Bureau, Thematic Mapping Section. 95 p.

Gianinetto, M., Rusmini, M., Candiani, G., Via, G.D., Frassy, F., Maianti, P., Marchesi, A., Nodari, F.R., & Dini, L. (2014). Hierarchical classification of complex landscape with VHR pan-sharpened satellite data and OBIA techniques. European Journal of Remote Sensing, 47, 229–250.

Giri, C., Ochieng, E., Tieszen, L.L., Zhu, Z., Singh, A., Loveland, T., Masek, J., & Duke, N. (2011). Status and distribution of mangrove forests of the world using earth observation satellite data. Global Ecology and Biogeography, 20, 154–159.

Green, E.P., Clark, C.D., Mumby, P.J., Edwards, A.J., & Ellis, A.C. (1998). Remote sensing techniques for mangrove mapping. International Journal of Remote Sensing, 19(5), 935–956.

Heenkenda, M.K., Maier, S.W., & Joyce, K.E. (2016). Estimating mangrove biophysical variables using WorldView-2 satellite data: Rapid Creek, Northern Territory, Australia. Journal of Imaging, 2(3),24. doi:10.3390/jimaging2030024

Hestir, E.L., Brando, V.E., Bresciani, M., Giardino, C., Matta, E., Villa, P., & Dekker, A.G. (2015) Measuring freshwater aquatic ecosystems: The need for a hyperspectral global mapping satellite mission. Remote Sensing of Environment, 167, 181–195.

Jia, M., Zhang, Y., Wang, Z., Song, K., & Ren, C. (2014). Mapping the distribution of mangrove species in the Core Zone of Mai Po Marshes Nature Reserve, Hong Kong, using hyperspectral data and high-resolution data. International Journal of Applied Earth Observation and Geoinformation, 33, 226–231.

Kamal, M., & Phinn, S. (2011). Hyperspectral data for mangrove species mapping: A comparison of pixel-based and object-based approach. Remote Sensing, 3, 2222–2242.

Kamal, M., Phinn, S., & Johansen, K. (2015). Object-based approach for multi-scale mangrove composition mapping using multi-resolution image datasets. Remote Sensing, 7, 4753–4783.

Kim, S., Prasad, A.K., El-Askary, H., Lee, W., & Kwak, D. (2014). Application of the Savitzky-Golay filter to land cover classification using temporal MODIS vegetation indices. Photogrammetric Engineering & Remote Sensing, 80(7), 675–685.

Klemas, V.V. (2009). The role of remote sensing in predicting and determining coastal storm impacts. Journal of Coastal Research, 25, 1264–1275.

Klemas, V.V. (2013a) Remote sensing of emergent and submerged wetlands: an overview. International Journal of Remote Sensing 34, 6286–6320.

Klemas, V.V. (2013b) Using Remote Sensing to Select and Monitor Wetland Restoration Sites: An Overview. Journal of Coastal Research, 29(4), 958–970.

Klemas, V.V. (2014) Remote Sensing of Riparian and Wetland Buffers: An Overview. Journal of Coastal Research, 30(5), 869 – 880

Kuenzer, C., Bluemel, A., Gebhardt, S., Tuan Vo, Q., & Dech, S. (2011). Remote sensing of mangrove ecosystems: A review. Remote Sensing, 3, 878–928

Lewis, R. R., Gilmore JR., R.G., Crewz, D.W. & Odum, W.E. (1985). Mangrove habitat and fishery resources of Florida. pp. 281–336 in: Seaman, W., Jr. (ed). Florida Aquatic Habitat and Fishery Resources. Florida Chapter, American Fisheries Society, Kissimmee, Florida. 543 p.

Lv, Z., Shi, W., Benedkitsson, J.A., & Ning, X. (2016). Novel object-based filter for improving land-cover classification or aerial imagery with very high spatial resolution. Remote Sensing, 8(12), 1023.

MacKay, H., Finlayson, C.M., Fernandez-Prieto, D., Davidson, N., Pritchard, D., & Rebelo, L-M. (2009). The role of Earth Observation (EO) technologies in supporting implementation of the Ramsar Convention on Wetlands. Journal of Environmental Management, 90, 2234–2242.

Martin, C.L., Momtaz, S., Gaston, T., & Motschaniwskyj, N.A. (2016) A systematic quanitative review of coastal and marine cultural ecosystem services: Current status and future research. Marine Policy, 74, 25–32. doi:10.1016/j.marpol.2016.09.004

McCarthy, M.J., Merton, E.J., & Muller-Karger, F.E. (2015). Improved coastal wetland mapping using very-high 2-meter spatial resolution imagery. International Journal of Applied Earth Observation and Geoinformation, 40, 11–18.

Mcleod, E., Chmura, G.L., Bouillon, S., et al. (2011). A blueprint for blue carbon: toward an improved understanding of the role of vegetated coastal habitats in sequestering CO_2. Frontiers in Ecology and the Environment, 9, 552–560.

Puetz, A.M., Lee, K., & Olsen, R.C. (2009). Worldivew-2 data simulation and analysis results. Proceedings of SPIE, 7334.

Raabe, E. A., Roy, L. C., & McIvor, C. C. (2012). Tampa Bay coastal wetlands: nineteenth to twentieth century tidal marsh-to-mangrove conversion. Estuaries and Coasts, 35(5), 1145–1162.

Schowengerdt, R.A. (1997). Remote Sensing: Models and Methods for Image Processing 2nd ed. San Diego: Academic Press

Sherwood, E.T., & Greening, H.S. (2014). Potential impacts and management implications of climate change on Tampa Bay estuary critical coastal habitats. Environmental Management, 53, 401–415.

Smith, T.J., Tiling, G., & Leasure, P.S. (2007). Restoring coastal wetlands that were ditched for mosquito control: A preliminary assessment of hydro-leveling as a restoration technique. Journal of Coastal Conservation, 11, 67–74.

Southwest Florida Water Management District (SWFWMD) (2011). Southwest Florida Water Management District Land Use Land Cover GIS dataset. http://data-swfwmd.opendata.arcgis.com/datasets/f325a3417c92444d9cba838154d6fa0d_11 (accessed 17.03.09)

Tiner, R.W. (1990) Use of high-altitude aerial photography for inventorying forested wetlands in the United States. Forest Ecology and Management, 33, 593–604.

Tiner, R.W. (1997) NWI maps: What they tell us. National Wetland Newsletter, 19, 7–12 .

Tiner, R.W., Lang, M.W., & Klemas, V.V., Eds. (2015) Remote Sensing of Wetlands: Applications and Advances. CRC Press, Boca Raton, FL. 574 pp.

Turpie, K.R. (2013) Explaining the Spectral Red-Edge Features of Inundated Marsh Vegetation. Journal of Coastal Research, 29(5),1111–1117.

Turpie, K.R., Klemas, V.V., Byrd, K., Kelly, M., Jo, Y-H. (2015) Prospective HyspIRI global observations of tidal wetlands. Remote Sensing of Environment 167:206-217.

Updike, T., & Comp, C. (2010). Radiometric use of WorldView-2 imagery. Technical note. Digital Globe.

Wang, L., Silvan-Cardenas, J.L., and Sousa, W.P. (2008). Neural network classification of mangrove species from multi-seasonal Ikonos imagery. Photogrammetric Engineering and Remote Sensing, 74, 921–927.

Wang, L., Sousa, W.P., Gong, P., & Biging, G.S. (2004). Comparison of IKONOS and QuickBird images for mapping mangrove species on the Caribbean coast of Panama. Remote Sensing of Environment, 91, 432–440.

Wolf, A. (2010). Using WorldView 2 Vis-NIR MSI Imagery to Support Land Mapping and Feature Extraction Using Normalized Difference Index Ratios. Colorado: DigitalGlobe.

Wu, J., Wang, D., & Bauer, M.E. (2005). Image-based atmospheric correction of QuickBird imagery of Minnesota cropland. Remote Sensing of Environment, 99, 315–325.

International Journal of Applied Earth Observation and Geoinformation 40 (2015) 11–18

Contents lists available at ScienceDirect

International Journal of Applied Earth Observation and Geoinformation

journal homepage: www.elsevier.com/locate/jag

Improved coastal wetland mapping using very-high 2-meter spatial resolution imagery

Matthew J. McCarthy [a,*], Elizabeth J. Merton [b], Frank E. Muller-Karger [a]

[a] Institute for Marine Remote Sensing, College of Marine Sciences, University of South Florida, 140 7th Ave. South, St. Petersburg, FL 33701, USA
[b] Geospatial Analytics Laboratory, Department of Environmental Science, Policy & Geography, University of South Florida St. Petersburg, 140 7th Ave. South, St. Petersburg, FL 33701, USA

ARTICLE INFO

Article history:
Received 15 January 2015
Accepted 13 March 2015

Keywords:
Wetlands
WorldView-2
Landsat 8 OLI
Tampa Bay
Mangroves

ABSTRACT

Accurate wetland maps are a fundamental requirement for land use management and for wetland restoration planning. Several wetland map products are available today; most of them based on remote sensing images, but their different data sources and mapping methods lead to substantially different estimations of wetland location and extent. We used two very high-resolution (2 m) WorldView-2 satellite images and one (30 m) Landsat 8 Operational Land Imager (OLI) image to assess wetland coverage in two coastal areas of Tampa Bay (Florida): Fort De Soto State Park and Weedon Island Preserve. An initial unsupervised classification derived from WorldView-2 was more accurate at identifying wetlands based on ground truth data collected in the field than the classification derived from Landsat 8 OLI (82% vs. 46% accuracy). The WorldView-2 data was then used to define the parameters of a simple and efficient decision tree with four nodes for a more exacting classification. The criteria for the decision tree were derived by extracting radiance spectra at 1500 separate pixels from the WorldView-2 data within field-validated regions. Results for both study areas showed high accuracy in both wetland (82% at Fort De Soto State Park, and 94% at Weedon Island Preserve) and non-wetland vegetation classes (90% and 83%, respectively). Historical, published land-use maps overestimate wetland surface cover by factors of 2–10 in the study areas. The proposed methods improve speed and efficiency of wetland map production, allow semi-annual monitoring through repeat satellite passes, and improve the accuracy and precision with which wetlands are identified.

1. Introduction

Wetlands are habitats located along the interface between land and either fresh- or saltwater environments, and are characterized by hydric soils that are flooded regularly (Cowardin et al., 1979; Lunetta and Balogh 1999). They are dominated by emergent, scrub, and forested vegetation. Wetlands are estimated to be worth billions of dollars to commercial and recreational fisheries by providing fish and wildlife habitat and nurseries (Dahl and Stedman, 2013; Ozesmi and Bauer 2002; Turner and Gannon 2014). They offer many other ecosystem services, including nutrient and suspended solid removal, flood protection, erosion control, recreation, aesthetics and other cultural values (Turner and Gannon 2014). The United States Environmental Protection Agency (US EPA) has estimated that the economic value of wetland services for even a single swamp is equivalent to up to $5 million in annual water pollution control costs, and up to $1.5 million in flood control costs (Turner and Gannon 2014). Wetlands provide habitat for wetland-dependent birds, which draw 50 million painters and photographers that contribute more than $10 billion per year to the U.S. economy. Nevertheless, the areal extent of wetlands declined rapidly in the 20th century, primarily as a result of development and pollution (Dahl and Stedman 2013; Raabe et al., 2012). This has led to important restoration efforts in the U.S. and elsewhere, which may conserve habitat biodiversity, and ecosystem services and goods (Nellemann and Corcoran 2010; Ozesmi and Bauer 2002; Rains et al., 2012). Because of their importance, wetlands are the only ecosystem covered by a global treaty, specifically the Ramsar Convention on Wetlands signed in 1971.

Wetland maps provide useful tools for wetland protection and management, including understanding impacts due to climate change or direct anthropogenic use (Rains et al., 2012). Wetland extent and change over time are typically evaluated with the help of synoptic mapping tools including aerial and satellite-derived

* Corresponding author. Tel.: +1 727 553 1186; fax: +1 727 553 1103.
E-mail address: mjm8@mail.usf.edu (M.J. McCarthy).

http://dx.doi.org/10.1016/j.jag.2015.03.011
0303-2434/

photographs and digital imagery (Gianinetto et al., 2014; Raabe et al., 2012; Rains et al., 2012; Rundquist et al., 2001; Steffen et al., 2010; Zhang et al., 2011).

The primary objective of this study was to develop a simple and robust methodology for assessing the extent of wetlands using new, high spatial resolution satellite imagery (~2 m and ~30 m) in specific coastal environments of the Tampa Bay estuary, Florida (USA), and compare the results with existing historical wetlands assessments for these regions. The study area was chosen because of its extensive estuarine and palustrine wetlands, and because these are of high relevance to the ecological health and economic vitality of Tampa Bay. Dominant wetland vegetation in the Tampa Bay watershed (~6550 km^2) includes red, white and black mangroves, and buttonwood.

Several existing wetland maps for the region differ in their estimate of wetland extent and location. For example, the land area classified as wetland in the National Oceanic and Atmospheric Administration (NOAA) Coastal-Change Analysis Program (C-CAP) maps does not match contemporary results from either the National Wetland Inventory (NWI) or the Southwest Florida Water Management District (SWFWMD). C-CAP overestimates the wetland class surface area estimates by a factor of almost three relative to the other two for similar mapping years, with a proportional underestimation of upland forest. The complementarity in error between these classes is likely due to the spectral and spatial mixing of wetland and non-wetland vegetation in the Landsat Thematic Mapper-class images (30 m) used for the analyses. Nevertheless, at least one accuracy validation study estimated that C-CAP wetlands, uplands, and water are classified to an accuracy of 95% (C-CAP, 2013).

2. Methods

2.1. Imagery used

To evaluate the applicability of much higher (order of 2 m per pixel) spatial resolution satellite data now available commercially, we examined two images collected by Digital Globe's WorldView-2 satellite sensors. These data, and wetlands classifications derived from them were compared with wetlands extent estimated with data from the Landsat 8 Operational Land Imager (OLI). These two sensor platforms feature different spatial, spectral and radiometric resolutions. Moreover, imagery from the latter are freely available for download, whereas those of the former are commercially dis-

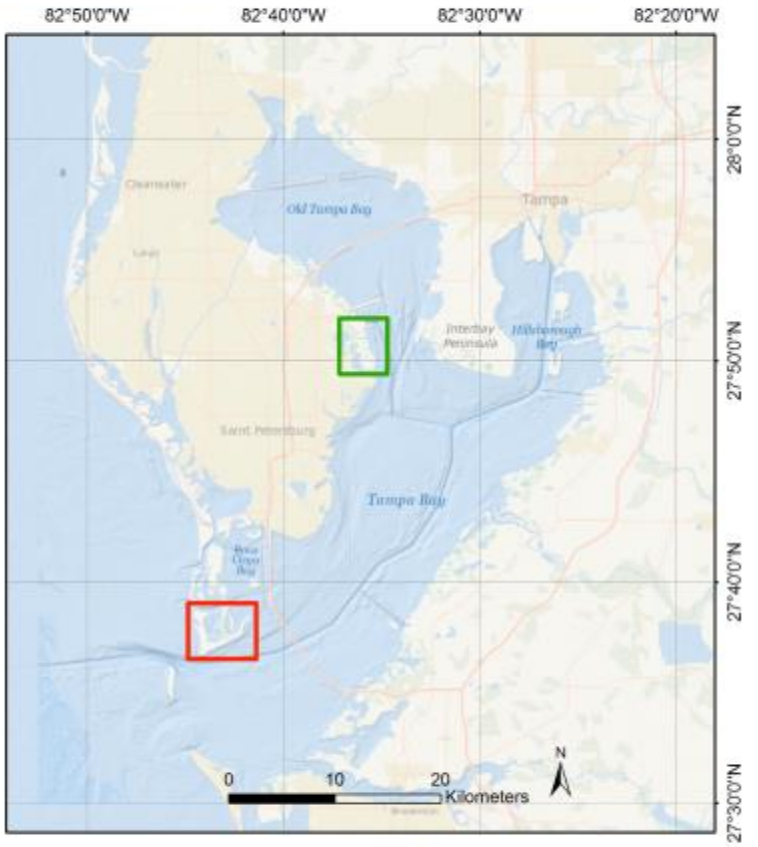

Fig. 1. Study areas in Tampa Bay: Weedon Island (Green box) and Fort De Soto (Red box). (For interpretation of the references to colour in this figure legend, the reader is referred to the web version of this article.)

Table 1
Landsat 8/OLI band specifications.

Band name	Band number	Center wavelength (nm)	Bandwidth (nm)
(Coastal/aerosol)	1	443	433–453
(Blue)	2	482	450–515
(Green)	3	562	525–600
(Red)	4	655	630–680
(NIR)	5	865	845–885
(SWIR 1)	6	1610	1560–1660
(SWIR 2)	7	2200	2100–2300
(PAN)	8	600	500–680
(CIRRUS)	9	1370	1360–1390

tributed – a potentially important factor in deciding which to use for monitoring efforts. We sought to evaluate the differences in the classes derived from these satellite sensors and compare the results with the most recent CCAP, SWFWMD and NWI wetland classes.

Landsat 8 OLI was launched on February 11, 2013. The instrument is a pushbroom system that uses a line of detectors arranged perpendicular to the flight direction collecting images with longer integration times, offering high signal to noise ratios (Vanhellemont and Ruddick, 2014). Imagery is acquired in eight spectral bands, with 12-bit radiometric resolution (Table 1) (Irons et al., 2012).

WorldView-2, launched on October 8, 2009, offers a spatial resolution of about 2 m (Digital Globe 2010). Worldview-2 is the first of the commercial, very high-resolution satellites to provide eight spectral bands in the visible and near-infrared, including coastal and red-edge bands (Table 2) (Digital Globe 2010; Tarantino et al., 2012). WorldView-2 offers an average revisiting time of 1.1 days (Tarantino et al., 2012).

The Landsat 8 OLI image covering both sites was collected in October 12, 2013. The WorldView-2 images were collected in November 8, 2012 (Weedon Island Preserve) and March 7, 2013 (Fort De Soto) (see Fig. 1 for location).

2.2. Study site

Two subregions within Tampa Bay were chosen for this study: Fort De Soto State Park and Weedon Island Preserve (Fig. 1). Fort De Soto is the largest park within the Pinellas County Park System, covering 4.59 km^2. Weedon Island Preserve is even larger at 12.91 km^2. Vegetation at both sites consists of mangroves, wetlands, palm hammocks, hardwoods, and grass flats. Developed land and beach, or barren land, are also prevalent.

2.3. Wetland definition

Wetlands were defined based on the prevalence of four species: *Rhizophora mangle* (red mangrove), *Avicennia germinans* (black mangrove), *Laguncularia racemosa* (white mangrove) and *Conocarpus erectus* (buttonwood). These forested wetlands appear to be frequently misclassified as non-wetland forest. This definition eliminated the need for soils or hydrology data, and allowed for spectral-based identification of the most prevalent wetland species for this area. This differs from the forested wetland definitions used by CCAP, SWFWMD and NWI, which require soil information, a quantification of vegetative cover, or the presence of a vaguely-defined 'hydrophytic vegetation' class.

Table 2
WorldView-2 band specifications.

Band name	Band number	Center wavelength (nm)	Bandwidth (nm)
MS7 (coastal)	1	427	396–458
MS4 (Blue)	2	478	442–515
MS3 (Green)	3	546	506–586
MS6 (Yellow)	4	608	584–632
MS2 (Red)	5	659	624–694
MS5 (Red edge)	6	724	699–749
MS1 (NIR1)	7	833	765–901
MS8 (NIR2)	8	949	856–1043
Panchromatic		627	447–808

2.4. Image pre-processing

Satellite images were radiometrically calibrated by converting digital numbers to radiance values by multiplying the metadata-based gain with the pixel value and adding the offset with ENVI's WorldView Radiance tool (Exelis Visual Information Solutions, Boulder, CO; version 4.5; see Exelis Visual Information Systems, 2014). Pu and Landry (2012) note that atmospheric effects can smear subtle spectral differences between cover types. Yet Harris (2012) confirmed that WorldView-2 radiance images without atmospheric correction are useful to observe objects surrounded by water, and that atmospheric correction of images using Dark Object Subtraction and Fast Line-of-sight Atmospheric Analysis of Hypercubes (FLAASH) markedly decreases the signal to noise ratio of the data. In this study we worked with raw radiances in order to retain any subtle differences in spectra between upland and wetland vegetation.

2.5. Unsupervised classification

A preliminary analysis was conducted to assess the capabilities of the two satellite sensors and determine which was better at identifying wetlands in Fort De Soto using a common, unsupervised classification approach. An unsupervised classification groups together pixels with similar spectral values. It is often used with no previous knowledge of the study area (Lillesand et al., 2008). This classification was first run before any fieldwork was conducted. A normalized difference water index (NDWI) was computed to identify water and exclude it from each image as a mask. Next, the images were segmented into five classes using ENVI's ISODATA unsupervised classification tool. These broad classes were chosen based on existing land cover maps of the area. To identify the land cover type to which each class corresponded, very-high resolution (0.15 m) aerial photographs were used visually as an independent reference. These aerial photographs were collected by the Florida Department of Environmental Protection in 2011 and downloaded from the Land Boundary Information System website (FDEP Land Boundary Information System, 2011). The unsupervised classification corresponded closely to marsh, upland, bare, developed, and grass classes. A second mask was created to exclude bare and developed land from each image. This allowed for the ISODATA algorithm, applied a second time, to distinguish between

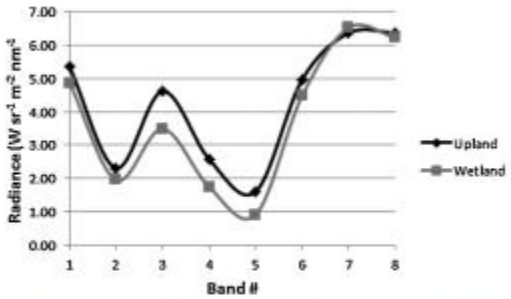

Fig. 2. Plot of average radiance for upland and wetland vegetation based on 780 and 720 spectral profiles, respectively.

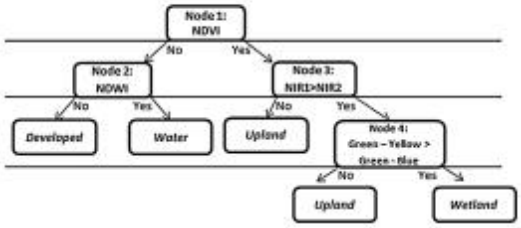

Fig. 3. Decision tree. Bold text indicates a node. Italicized text indicates an identified class.

Table 3
Upland ($n = 780$) and wetland ($n = 720$) radiance ($W\,sr^{-1}\,m^{-2}\,mm^{-1}$) spectral profile assessments combined from both sites. Averages are shown with uncertainties based on one standard deviation.

	Upland	Wetland
Band	Average	Average
1	5.35 ± 0.44	4.88 ± 0.31
2	2.31 ± 0.31	1.95 ± 0.19
3	4.62 ± 0.84	3.49 ± 0.43
4	2.57 ± 0.63	1.74 ± 0.19
5	1.60 ± 0.59	0.91 ± 0.17
6	4.97 ± 1.08	4.48 ± 0.69
7	6.37 ± 1.40	6.53 ± 1.06
8	6.38 ± 1.36	6.24 ± 0.96

vegetation classes. The result was two classified vegetation maps, specifically one from Landsat 8 OLI and one from WorldView-2.

2.6. Field survey

Ground reference points (GRPs) were collected in the field for use in conducting a classification accuracy assessment. We used a Trimble GeoExplorer 6000 series GPS unit (horizontal accuracy of 2.5 cm and vertical accuracy of 4 cm) during May 2014. Habitat classes were identified throughout both study sites where access was feasible. Location was recorded for at least 10 points per class (Barren Land, Developed, Upland, Marsh and Grass). Water was not included in the collection. The points were overlaid on the images using ENVI to confirm congruence with features in the images. All points were separated by at least 20 m to minimize spatial autocorrelation effects (McCarthy and Halls 2014). The GRPs that fit these criteria (55 GRPS for Fort De Soto, 52 for Weedon Island) were then used with ENVI's confusion matrix tool to generate an accuracy assessment for each classified map.

2.7. Decision tree node development and classification

We used a decision tree to conduct classifications. A decision tree is a multi-stage image classifier tool that uses a series of binary decisions to determine the correct class for each image pixel. Each decision node divides the data into one of two classes or groups of classes. No single decision performs the complete segmentation of the image into classes (ENVI Tutorial, 2011). Lu and Weng (2009) found that a decision-tree approach provided an overall accuracy of 92% in land-use classification and that other supervised classification methods yielded lower accuracies. A relatively "mature" classification tool, the decision tree is not a novel approach in itself. Innovative use of one lies in the development of the nodes used to hierarchically identify each pixel's land cover class accurately.

Our decision tree was built to identify 4 land classes: developed/bare, water, upland, and wetland. We were primarily interested in obtaining the highest accuracy of wetlands extent. The results of the unsupervised classification of the WorldView-2 data covering Fort De Soto provided a map of higher accuracy than that of Landsat 8 OLI. The spectral data from the WorldView-2 images were therefore used to define a decision tree based on field-validated locations of specific classes. The decision tree was then used to re-classify the WorldView-2 images of Fort De Soto and Weedon Island.

A normalized difference vegetation index (NDVI) was used in the first node of the decision tree to distinguish vegetated from non-vegetated classes (Eq. (1)) (Wolf 2010). The second Near Infrared band (NIR2, band 8) and the Red band (band 5), centered at 950 and 660 nm, respectively (Table 1), were chosen for this index. In the second node, water was distinguished from developed/bare land using a normalized difference water index (NDWI) (Eq. (2)) using the Coastal band (band 1) and NIR2 (Table 1) (McFeeters 1996).

$$\text{Index} = \frac{(\text{NIR2} - \text{Red})}{(\text{NIR2} + \text{Red})} \quad (1)$$

$$\text{Index} = \frac{(\text{Coastal} - \text{NIR2})}{(\text{Coastal} + \text{NIR2})} \quad (2)$$

Wetland vegetation and upland forest showed similar spectral reflectance patterns (Fig. 2). To identify consistent differences between these vegetation types, 720 wetland and 780 upland spectral profiles from separate pixels were examined for Fort De Soto and Weedon Island field-validated regions. The profiles for both locations were averaged for each class (Table 3 and Fig. 2).

We found that 56% of our collected upland vegetation pixels had maximum radiance values in band 8 (NIR2), whereas 90% of wetland pixels had a maximum in band 7 (NIR1) (Fig. 2; Table 3). These differences in the spectra were used to identify upland vegetation in the third decision-tree node. The difference between band 3 (Green) and band 2 (Blue) radiances was greater for upland in 67% of pixels, and the difference between band 3 (Green) and band 4 (Yellow) radiances was greater for wetland in 96% of pixels. This pattern was used in the fourth and final decision-tree node (Fig. 3) to further distinguish between wetland and upland pixels. These relationships were consistent between the two study sites and for the image acquisition times of March and November.

2.8. Post-processing and accuracy assessment

Classification maps were then filtered using a 3 × 3 pixel median filter in ENVI's Convolutions and Morphology tool to generate more homogenous maps and improve accuracy by replacing isolated cells with the class that corresponds to the median value of cells within a 3 × 3 pixel matrix (McCarthy and Halls, 2014). This is done because habitats tend not to be found in isolation, and isolated pixels are, therefore, likely to be erroneous in classification maps. Accuracy assessment was conducted using ENVI's confusion matrix tool on

Table 4
Confusion matrix results for Fort De Soto (90.9% overall accuracy, Kappa 0.8569).

Class	Producer's accuracy (%)	User's accuracy (%)	Commission error (%)	Omission error (%)
Wetland	81.82	90.00	10.00	18.18
Upland	90.48	90.48	9.52	9.52
Bare/Developed	95.65	91.67	8.33	4.35

Table 5
Confusion matrix results for Weedon Island (84.6% overall accuracy, Kappa 0.7245).

Class	Producer's accuracy (%)	User's accuracy (%)	Commission error (%)	Omission error (%)
Wetland	94.44	77.27	22.73	5.56
Upland	82.76	88.89	11.11	17.24
Bare/Developed	60.00	100.00	0.00	40.00

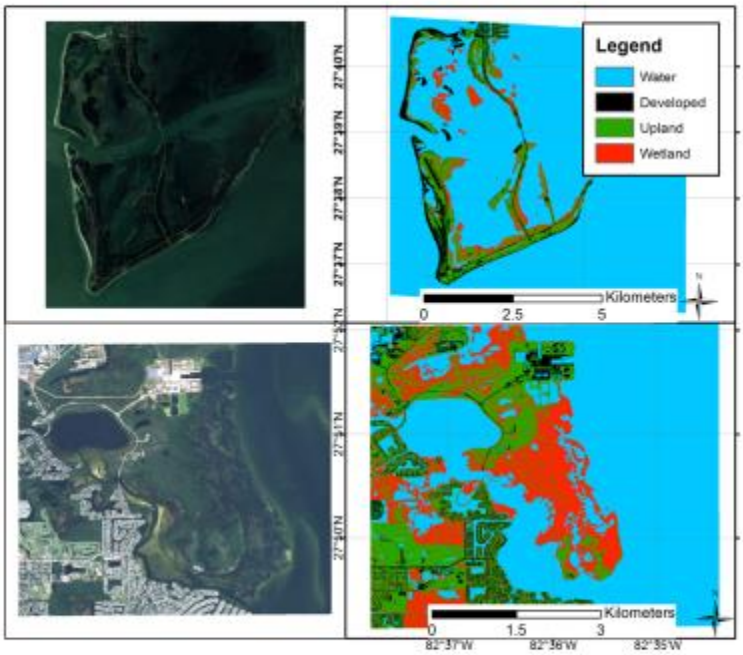

Fig. 4. WorldView-2 image and Decision tree classification maps for Fort De Soto (upper left and right) and Weedon Island (lower left and right).

three classes using the collected GRPs: Wetland, Upland, and Developed/Bare.

3. Results

3.1. Unsupervised classifications

The initial unsupervised classifications of Fort De Soto using WorldView-2 data yielded a Wetland accuracy of 82%, while using Landsat 8 OLI the accuracy was 46%. Upland and Grass accuracies were 67% and 22%, respectively, for WorldView-2, and 58% and 67%, respectively, for Landsat 8 OLI. Because our primary interest was to improve existing wetland maps, we selected WorldView-2 for further analysis to generate the spectral profiles, and train and apply the decision tree.

3.2. Decision tree classifications

The WorldView-2 product derived with the decision tree classification yielded an accuracy (producer's accuracy) of 82% for Wetland in Fort De Soto and 94% in Weedon Island (Tables 4 and 5). Identification of Upland vegetation accuracy was 90% in Fort De Soto and 83% in Weedon Island. User's accuracy for the Wetland class – an index that would be low if wetlands were misclassified as other classes – was 90% for Fort De Soto and 77% for Weedon Island. Producer's accuracy for Developed land was 96% for Fort De Soto and 60% for Weedon Island. None of the Developed-land GRPs were found to be misclassified as Wetland. Decision tree classification maps for each study site are shown with the original images in Fig. 4.

4. Discussion

Remote sensing observations collected at very high spatial resolution, and at high radiometric and spectral resolution, have advanced studies of land use over large areas (Gianinetto et al., 2014). Our study finds that land classification maps derived for two specific coastal habitats within the Tampa Bay estuary using WorldView-2 images had higher accuracy relative to maps derived with Landsat 8 OLI, using ground observations as a reference. In general, the radiometric quality of the Landsat 8 OLI data is comparable to that of the WorldView-2 data (Irons et al., 2012; Tarantino et al., 2012). Also, the spectral resolution of the bands used from each of these sensors is similar (see Tables 1 and 2). Thus, differences in accuracy between the maps derived from the two sensors are likely due to the difference in spatial resolution. Our field evaluations confirmed that many coastal wetland habitats in the two study areas were patchy and often narrow (approximately 5–10 m

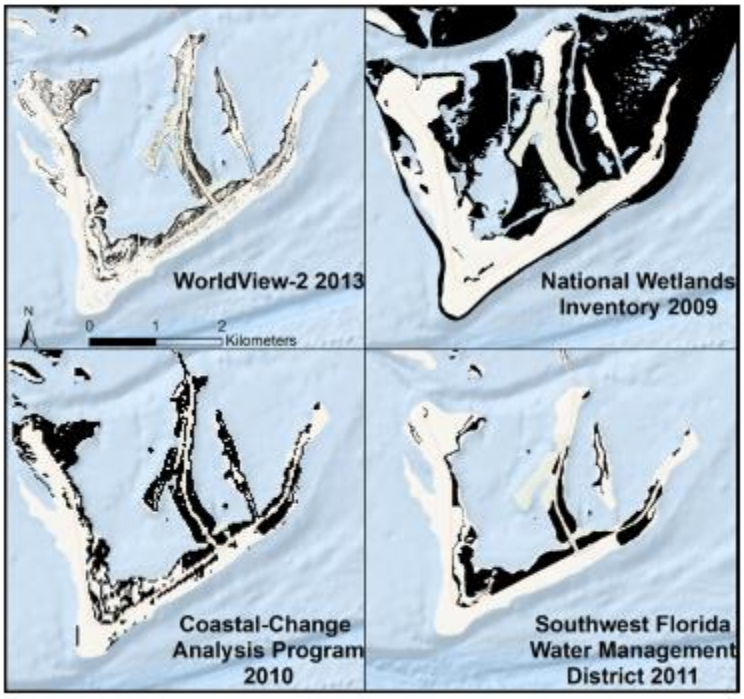

Fig. 5. Wetlands (black) of Fort De Soto from this study (top left) and comparable mapped products with map source and year of remotely sensed data.

wide strips). The 30 m × 30 m pixels of Landsat 8 OLI do not resolve these areas or the mixed vegetation that would be aggregated within each 30 m pixel. In contrast, the very high resolution of WorldView-2 images is able to resolve these vegetation classes (Fig. 5).

One of the goals of this project was to develop a method that could be implemented with relatively minimal resources, and without need for training data. The decision tree tool can be found or created in common image-processing software, and our novel combination of nodes can be copied from this manuscript and applied. We believe that this work has high potential for monitoring in the future when a substantial time series of WorldView-2 imagery is available. Moreover, while we have only validated this approach for the WorldView-2 sensor, it may be applicable to other digital remote sensing data with similar spectral and radiometric resolutions. The decision tree that we developed led to a capability to identify wetland vegetation to greater than 80% accuracy in an objective, automated process using WorldView-2 images. This process did not require ancillary data such as soil or hydrology information. Accurate identification of upland vegetation was also greater than 80%. This process substantially decreased overestimation of wetland area by reducing misclassification of non-wetland vegetation as wetland when compared with other groups' mapped products.

The NIR2 and Yellow bands of the WorldView-2 sensor allowed the segregation of upland and wetland in the decision tree consistently across the two different study areas and in imagery acquired during different seasons. Wang and Sousa (2009) present figures of the mean and standard deviations of mangrove spectral reflectance patterns across visible and near infrared wavelengths for healthy and stressed plants. Variance in reflectance, and differences between spectra of healthy and stressed species, are smaller in the visible wavelengths used in our study than at wavelengths greater than 1000 nm (Wang and Sousa, 2009). Seasonal differences are expected to influence vegetation spectra patterns. Yet Flores-de-Santiago et al. (2012) found no differences in reflectance patterns of healthy or stressed mangrove species in western Mexico along the Gulf of California from the dry to the wet season. The climate in the Tampa Bay area is more moderate than their study area, and the low spectral radiance variation in our wetlands pixels was consistent with that study. We therefore, expect that the spectral patterns of wetlands identified in this study are stable. Future research is needed to validate across greater spatio-temporal ranges the consistent radiance patterns found here.

Benefits of this methodology for future wetland monitoring efforts include further standardization of wetland classification, efficient mapping with a four-node decision tree on digital data, and improved precision of wetland area identification with very high resolution imagery. The implication is that wetlands can now be identified faster and more precisely than before with higher accuracy.

C-CAP, NWI and SWFWMD products used different data and methods for identifying wetlands (C-CAP, 2013; Cowardin et al., 1979; Kawula 2009; National Wetlands Inventory Program, 2014; Southwest Florida Water Management District, 2011). Those products show substantial inconsistencies between wetlands coverage (Figs. 5 and 6). While C-CAP reports an overall accuracy of >80%, large errors were reported in the user's and producer's accuracies for wetland classes (NOAA, 2006). The NWI maps were created by digitizing polygons in a geographic information system using

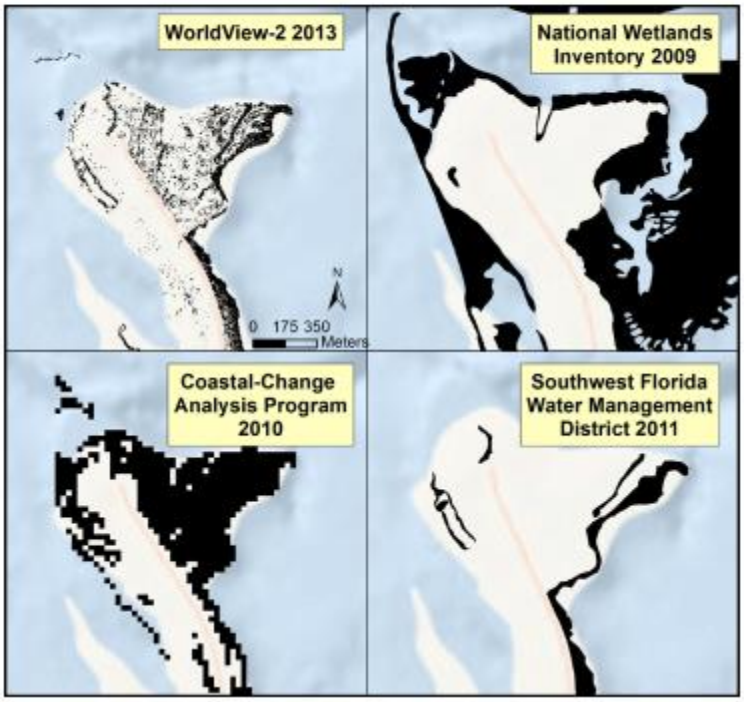

Fig. 6. Wetlands (black) of North Beach subsection of Fort De Soto from this study (top left) and comparable mapped products with map source and year of remotely sensed data.

Table 6
Wetland area computed from map products of Fort De Soto (22 km^2 region of interest), and Weedon Island (27 km^2 region of interest).

	Fort De Soto		Weedon Island	
Map source	Wetland area (km^2)	Factor difference from this study	Wetland area (km^2)	Factor difference from this study
WorldView-2	0.94	N/A	6.17	N/A
SWFWMD	2.49	2.64	8.19	1.33
C-CAP	4.99	5.31	12.74	2.06
NWI	9.92	10.55	12.43	2.01

aerial photographs. The SWFWMD maps were created using a process similar to that used by the NWI (Raabe et al., 2012; Rains et al., 2012). All three products overestimate wetland area relative to our high-resolution WorldView-2 product in both Fort De Soto and Weedon Island (Table 6). The SWFWMD map shows more than double the wetland area, and the CCAP maps report more than five times the wetland area than our product. The ten-fold greater NWI wetland area includes submerged wetlands, which were not considered in the other three maps. We found similar discrepancies for the Weedon Island study area, which includes residential areas of Pinellas County outside the preserve (Table 6).

Given the high accuracy and low misclassification error of this study's wetland maps, we conclude that wetland areas in the C-CAP, NWI and SWFWMD data sets have been overestimated. The latter wetland maps have been used historically to guide restoration efforts in the Tampa Bay watershed (Rains et al., 2012; Robison 2010). We recommend that the methodology used for setting restoration goals be reviewed. It may be appropriate to adopt new methodologies for land classification, such as those used in this study, to establish a more accurate baseline of current wetland area. This would be a better baseline against which to monitor future wetland change.

Additional research is needed to improve the identification of other vegetation types, including forested wetland, scrub-shrub wetland, and emergent wetland. Also, further studies would help to expand the decision tree's capability to identify inland wetlands, which would include distinguishing between palustrine and estuarine wetlands.

6. Conclusions

The goals of this research were to test the applicability of very high spatial resolution (2 m) WorldView-2 satellite observations to quantify wetland area in two regions of interest in the Tampa Bay Florida, USA, watershed. A decision-tree image classification method was used to derive various traditional land and land-use classes. Our methodology identified wetlands with high accuracy and higher precision than previously achieved using satellite and aerial photograph based

data. The decision tree method was rapid and efficient. Our results show that the area of coastal wetland vegetation in our study areas around Tampa Bay is about half that reported in publicly-available products derived from remote sensing methods. Very high resolution WorldView-2 imagery and the decision tree methodology developed here may be useful tools to help focus future monitoring and restoration efforts.

Conflict of interest

The authors declare that they have no conflict of interest.

Acknowledgements

Support for this study was provided by grant to FMK. WorldView-2 images were facilitated by Digital Globe under licensed agreement with the National Science Foundation and were provided by D. Paul Morin of the Polar Geospatial Center, University of Minnesota. The authors thank Tampa Bay Estuary Program employees Lindsay Cross and Ed. Sherwood for their comments in preparation of this work. We also thank Pinellas Country for granting permission to conduct research in Fort De Soto and Weedon Island. Field work was assisted by Lindsey Brendis, Steven Douglas, Jennifer Granneman, Kimberly Lyons, and Devlin Munion. We thank Dr. Barnali Dixon (University of South Florida, St. Petersburg) for her encouragement and advice during this project.

References

C-CAP, 2013. Assessment report of wetland mapping improvement to NOAA's Coastal Change Analysis Program (C-CAP) land cover in western Washington State. State of Washington Department of Ecology. <http://www.ecy.wa.gov/programs/sea/wetlands/pdf/C-CAPWetlandAssessmentReport.pdf/>. (accessed 20.04.14.).

Cowardin, L., Carter, V., Golet, F., LaRoe, E., 1979. Classification of Wetlands and Deepwater Habitats of the United States, FWS/OBS79/31. U.S. Fish and Wildlife Service, Washington.

Dahl, T., Stedman, S., 2013. Status and trends of wetlands in the coastal watersheds of the Conterminous United States 2004 to 2009. U.S. Department of the Interior, Fish and Wildlife Service and National Oceanic and Atmospheric Administration, National Marine Fisheries Service. (46 p.).

Digital Globe, 2010. The Benefits of the Eight Spectral Bands od WorldView-2. Available in <http://www.digitalglobe.com/sites/default/files/DG-8SPECTRAL-WP.pdf/>. (accessed 26.06.14.).

ENVI Tutorial, Decision Tree Classification. <http://www.ittvis.com/language/en-us/productsservices/envi/tutorials.aspx/>. (accessed 15.05.14.).

Exelis Visual Information Systems, 2014. Radiometric Calibration. Calibrating Images Tutorial. <http://www.exelisvis.com/docs/RadiometricCalibration.html/>. (accessed 21.04.14.).

FDEP Land Boundary Information System, 2011. Pinellas [air photo], 1:6,000. Photo #B089. Brooksville, FL.

Flores-de-Santiago, Kovacs, J.M., Flores-Verdugo, F., 2012. Seasonal changes in leaf chlorophyll a content and morphology in a sub-tropical mangrove forest of the Mexican Pacific. Mar. Ecol. Prog. Ser. 444, 57–68.

Gianinetto, M., Rusmini, M., Candiani, G., Via, G.D., Frassy, F., Maianti, P., Marchesi, A., Nodari, F.R., Dini, L., 2014. Hierarchical classification of complex landscape with VHR pan-sharpened satellite data and OBIA techniques. Eur. J. Remote Sens. 47, 229–250.

Harris, T., 2012. Spectral Target Detection for Detecting and Characterizing Floating Marine Debris. American Geophysical Union, San Francisco, CA, Dec. 3–7.

Irons, J.R., Dwyer John, L., Barsi Julia, A., 2012. The next landsat satellite: the landsat data continuity mission. Remote Sens. Environ. 122, 11–21.

Kawula R., 2009. Florida Land Cover Classification System. <http://myfwc.com/media/1205712/SWG%20T-13%20Final%208pt,0118pdf/>. (accessed 21.04.14.).

Lillesand, T., Kiefer, R., Chipman, J., 2008. Remote Sensing and Image Interpretation, 6th ed. John Wiley & Sons, Inc., Hoboken, NJ, USA.

Lu, D., Weng, Q., 2009. Extraction of urban impervious surfaces from an IKONOS image. Int. J. Remote Sens. 30, 1297–1311.

Lunetta, R., Balogh, M., 1999. Application of multi-temporal Landsat 5 TM imagery for wetland identification. Photogr. Eng. Remote Sens. 65, 1301–1310.

McCarthy, M.J., Halls, J., 2014. Habitat mapping and change assessment of coastal environments: an examination of WorldView-2, QuickBird, and IKONOS satellite imagery and airborne LiDAR for mapping barrier island habitats. Int. J. Geo-Information 3, 297–325.

McFeeters, S.K., 1996. The use of the normalized difference water index (NDWI) in the delineation of open water features. Int. J. Remote Sens. 17, 1425–1432.

National Wetlands Inventory Program [NWI], 2014. NWI Program Overview. Available in <http://www.fws.gov/wetlands/NWI/Overview.html/>. (accessed 29.05.14.).

Nellemann, C., Corcoran, E., 2010. Dead Planet, Living Planet. Biodiversity and Ecosystem Restoration for Sustainable Development, a Rapid Response Assessment. United Nations Environment Programme, GRID-Arendal, Arendal, Norway. pp. p.100.

NOAA Coastal Change Analysis Program (C-CAP) Land Cover and Change Data [computer file], Charleston, SC: NOAA Coastal Change Analysis Program (C-CAP), 2006. Available at: LAGIC <http://lagic.lsu.edu/data/losco/landcover_la_noaa_2005html#8/>. (accessed 21.04.14.).

Ozesmi, S.L., Bauer, M.E., 2002. Satellite remote sensing of Wetlands. Wetlands Ecol. Manage. 10, 381–402.

Pu, R., Landry, S., 2012. A comparative analysis of high spatial resolution IKONOS and WorldView-2 imagery for mapping urban tree species. Remote Sens. Environ. 124, 516–533.

Raabe, E., Roy, L., McIvor, C., 2012. Tampa Bay coastal wetlands: nineteenth to twentieth century tidal marsh-to-mangrove conversion. Estuaries and Coasts 35, 1145–1162.

Rains, M., Landry, S., Seidel, V., Crisman, T., 2012. Prioritizing habitat restoration goals in the Tampa Bay watershed. Technical report to the Tampa Bay Estuary Program # 10–12. <http://www.tbeptech.org/TBEP_TECH_PUBS/2012/TBEP_10_12_USF_Prioritizing_Habitat_Restoration_Goals_2012_04pdf/>. (accessed 18.05.14.).

Robison, D., 2010. Tampa Bay Estuary Program habitat master plan update. Technical report to the Tampa Bay Estuary Program # 06–09. Available in <http://www.tbeptech.org/TBEP_TECH_PUBS/2009/TBEP_06_09_Habitat_Master_Plan_Update_Report_July_2010pdf/>. (accessed 18.05.14).

Rundquist, D.C., Naraumalani, S., Narayanan, R.M., 2001. A review of wetlands remote sensing and defining new considerations. Remote Sens. Rev. 20 (3), 207–226.

Southwest Florida Water Management District [SWFWMD], 2011. Land Cover Land Use. 2011. <http://www.swfwmd.state.fl.us/data/gis/libraries/physical_deuse/lu11php/>. (accessed 29.05.14.).

Steffen, M., Estes, M., Al-Hamdan, M., 2010. Using remote sensing data to evaluate habitat loss in the Mobile, Galveston and Tampa Bay watersheds. Coastal Education and Research Foundation, p.24. <http://weather.msfc.nasa.gov/applied_science/Wetland_Paper_Final.pdf/> (accessed 20.03.14.).

Tarantino, C., Adamo, M., Pasquariello, G., Lovergine, F., Blonda Tomaselli, P.V., 2012. 8-band image data processing of the worldview-2 satellite in a wide area of applications. In: Rustamov, R. (Ed.), Earth Observation., http://dx.doi.org/10.5772/27499, ISBN: 978-953-307-973-8, InTech, Available from: http://www.intechopen.com/books/earth-observation/8-band-image-data-processing-of-the-worldview-2-satellite-in-a-wide-area-of-applications

Turner, M., Gannon, R., 2014. Values of Wetlands. North Carolina State University. <http://www.water.ncsu.edu/watersheds/info/wetlands/values.html/> (accessed 21.04.14.).

Vanhellemont, Q., Ruddick, K., 2014. Turbid wakes associated with offshore turbines observed with Landsat 8. Remote Sens. Environ. 145, 105–115.

Wang, L., Sousa, W.P., 2009. Distinguishing mangrove species with laboratory measurements of hyperspectral leaf reflectance. Int. J. Remote Sens. 30 (5), 1267–1281.

Wolf, A., 2010. Using WorldView-2 Vis-NIR MSI imagery to support land mapping and feature extraction using normalized difference index ratios. Digital Globe: 8-band challenge. Longmont, CO. <http://www.exelisvis.com/portals/0/pdfs/envi/8_bands_Antonin_Wolf.pdf/> (accessed 5.06.14.).

Zhang, Y., Lu, D., Yang, B., Sun, C., Sun, M., 2011. Coastal wetland vegetation classification with a landsat thematic mapper image. Int. J. Remote Sens. 32 (2), 545–561.

Satellite Remote Sensing for Coastal Management: A Review of Successful Applications

Matthew J. McCarthy, Kaitlyn E. Colna, Mahmoud M. El-Mezayen, Abdiel E. Laureano-Rosario, Pablo Méndez-Lázaro, Daniel B. Otis, et al.

Environmental Management

ISSN 0364-152X
Volume 60
Number 2

Environmental Management (2017)
60:323-339
DOI 10.1007/s00267-017-0880-x

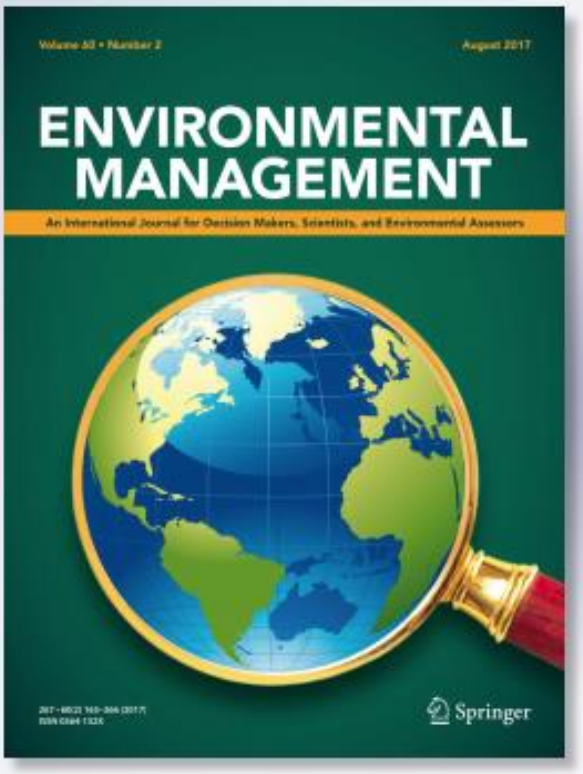

Springer

Environmental Management (2017) 60:323–339
DOI 10.1007/s00267-017-0880-x

Satellite Remote Sensing for Coastal Management: A Review of Successful Applications

Matthew J. McCarthy[1] · **Kaitlyn E. Colna**[1] · **Mahmoud M. El-Mezayen**[1,2] · **Abdiel E. Laureano-Rosario**[1] · **Pablo Méndez-Lázaro**[3] · **Daniel B. Otis**[1] · **Gerardo Toro-Farmer**[1] · **Maria Vega-Rodriguez**[1] · **Frank E. Muller-Karger**[1]

Received: 4 January 2017 / Accepted: 25 April 2017 / Published online: 8 May 2017

Abstract Management of coastal and marine natural resources presents a number of challenges as a growing global population and a changing climate require us to find better strategies to conserve the resources on which our health, economy, and overall well-being depend. To evaluate the status and trends in changing coastal resources over larger areas, managers in government agencies and private stakeholders around the world have increasingly turned to remote sensing technologies. A surge in collaborative and innovative efforts between resource managers, academic researchers, and industry partners is becoming increasingly vital to keep pace with evolving changes of our natural resources. Synoptic capabilities of remote sensing techniques allow assessments that are impossible to do with traditional methods. Sixty years of remote sensing research have paved the way for resource management applications, but uncertainties regarding the use of this technology have hampered its use in management fields. Here we review examples of remote sensing applications in the sectors of coral reefs, wetlands, water quality, public health, and fisheries and aquaculture that have successfully contributed to management and decision-making goals.

Keywords Coastal resources · Coral reefs · Wetlands · Water quality · Public health · Fisheries

✉ Matthew J. McCarthy
mjm8@mail.usf.edu

[1] Institute for Marine Remote Sensing, College of Marine Science, University of South Florida, 140 7th Ave. South, St. Petersburg, FL 33701, USA

[2] Aquaculture Department, National Institute of Oceanography and Fisheries (NIOF), Alexandria, Egypt

[3] Environmental Health Department, Graduate School of Public Health, University of Puerto Rico, Medical Sciences Campus, PO Box 365067, San Juan, PR 00936-5067, USA

Introduction

As of 2010, over 2.5 billion people (~40% of the global population) live in coastal ecosystems that are increasingly vulnerable to natural and anthropogenic influences (Sale et al. 2014). In the next few decades, these areas will be affected by changing atmospheric and ocean temperatures, sea levels, ocean chemistry, weather patterns, and the increased demands of a growing global population. Without proper strategies to manage our use of resources, these changes will result in increased risks to human health, property, economic vitality, and further damage to services we derive from these ecosystems (Pereira et al. 2010; Pettorelli et al. 2014; Sale et al. 2014; Wigbels 2011). To improve coastal ecosystem management, decision-makers should take further advantage of the synoptic, frequently sampled, and often freely accessible satellite remote sensing technology that is available today (Kachelreiss et al. 2014; Pettorelli et al. 2012).

Remote sensing techniques have substantially improved our ability to observe the environment and its processes (De La Rocque et al. 2004; Heumann 2011). Currently, however, remote sensing technologies are underutilized in environmental management (Heumann 2011; Pettorelli et al. 2014). Based on an internal survey of Environmental Protection Agency personnel, who were responsible for integrating scientific research into decisions related to policy and management, Schaeffer et al. (2013) identified four main themes regarding why these technologies may be

underutilized: costs and accuracy of data products, uncertainty about satellite mission continuity, and difficulty in obtaining administrative approval for using remote sensing in decision-making. Additionally, managers may be unfamiliar with the breadth of current satellite data, and therefore under the impression that available imagery may be insufficient to meet their needs.

Our goal with this review is to illustrate applications of satellite remote sensing techniques that have successfully improved management capabilities in coastal sectors, and summarize the data that is currently available for management use. We provide examples in coral reefs and wetlands, assessments of water quality and public health, and support to fisheries and aquaculture activities.

Each satellite sensor is designed for particular sets of applications. Trade-offs exist between spectral, spatial, and temporal resolution for different sensors. Specifically, spatial resolution is the spatial "footprint", or pixel (picture element) size, which is the smallest portion of the Earth's surface discretely sampled by a device. Figure 1 compares the spatial resolution of the Landsat 8 sensor (30 meter) to that of WorldView-2 (2 meter), as well as the additional trade-off of greater geographical coverage per image "tile" with coarser resolution imagery. Spectral resolution is the smallest window in wavelength or frequency space of the electromagnetic spectrum that is discretely sampled by a sensor. Sensors typically have several spectral bands that sample different parts of the electromagnetic spectrum at different spectral resolutions. Temporal resolution is the frequency or revisit time at which a sensor collects subsequent measurements of the same location. In addition, sensors and the satellite platforms on which they fly need to be designed to satisfy a number of minimum requirements in order to observe particular phenomena.

For example, many satellite sensors designed for viewing the ocean in the visible range of the electromagnetic spectrum (reflected color) and in the infrared (emitted thermal radiation) have nominal spatial resolutions of about one square kilometer. This allows capturing mesoscale and larger spatial variability of the open ocean at near daily

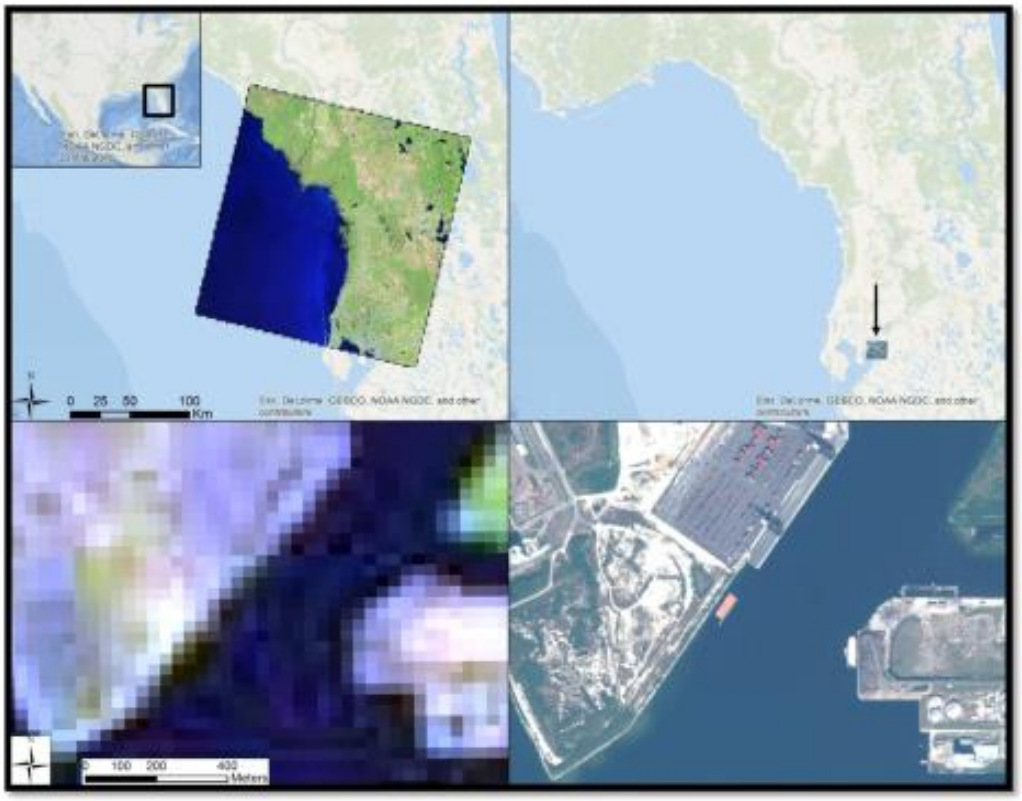

Fig. 1 Geographic coverage per image "tile" (*top*), and spatial resolution (*bottom*) of Landsat 8 (*left*) and WorldView-2 (*right*) are compared

revisit time from orbits at altitudes of about 600–800 km above the Earth. Medium-resolution sensors such as those flown on the Landsat series have a spatial resolution on the order of 30 m, wide spectral bands (~ 60 nm bandwidth), and a revisit time of 16 days. The European Sentinel-2 satellite has a spatial resolution from ~ 10 to 60 m depending on the band, spectral bandwidths from 10 to 60 nm, and a revisit period of ~ 2–3 days. Geostationary sensors operate from an orbit of about 36,000 km above the Earth and can collect data several times per day from low-latitudes to mid-latitudes in a single hemisphere. Many weather satellites have such hemispheric coverage. The Korean Geostationary Ocean Color Imager (GOCI) focuses on a small geographic area with a spatial resolution of ~ 500 m. Satellite sensors such as these will be discussed in the following management sectors for which they are most applicable. Table 1 summarizes the sensors mentioned here by resolutions, years of available data, relevant management uses, and locations from which data may be downloaded or requested.

Management Sectors

Coral Reefs

Shallow-water tropical coral reefs are some of the most diverse and productive ecosystems in the ocean (Bellwood and Hughes 2001; Small et al. 1998). Globally, the economic value of reefs is ~ US $30 billion annually (Chen et al. 2015). They are critical for the social and economic well-being of people living in coastal regions as they provide seafood, pharmaceuticals, recreation, and coastal protection (Burke et al. 2011). Despite these ecological and social benefits, coral reefs are undergoing major habitat loss (Baker et al. 2008; Gardner et al. 2003).

The progressive warming of global sea surface temperature (SST) is one of the most important environmental stressors responsible for decline in coral cover (Chollett et al. 2012; Eakin et al. 2010; Hoegh-Guldberg and Bruno 2010; Kleypas et al. 1999; Soto Ramos et al. 2011). Widespread coral bleaching and mortality are linked to anomalously warm water driven by El Niño Southern Oscillation events (Baker et al. 2008; Goreau et al. 2000; Goreau and Hayes 1994). Reductions in coral cover of key reef-building species is changing the biodiversity in these ecosystems, and reducing critical habitat for many marine species including reef fishes (Goreau et al. 2000; Somerfield et al. 2008; Soto Ramos et al. 2011; Vega-Rodriguez et al. 2015). Thus, loss of reef services (e.g., tourism and recreational activities) due to decreased coral cover and biodiversity has been estimated to be approximately US $4–$24 billion annually (Chen et al. 2015).

Building stronger coral reef management strategies requires identifying regional stressors (e.g., SST, decreased water quality due to coastal erosion or runoff) and evaluating them in the context of species-specific responses and reef connectivity (Aswani et al. 2015). Satellite-based observations have successfully provided inexpensive real-time data used to enhance our understanding of coral reef dynamics. Extensive reviews cover remote sensing methods and applications for coral reef observations and monitoring (Eakin et al. 2010; Goodman et al. 2013; Hedley et al. 2016; Hochberg 2011). Specifically, satellite-derived products have been used to monitor and forecast global coral bleaching and mortality, map global distributions of coral reef habitats, provide synoptic views of large-scale oceanographic processes, and evaluate changes in water quality.

Management applications

Satellite observations, combined with local in situ time series of bio-geochemical observations and forecasting models, are required for better support of ecosystem based Management (EBM) initiatives (IOCCG 2009; Lorenzoni and Benway 2013; Sherman et al. 2011; Stuart et al. 2011). For example, newly derived thermal stress products (e.g., bleaching alert areas; Fig. 2) were developed by the National Oceanic and Atmospheric Administration (NOAA) Coral Reef Watch Program (Liu et al. 2014) in response to coastal and reef manager needs. NOAA's next-generation of daily global geostationary and polar-orbiting SST images reliably monitor thermal-stress conditions on 95% of reefs worldwide (Liu et al. 2014). These operational and freely accessible products have been incorporated into the monitoring and management efforts of the NOAA Coral Reef Conservation Program, the states of Florida and Hawaii, The Nature Conservancy, Guam, and the Commonwealth of the Northern Mariana Islands, among others (Liu et al. 2014). In the Florida Keys, these products are frequently used as part of the Coral Bleaching Early Warning Network conditions reports (Walter 2015). Based on satellite SST products, prediction-based models have been integrated within early warning systems in Australia and are used to understand and target increased incidence of coral disease outbreaks (Maynard et al. 2011). These models, combined with volunteer-based ground-truth monitoring networks, help management responses to succeed. Additionally, acute changes in the coastal water quality that surrounds coral reefs could potentially alter reef health. The impact of sediment plumes, another concern for reef managers, has been associated with increased incidence of coral disease (Pollock et al. 2014). The extent of sediment plumes, caused by dredging activities or river discharge, has been estimated along coastal areas and nearby reefs using freely accessible high spatial-resolution and

Table 1 Satellite sensors discussed in this review and their specifications

Sensor	Free to Public?	Spatial resolution	Spectral resolution	Temporal resolution	Years of available data	Management uses	Data source
ALOS	Yes	2.5–10 m	6 bands: Vis, IR, MW	46 days	2006–2011	Wetlands, aquaculture	https://earth.esa.int/web/guest/home
AMSR-E	Yes	6–75 km	6 bands: MW	3 days	2002–2011	Public health	https://giovanni.sci.gsfc.nasa.gov/giovanni/
ASAR	Yes	30 m	1 band: MW	35 days	2002–2012	Wetlands, aquaculture	https://earth.esa.int/web/guest/home
AVHRR series	Yes	1.1 km	4–5 bands: Vis, IR	1 day	1978–present	Fisheries, aquaculture, corals	https://earth.esa.int/web/guest/home
CZCS	Yes	825 m	6 bands: Vis, IR	1 day	1978–1986	Fisheries	https://oceancolor.sci.gsfc.nasa.gov/
GOCI	Yes	500 m	8 bands: Vis	8 images per day	2010–present	Water quality	https://oceancolor.sci.gsfc.nasa.gov/
IKONOS	Some	1–4 m	5 bands: Vis, IR	3 days	1999–present	Wetlands	https://earth.esa.int/web/guest/home
Landsat series	Yes	15–120 m	Up to 11 bands: Vis, IR	16–18 days	1972–present	Wetlands, corals, water quality, aquaculture	https://landsatlook.usgs.gov/
MERIS	Yes	300 m–1.2 km	15 bands: Vis, IR	3 days	2002–2012	Wetlands, corals, water quality, aquaculture	https://oceancolor.sci.gsfc.nasa.gov/
Meteosat series	Yes	1–5 km	Up to 12 bands: Vis, IR	Up to 15 minutes	1977–present	Fisheries	http://www.eumetsat.int/website/home/Data/index.html
MODIS	Yes	250 m–1 km	36 bands: Vis, IR	1–2 days	2000–present	Corals, water quality, aquaculture	https://giovanni.sci.gsfc.nasa.gov/giovanni/
OMI	Yes	24 km	740 bands: Vis, UV	1 day	2004–present	Public health	https://giovanni.sci.gsfc.nasa.gov/giovanni/
QuickBird	Some	0.6–2.9 m	5 bands: Vis, IR	1–3 days	2001–present	Wetlands	https://earth.esa.int/web/guest/home
SeaWiFS	Yes	1 km	8 bands: Vis	1 day	1997–2010	Water quality, public health, aquaculture	https://giovanni.sci.gsfc.nasa.gov/giovanni/
Sentinel-2	Yes	10–60 m	13 bands: Vis, IR	5 days	2015–present	Wetlands	https://earth.esa.int/web/guest/home
SSMI	Yes	15–69 km	4 bands: MW	1 day	1987–present	Aquaculture	http://www.remss.com/missions/ssmi
SPOT-5	No	2.5–20 m	5 bands: Vis, IR	2–3 days	2002–2015	Wetlands, aquaculture	https://www.spot-take5.org/client/#/home
WorldView-2	Some	0.5–2 m	9 bands: Vis, IR	1–3 days	2009–present	Wetlands	https://earth.esa.int/web/guest/home

Note: Some data sources require user registration or additional criteria

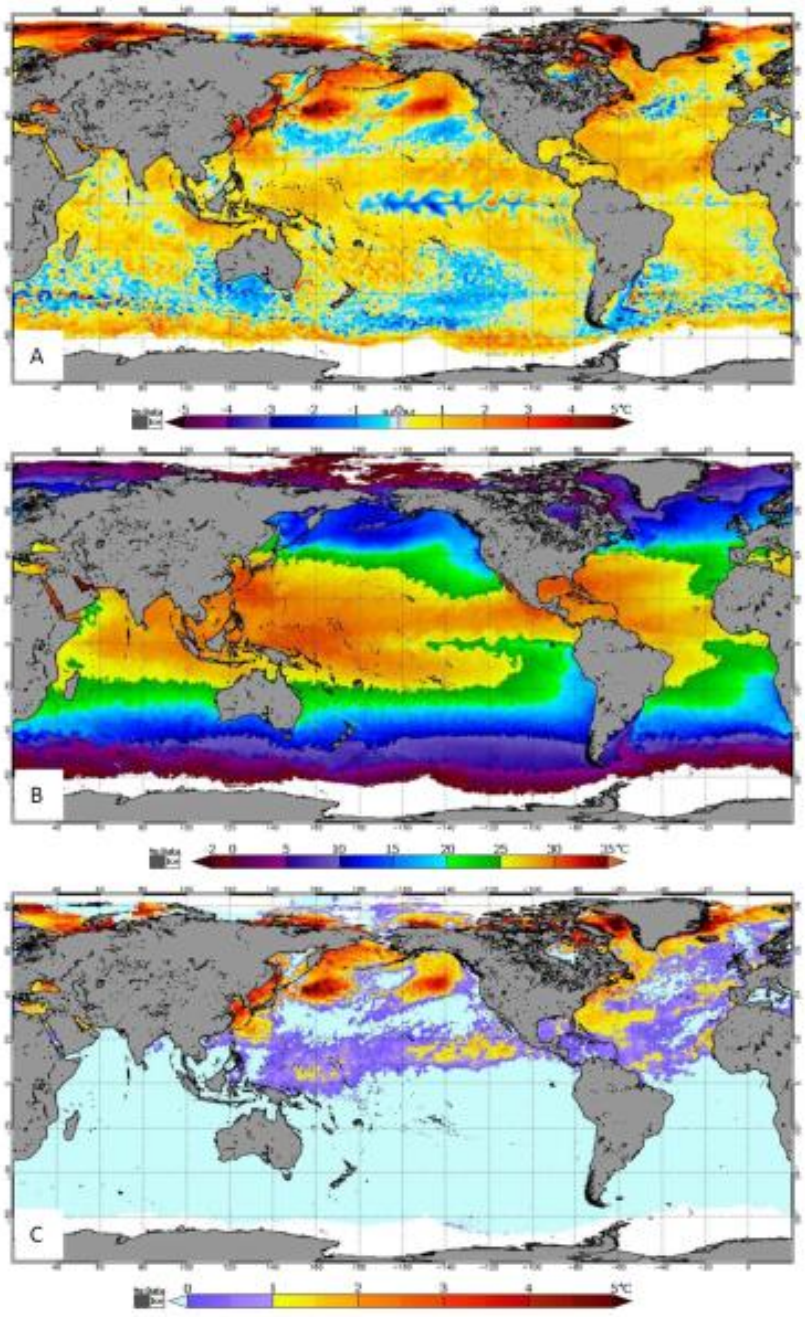

Fig. 2 NOAA Coral Reef Watch 5-km spatial-resolution thermal-stress products for August 22, 2016: **a** SST anomaly, **b** SST, and **c** Coral Bleaching Hot Spots (https://coralreefwatch.noaa.gov/satellite/index.php)

temporal-resolution remote sensing data from sensors such as the Moderate Resolution Imaging Spectroradiometer (MODIS) and Landsat (Barnes et al. 2015; Evans et al. 2012).

The combination of high spatial-resolution satellite imagery (e.g., IKONOS) with aerial photography and Light Detection And Ranging data, which uses multiple returns of laser surveying to build digital elevation models, has led to the creation of accurate benthic habitat maps for Caribbean reefs, including some endangered stony coral species (e.g., *Acropora spp.*) (Wirt et al. 2015). Researchers at the Florida Fish and Wildlife Commission successfully used these habitat maps to identify the distribution of *A. palmata* and *A. cervicornis* in the Florida and Caribbean regions and to identify areas of suitable substrate for *Acropora* spp. coral larvae settlement (Wirt et al. 2015). Satellite-derived data have also been used to identify and manage marine protected areas, which include important reefs. For example, in Brazil, proxies for habitat quality derived from satellite observations (e.g., thermal stress, sedimentation) combined with high-resolution coral-reef habitat maps derived from Landsat images were used to select priority reef-conservation areas (Magris et al. 2015).

Wetlands

Global wetlands are estimated to be worth billions of dollars for their ecosystem services (i.e., the direct and indirect contributions of ecosystems to human well-being). These include commercial-fish and recreational-fish habitat and nurseries, nutrient and suspended-solid filtration and removal, flood protection, erosion control, recreation, aesthetics, and other cultural values (Dahl and Stedman 2013; Ozesmi and Bauer 2002; Turner and Gannon 2014). Wetlands are, in fact, the only ecosystem covered by a global treaty—the Ramsar Convention on Wetlands, signed in 1971. Despite their significance, the areal extent of wetlands declined substantially in the 20th century as a result of development, pollution, and sea-level rise, among other contributors (Dahl and Stedman 2013; Raabe et al. 2012).

In response, management agencies around the world have identified wetland restoration and conservation as priority goals, and many have employed remote sensing technologies to help achieve those goals. In fact, the use of aerial-based imagery for wetland management is relatively well-established (see Green et al. 1996 for a review of aerial and early satellite sensor applications). Recent advances, however, in the spatial, spectral, and temporal resolutions of satellite-based sensors, as well as declining costs associated with data acquisition and processing, have increased the viability of satellite sensors as wetland-management tools (see Heumann 2011, for a comprehensive summary of satellite sensors available through 2010 and their applicability for mapping mangroves).

Management applications

The following management needs have been served through remotely sensed data: mapping at site, basin, and global levels; inventory and baseline assessment; status and trends assessment; monitoring and reporting; and management planning and implementation (MacKay et al. 2009). Mapping wetlands is considered "critical for practical management and decision-making purposes" (MacKay et al. 2009), and many studies have employed satellite data for mapping purposes (Giri et al. 2011; Jia et al. 2014; MacAlister and Mahaxay 2009; McCarthy et al. 2015). Using Landsat imagery, MacAlister and Mahaxay (2009) successfully mapped wetlands of the Lower Mekong Basin in Southeast Asia. They identified 31 wetland and 23 non-wetland categories in five pilot study areas. Images were classified using the common Maximum Likelihood approach to a minimum mapping unit of 60 m. Field surveys were used to assess their classification accuracy, which ranged from 77.2–93.8% across the five sites. The maps are now in use for resource and conservation planning at provincial and national levels in the countries of Laos, Cambodia, and Vietnam. They have also been used for Ramsar site delineation, water-use planning, fire and water strategies, and site conservation management plan development (MacAlister and Mahaxay 2009).

Herrero and Castañeda (2009) used Landsat imagery to map, delineate, and monitor wetlands. They evaluated small (<2 to >200 ha) saline wetlands in northeastern Spain with 52 Landsat images from 1984–2004. Unsupervised classification methods were combined with field observations to identify five soil surface covers in each image. These were used to determine the conservation status, limits and functions of 53 wetlands. They found that 60% of the habitats were highly vulnerable to a variety of environmental and anthropogenic stressors, including agricultural intensification, waste dumping, and loss of native vegetation. Landsat imagery proved useful not only for the consistent and comprehensive assessment of wetland conditions, but also for its ability to fill historical gaps of scarce field records (Herrero and Castañeda 2009).

Dabrowska-Zielinska et al. (2009) demonstrated the use of both visible-light and microwave remote sensing data to monitor wetlands. They studied the Biebrza Wetlands in northeastern Poland—a Ramsar test site, and one of the largest wetland ecosystems in Europe. This fragile ecosystem has been intensively drained by development ventures in recent years, but is a target area for restoration and conservation. In order to develop a management strategy, managers needed the remaining wetlands to be mapped, and

the marshland habitats characterized. Due to the size, isolation, and challenging terrain, traditional field survey methods were not feasible. The circumstances provided an opportunity for researchers to explore new ways to map wetlands while fulfilling a fundamental wetland-management requirement. Data from multiple microwave-range and visible-range satellite sensors were compared to determine the best vegetation indices for distinguishing marshland vegetation classes remotely. The authors concluded that the Enhanced Vegetation Index (EVI) and Global Environmental Monitoring Index from SPOT VEGETATION, and the EVI from ENVISAT MERIS were most effective in identifying marshland habitat classes. The Leaf Area Index derived from microwave Advanced Synthetic Aperture Radar data was also used for soil moisture estimation, and proved effective even under cloudy conditions when optical data was not useful. The results of this study showed that relatively coarse resolution imagery could be successfully used for identifying and characterizing sufficiently large wetland habitats to be managed, and for monitoring changes in wetland vegetation caused by soil moisture and humidity changes that result from anthropogenic wetland drainage.

Water Quality

Routine coastal water-quality monitoring is carried out in the field by management agencies but is often costly and labor intensive (Bierman et al. 2011). Due to cost constraints, sampling stations may only represent a small portion of the water body and can only provide a snapshot of water quality conditions in one location at one point in time. Herein, remotely sensed water quality is defined as the simultaneous measurement of three color-producing agents that contribute to the overall "color" of a water body: chlorophyll-a (Chla), suspended minerals, and colored dissolved organic matter (CDOM). These parameters absorb and scatter light in the water column to a degree that can be measured from space (Bukata 2005). They have unique optical signatures in terms of scattering and absorption, which allows for their relative contributions to the overall color of the water to be differentiated. Chla, a proxy for the biomass of algal particles (phytoplankton), is a fundamental parameter in the study of coastal water quality and can indicate increased nutrients in a water body (Bukata 2005; Devlin et al. 2011; Schaeffer et al. 2012). CDOM is defined as the colored portion of the pool of dissolved organic carbon (Blough and Del Vecchio 2002).

Water clarity is another parameter of interest in coastal water-quality management related to light absorption and scattering by mineral particles. Often reported as turbidity or total suspended sediments, water clarity is a measure of reduced light penetration within the water column, which may lead to degraded water quality that can impact the productivity and health of coastal ecosystems (Cloern et al. 2013; May et al. 2003; Wofsy 1983). As an example for Tampa Bay, FL, three constituents (CDOM, turbidity, and Chla) can be simultaneously assessed with the MODIS sensor using the methods of Chen et al. (2007a, b) and Le et al. (2012), respectively. It is important to note that these approaches, particularly for Chla, are quite localized and cannot be broadly applied to a variety of environments.

Management applications

Satellite observations have been used to assess and monitor coastal water-quality in numerous studies. "Black water" events in southwest Florida were observed using MODIS and Sea-viewing Wide Field-of-View Sensor (SeaWiFS) data by Zhao et al. (2013). A study by Thompson et al. (2014) discovered marked seasonal variability in water quality on the Great Barrier Reef in Australia using data from the MODIS sensor. Barnes et al. (2013a) used data from the Landsat and MODIS sensors to investigate historical changes in water quality in the Florida Keys from the 1980's until present. Using the recently launched GOCI, Jang et al. (2016) developed water quality indices for coastal areas in Korea. The technology exists for the remote sensing community to provide useful, synoptic measurements of relevant water quality indicators to managers (Bukata 2005), but these products are currently underutilized in an operational manner (Schaeffer et al. 2013).

To assist managers in assessing water quality conditions, a decision-support tool for Tampa Bay, Florida was developed by Le et al. (2013) using a satellite-based Water Quality Decision Matrix (WQDM). Based upon previously established targets and thresholds of water clarity and Chla concentration (Janicki et al. 2000), satellite-derived indices of these two parameters were used to create the WQDM, which tracks annual mean water-quality conditions to help inform managers when making decisions. A "*green*" color in the WQDM indicates "good" conditions requiring no direct action by managers. A "*yellow*" color indicates that one of the two water quality indices has exceeded its threshold by more than one standard deviation. *Yellow* conditions indicate that managers should be alert to changing conditions. A "*red*" condition exists if both water quality indices exceed their thresholds by over two standard deviations and indicates poor water quality conditions. If "*red*" conditions persist for two consecutive years, management action is required (Fig. 3). While these WQDM matrices are produced on an annual basis in Tampa Bay Estuary Program reports largely based on in-situ data, satellite-based water quality data that may be used to derive them can be found at the University of South Florida Optical Oceanography

Year	OTB	HB	MTB	LTB
1998	Yellow	Yellow	Red	Yellow
1999	Green	Green	Green	Green
2000	Green	Green	Green	Green
2001	Green	Green	Yellow	Yellow
2002	Green	Green	Yellow	Green
2003	Red	Yellow	Red	Yellow
2004	Red	Yellow	Yellow	Yellow
2005	Green	Green	Yellow	Yellow
2006	Green	Green	Green	Green
2007	Green	Green	Green	Green
2008	Green	Green	Green	Green
2009	Green	Green	Green	Green
2010	Yellow	Green	Green	Green
2011	Green	Green	Green	Green

Year	OTB	HB	MTB	LTB
1998	Yellow	Yellow	Red	Red
1999	Green	Green	Yellow	Green
2000	Green	Green	Green	Green
2001	Green	Green	Yellow	Yellow
2002	Green	Green	Yellow	Green
2003	Red	Red	Red	Yellow
2004	Yellow	Yellow	Yellow	Yellow
2005	Green	Yellow	Yellow	Yellow
2006	Green	Green	Green	Green
2007	Green	Green	Green	Green
2008	Green	Green	Green	Green
2009	Green	Green	Green	Green
2010	Green	Green	Green	Green
2011	Green	Green	Green	Green

Fig. 3 Table 4 from Le et al. (2013) comparing annual mean water-quality conditions in four sections of Tampa Bay, Florida based on indices derived from (*left*) historical field data, and (*right*) satellite data. *OTB* Old Tampa Bay, *HB* Hillsborough Bay, *MTB* Middle Tampa Bay, *LTB* Lower Tampa Bay

Laboratory website (http://optics.marine.usf.edu/projects/vbs.html).

Public Health

Remote sensing techniques have been widely applied in coastal areas to assess public health concerns (Glasgow et al. 2004; Hay 2011). Global air pollution is one of the most critical environmental health risks, estimated to cost 2 million premature deaths, and it is largely due to enhanced anthropogenic activities such as burning fossil fuels (Wigbels 2011). Global observations of air pollutants such as aerosols, tropospheric ozone, tropospheric nitrogen dioxide, carbon monoxide, formaldehyde, and sulfur dioxide are now widely available (Paciorek and Liu 2009; Wang et al. 2015). Among air pollution variants, airborne dust carrying heavy metals, and particulate matter (PM) is considered one of the most harmful (Yan et al. 2015). Urban air pollution is one of the top 15 causes of death and disease globally, and it is always ranked in the top 10 for high-income countries (Bechle et al. 2013). Reliable predictions of public health risks such as heat waves, extreme and prolonged heat episodes, atmospheric ozone, dust and other aerosols that trigger asthmatic responses are vital to improving public health (Shamir and Georgakakos 2014).

Additionally, vector-borne diseases (VBD) such as those carried by mosquitoes, ticks, and flies are currently responsible for more deaths in humans than all other causes combined (Kalluri et al. 2007). Improved methods are required for forecasting, early warning systems, prevention, and control of VBD due to the increasing trend of large-scale epidemics such as malaria, dengue, and chikungunya (Chuang et al. 2012).

Management applications: Air pollution

Remotely sensed estimations of aerosols could lead to better assessments of air quality, particularly in suburban and rural areas that are often far from in-situ sensors (Basly and Wald 2010; Bechle et al. 2013; Malakar et al. 2014). For example, satellite-based observations of nitrogen dioxide from the Ozone Monitoring Instrument provide reliable measurements of ground-level nitrogen-dioxide exposure within a large area (Bechle et al. 2013). Additionally, researchers at the Hong Kong Polytechnic University used remote sensing and in-situ data to assess dustfall distribution in urban areas (Yan et al. 2015). Yan et al. (2015) showed that construction sites and low-rise buildings with inappropriate land-use were two main sources of dust pollution. This technique offered a low-cost and effective method for monitoring and managing dustfall in an urban environments.

In Spain, the Ministry of Agriculture and Fisheries, Food, and Environment, and the National Weather Agency have adopted the forecasts of dust surface concentration and dust optical depth released by the Barcelona Dust Forecast Center (BDFC). The BDFC is the first Regional Specialized Meteorological Centre specializing in atmospheric sand and dust forecasting, as designated by the World Meteorological Organization. It produces dust forecasts for Northern Africa, the Middle East and Europe (http://dust.aemet.es/news/dust-forecasts-available-on-the-wmo-website). Additionally, the Government of the Hong Kong Special Administrative Region, China Meteorological Authority, and Japan Meteorological Authority have adopted maps of dust pollution for monitoring and management, including the development of several tools based on satellite imagery for monitoring sand and dust weather (Sand and Dust Storm Warning Advisory and Assessment System).

Previous studies suggest that oceanic harmful algal bloom toxins can either be released into the air or accumulate in shellfish, leading to public health concerns such as asthma, ciguatera and paralytic, neurotoxic, amnesic and diarrhetic shellfish poisoning (Backer 2002, 2003, 2005; Fleming et al. 2007; Pitois et al. 2000; Randolph et al. 2008; Van Dolah 2000). Along the West Florida Shelf, blooms of *Karenia brevis* have been studied using Chla and fluorescence line height (FLH) remote sensing products derived from SeaWIFS and MODIS satellites (Hu et al. 2007; Soto Ramos et al. 2017; Stumpf et al. 2003). Satellite-derived SST, FLH, and Chla provide the tools for large-scale, early warning identification and mitigation techniques to reduce risks due to these blooms.

Management applications: Heat vulnerability

To better manage heat-related health risks, information is required on the intra-urban variability of vulnerability to heat wave events (Wolf and McGregor 2013). In Brisbane, Australia, MODIS Land Surface Temperature data were used to examine the impact of temperature on childhood pneumonia (Xu et al. 2014). Mohan and Kandya (2015) investigated the effect of urbanization on the land surface temperature in India by using Terra and Aqua MODIS land surface data obtained from the Monsoon Asia Integrated Regional Study program. They called for strong and urgent heat-island mitigation measures after finding that the level of human mortality risk remained high during a prolonged extreme heat episode. This type of information has been widely used to determine heat vulnerability in different cities around the world, primarily in continental areas and mid-latitudes such as London, Toronto, Rome, Florence, Philadelphia, and Chicago (Bao et al. 2015; Morabito et al. 2015; Rinner and Hussain 2011; Wolf and McGregor 2013).

Management applications: VBD

The use of satellite data for epidemiological purposes, including characterizing the environments in which vectors thrive, has improved our ability to determine disease distributions, their impacts on populations, and their changes through time (Buczak et al. 2012; Garni et al. 2014; White-Newsome et al. 2013; Young et al. 2013). Variability in environmental components, such as temperature and precipitation, has important influences on mosquito life cycles. Understanding the spatial and temporal patterns of mosquito populations is critical for control and prevention of VBD (Chuang et al. 2012). Research conducted by South Dakota State University from 2005 to 2010, used NASA's Advanced Microwave Scanning Radiometer (AMSR-E) and in-situ weather station data to successfully identify environmental metrics (e.g., air and SST, humidity, and rainfall) and better predict population dynamics of mosquitoes *Aedes vexans* and *Culex tarsalis* while improving the effectiveness of mosquito-borne disease early warning systems (Chuang et al. 2012; Méndez-Lázaro et al. 2014).

Satellite sensors provide information about a wide variety of water parameters (e.g., SST, water clarity, Chla estimates, and FLH) that can be used to understand spatiotemporal variations of vector-borne and water-borne diseases (Colwell 1996; Ritchie et al. 2003; Rodó et al. 2013). Cholera thrives in warmer waters (Colwell 2004; Epstein et al. 1993; Huq et al. 1984); therefore a combination of remote-sensing techniques and historical cholera-case data, can enable researchers to understand patterns in Cholera outbreaks. Lobitz et al. (2000) used satellite-derived SST to assess how increased water temperatures were related with increased numbers of cholera cases in coastal areas (Pascual et al. 2000; Speelman et al. 2000).

These activities have led to improvements in health management within coastal areas, especially by creating early warning systems to decrease outbreaks on coastal communities (Ho et al. 2005; Rose et al. 2001). For example, Anyamba et al. (2009) were able to produce risk-mapping models using satellite-derived SST, rainfall, and a vegetation index to accurately predict the location and timing of Rift Valley Fever activity with a 2 to 6 week period of warning for the Horn of Africa that facilitated disease-outbreak response and mitigation activities. Further, Malaria Early Warning Systems use transmission risk indicators, such as unusually elevated rainfall, to predict the timing and severity of a malaria epidemic 2 to 4 months in advance (Thomson et al. 2005; World Health Organization 2001). Early detection of the outbreaks has allowed early activation of vector control and the implementation of other effective control measures (Kiang 2009; Lee et al. 2010; Lowe et al. 2011; World Health Organization 2001).

Fisheries and Aquaculture

There is currently a global food shortage, and therefore a need for enhanced food production (FAO 2015). A potential solution to this problem involves improving fisheries management, and the expansion of sustainable aquaculture from small-scale family practice to a highly commercial industry. To expand this renewable, rapid-growth resource, the industry needs to overcome substantial bio-physical, socio-economical, and spatiotemporal constraints (IOCCG 2009; Nath et al. 2000). The application of remote sensing and geographical information systems, in addition to traditional data and methods, may substantially improve the ability of managers to address these constraints (Meaden and Aguilar-Manjarrez 2013). Remote sensing offers a useful suite of tools that can rapidly monitor aquatic environments in terms of physical water-quality parameters (e.g., sea-surface temperature, sea-surface salinity, sea-level rise, turbidity, currents, CDOM, ice coverage, bathymetry, red tides, and oil spills), and biological processes (e.g., Chla and net primary productivity), and support facilities that influence fisheries and aquaculture planning.

Management applications: Fisheries

SST observations are used to identify areas of upwelling (nutrient-rich deeper waters brought to the surface), which drive primary production and support productive fisheries (Muller-Karger et al. 2001; Rueda-Roa 2012). Fisheries managers rely on these remote-sensing products to predict fish aggregations in space and time, and to manage marine fishery resources (Santos and Miguel 2000; Lindo-Atichati et al. 2012; Habtes 2014). The search time of some US commercial fisheries is reduced by 25–50% due to the use of satellite-derived fishery aid charts (Santos and Miguel 2000). Several early studies of fisheries used the Advanced Very High Resolution Radiometer (AVHRR) and Coastal Zone Color Scanner satellite sensors to aid in monitoring tuna off of the California coast (Bakun 2006; Fiedler 1983; Laurs et al. 1984). The migration, distribution, availability, and catchability of tuna are influenced by oceanographic conditions (Laurs et al. 1984; Lindo-Atichati et al 2012). Tuna tend to aggregate along the coast near surface frontal boundaries that are associated with coastal upwelling along the central California coast. Upwelling intensity was identified via SST images from AVHRR. Fiedler (1983) studied tuna that were caught when upwelling was not constant. He found that tuna was grouped based on distance to the upwelling filaments, and the mean length and stomach volume increased with distance away from the upwelling filament. The diet of the tuna that were caught closest to the upwelling filament indicated that juvenile anchovies were in high abundance in this area as well, which helped define the limits of the spawning activity of the anchovy. Managers may use remotely sensed upwelling observations to predict the prevalence and catchability of tuna and anchovy populations in coastal regions.

The recruitment of octopi is also influenced by environmental indices such as coastal upwelling (Faure et al. 2000). Faure et al. (2000) studied the relationship between octopus recruitment and environmental indices, both of which fluctuate annually and seasonally off the Mauritanian coast. This study utilized the Meteosat sensor for SST data, and obtained wind turbulence data from the Comprehensive Ocean Atmosphere Data Set. The Mauritanian coast experiences trade winds that generate seasonal upwelling from October to June, with maximum upwelling from January to May (Faure et al. 2000). Faure et al. (2000) found that spawning takes place in and out of upwelling seasons. It was discovered that upwelling and wind-induced turbulence were linear and positive with summer recruitments, confirming that coastal upwelling primarily contributes to the summer recruitment variability of octopi. High-intensity upwelling events combined with wind turbulence create a high encounter rate between food and larvae, which favors larvae survival. Fisheries managers may use this information to identify favorable conditions for reproduction in similar fashion to commercial operations like Roffer's Ocean Fishing Forecast Service, Inc. (https://www.roffs.com/), which processes SST and other satellite-derived data to produce maps guiding fishermen to productive grounds.

Management applications: Aquaculture

The top priority for sustainable aquaculture development is appropriate site selection. The process of selecting sites where natural conditions suit the cultured fish species and the impact on the surrounding environment is minimized may be substantially improved with the use of remote sensing tools and techniques (Alexandridis et al. 2008; Boyd and Schmittou 1999; IOCCG 2009; Radiarta and Saitoh 2008). Mustapha and Saitoh (2008) demonstrated the utility of remote sensing data for scallop aquaculture site selection in Japan along Funka Bay, Hokkaido by using Special Sensor Microwave Imager microwave and SeaWiFS data of ice cover and wind stress that affect the spring bloom. Others have used MODIS, SeaWiFS, and Advanced Land Observing Satellite data sets of SST, Chla, turbidity, suspended solids, and bathymetry for site selection mapping (Radiarta and Saitoh 2008; Radiarta and Saitoh 2009). Suitability modeling of the data revealed that about 83% of the bay area has optimum conditions for scallop culture (Radiarta and Saitoh 2009).

Bivalve aquaculture tended to be practiced close to the coastline where suspended PM supports phytoplankton

(Dowd 2005; Noren et al. 1999). Thomas et al. (2006) evaluated the carrying capacity of the mussel-cultured areas in the Mont St. Michel Bay, France, as well as discovering new, potential sites using daily SeaWiFS imagery. Modeling the Chla and SST data derived from the sensor and verified on the ground resulted in maps of prediction scenarios for mussel production. In New Zealand, the aquaculture of suspended mussels was practiced in the Bay of Plenty. A series of studies using AVHRR images, and SeaWiFS images for SST and Chl-a, respectively, identified the most productive regions based on bathymetry, currents, and upwelling conditions (Longdill et al. 2007; Longdill et al. 2008a, b, c). After multiplying the normalized monthly climatological anomalies of SST and Chla together, all layers were converted to 200 m^2 spatial resolution excluding the locations more than 30 km from the coast or deeper than 100 m. The output models were subjected to multi-criteria evaluation techniques to achieve the best sustainable management plan for the mussel culture (Aguilar-Manjarrez 1996; Arnold et al. 2000; Carrick and Ostendorf 2007; Vincenzi et al. 2006). The results of Longdill et al. (2008c) showed that only 18% of the bay area was classified as most suitable for mussel aquaculture, and 46% was classified as unsuitable (Fig. 4).

Coastal aquaculture has increased rapidly in recent years all over the world, as has interest in monitoring such practices. In 2007, South Africa launched a satellite designed to track aquaculture production and to predict fish yield. The 15 m spatial resolution, hyperspectral satellite named Multi-sensor Microsatellite Imager has 200 spectral channels, and a revisit time of 10 days (Steyn 2010; Quansah et al. 2007). Delineating aquaculture coasts is difficult when using traditional automated mapping methods due to the spectral similarities between aquaculture regions and ocean. However, a process called object-based region growing integrated with edge detection (OBRGIE) was achieved to delineate aquaculture coastlines by Zhang et al. (2013). The OBRGIE method was found to be much more effective than the spectral attribute in separating land and sea in aquaculture coasts of the Bohai Sea in Northern China and Zhujiangkou Estuary in Southern China using Landsat and SPOT-5 multispectral images, respectively.

Challenges

Many challenges in the interpretation of satellite data for coastal-management applications remain. For example, cloud cover interferes with visible light, and therefore hampers the use of imagery collected in the visible and infrared range of the electromagnetic spectrum. This issue may be avoided, depending on the research application, by using imagery collected in the microwave range of the

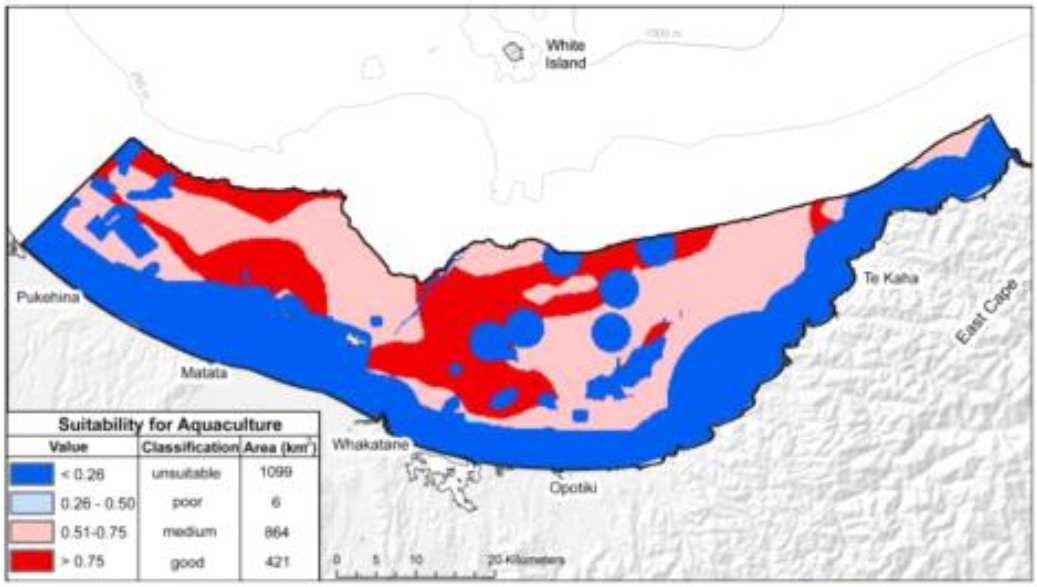

Fig. 4 Suitability map for offshore bivalve aquaculture in the Bay of Plenty, New Zealand (Longdill et al. 2008c). Suitability determination incorporated SST and Chl-a estimates from AVHRR and SeaWIFS sensors

electromagnetic spectrum because it is not affected by cloud cover (Dabrowska-Zielinska et al. 2009), or by using imagery with high temporal-resolution (i.e., frequent repeat times), which may provide more opportunities for acquiring cloudless imagery. Also, variability in the concentration and type of light-absorbing aerosols is quite high in the coastal zone, a problem that can easily confound existing approaches to atmospheric correction. Therefore, accurate atmospheric correction is vital to the generation of usable remote sensing products.

In addition to atmospheric corrections, reflectance from the seafloor in coastal shallow areas has to also be removed from remotely sensed data when studying properties of the water column itself. Algorithms designed to estimate Chla concentration from satellite data, for example, rely on the use of spectral bands in the visible portion of the spectrum where light readily penetrates the water and reflects off the bottom (Bukata 2005). The removal of bottom contribution to satellite images, specifically for optically clear waters, continues to be a difficult task, although important advances have been made (Barnes et al. 2013b). One solution is to simply mask or eliminate areas shallower than a specific depth using bathymetry data.

When mapping wetlands and other coastal habitats, tides and other water level variations must be accounted for, especially when comparing images acquired at different times of day or year (McCarthy and Halls 2014). Maps of submerged and intertidal vegetation may be especially affected by variations in water level, as well as by water column components (i.e., suspended sediments, phytoplankton, and dissolved organic matter). Ideally, time series images will be selected with acquisition times that coincide with identical water levels. Accurate water levels are necessary to account for these variations. More broadly, we recommend that accuracy assessments of any satellite-derived product be gathered either ad hoc by data users, or from data providers upon request.

Many coastal management studies have utilized the freely available MODIS, SeaWiFS, AVHRR, Landsat imagery, which includes several decades of continuous data coverage, and offers a medium-spatial to high-spatial resolution that affords near-global coverage of land areas every year. Higher spatial-resolution commercial imagery, such as that from IKONOS, QuickBird, and WorldView-2, has been used for local/regional coastal resource case studies, but it may be cost-prohibitive to expand the use of such imagery to larger study areas for now (Alexandridis et al. 2008; Belluco et al. 2006; Chust et al. 2008; IOCCG 2009; Ghioca-Robrecht et al. 2008; McCarthy and Halls 2014; McCarthy et al. 2015). Nevertheless, MacKay et al. (2009) noted that, for wetland mapping, high-spatial resolution imagery (i.e., 1–4 m resolution) is likely more useful than high-spectral and medium-spatial (i.e., 10–30 m) resolution imagery due to the small, heterogeneous spatial structure of wetlands worldwide.

For many applications of remote sensing data to management goals, additional interdisciplinary research between coastal managers and environmental scientists is needed. Web-based portals are emerging as powerful platforms for managers, scientists, and the public to obtain historical and near-real time satellite data. Despite discussions on shared regional governance of living marine resources (Chakalall et al. 2007; Fanning et al. 2009), limited integrated environmental data analysis and visualization tools exist for the US territories and international community. Local management initiatives for the sectors discussed here, among others, could benefit from readably accessible online portals, such as NOAA's Coral Reef Watch website (https://coralreefwatch.noaa.gov/satellite/index.php; Cho 2005; Ortiz-Lozano et al. 2007).

Conclusions

As the global population continues to rise and concentrate along coasts, current approaches to managing coastal resources require updating. Successful management requires local interventions coordinated across ecologically appropriate spatial scales, and is best guided by frequent and synoptic sampling and monitoring (Sale et al. 2014). This work reviews recent, demonstrated applications of remote sensing technology for management of coral reefs, wetlands, water quality, fisheries and aquaculture, and public health. Challenges to the use of remote sensing data for these purposes have been addressed here, and must be considered before implementing these approaches for coastal-resource management. Space-based remote sensing tools enhance the ability of coastal-resource managers to keep pace with increasing population-pressure on coastal resources, and improve climate change adaptation strategies. We encourage coastal managers to take advantage of this technology to supplement traditional management approaches toward the goal of preserving both human and ecosystem health.

Acknowledgements This manuscript is a contribution to the Marine Biodiversity Observation Network. Funding for this work was provided by the National Aeronautic and Space Administration (NASA) Earth and Science Fellowship Program (grant numbers NNX12AN94H and NNX15AN60H), the National Science Foundation FG-LSAMP Bridge to the Doctorate (HRD #0929435), the National Science Foundation Partnerships for International Research (PIRE) (grant number 1243510), the Environmental Protection Agency Science To Achieve Results (grant number 83519301O), NASA's Airborne Science program for UAS Enabled Earth Science Program (grant number NNH10ZDA001NRA-UAS), NASA and the National Oceanic and Atmospheric Administration (NOAA) Integrated Ocean Observing System (IOOS) Program Office (grant number

NNX14AP62A), the National Science Foundation (grant number AGS-278 1444755), the University of South Florida (USF) College of Marine Science Bridge to the Doctorate Endowed & Alfred P. Sloan Fellowships, the USF Dissertation Completion Fellowship, the Linton Tibbetts Endowed Fellowship, the Sanibel Captiva Fellowship, and the 2016 Gulf Oceanographic Charitable Trust Fellowship. This paper is a result of research funded by the National Oceanic and Atmospheric Administration's RESTORE Act Science Program under award NA15NOS4510226 to The University of Miami.

Compliance with Ethical Standards

Conflict of Interest The authors declare that they have no competing interests.

References

Aguilar-Manjarrez J (1996) Development and evaluation of GIS-based models for planning and management of coastal aquaculture: A case study in Sinaloa. Dissertation, University of Stirling

Alexandridis TK, Topaloglou CA, Lazaridou E, Zalidis G (2008) The performance of satellite images in mapping aquacultures. Ocean Coast Manage 51:638–644

Anyamba A, Chretien JP, Small J, Tucker CJ, Formenty PB, Richardson JH, Britch SC, Schnabel DC, Erickson RL, Linthicum KJ (2009) Prediction of a Rift Valley fever outbreak. P Natl Acad Sci USA 106:955–959

Arnold WS, White MW, Norris HA, Berrigan ME (2000) Hard clam (Mercenaria spp) aquaculture in Florida USA: geographic information system applications to lease site selection. Aquacult Eng 23:203–231. doi:101016/S0144-8609(00)00042-X

Aswani S, Mumby PJ, Baker AC, Christie P et al. (2015) Scientific frontiers in the management of coral reefs. Front Marine Sci 2 (50):1–13

Backer LC (2002) Cyanobacterial harmful algal blooms (Cyano-HABs): developing a public health response. Lake Reserv Manage 18(1):20–31

Backer LC, Fleming LE, Rowan A, Cheng YS, Benson J, Pierce RH, Zaias J, Bean J, Bossart GD, Johnson D, Quimbo R, Baden DG (2003) Recreational exposure to aerosolized brevetoxins during Florida red tide events. Harmful Algae 2(1):19–28

Backer LC, Kirkpatrick B, Fleming LE, Cheng YS, Pierce R, Bean JA, Clark R, Johnson D, Wanner A, Tamer R, Zhou Y, Baden DG (2005) Occupational exposure to aerosolized brevetoxins during Florida red tide events: effects on a healthy worker population. Environ Health Persp 113(5):644–659

Baker A, Glynn PW, Riegl B (2008) Climate change and coral reef bleaching: an ecological assessment of long-term impacts recovery trends and future outlook. Estuar Coast Shelf Sci 80:435–471

Bakun A (2006) Front and eddies as key structures in the habitat of marine fish larvae: opportunity, adaptive response and competitive advantage. Sci Mar 70(S2):105–122

Bao J, Li X, Yu C (2015) The construction and validation of the heat vulnerability index a review. Int J Environ Res Public Health 12:7220–7234. doi:103390/ijerph120707220

Barnes BB, Hu C, Holekamp KL, Blonski S, Spiering BA, Palandro D, Lapointe B (2013a) Use of Landsat data to track historical water quality changes in Florida keys marine environments. Remote Sens Environ 140:485–496

Barnes BB, Hu C, Kovach C, Silverstein R (2015) Sediment plumes induced by the Port of Miami dredging: analysis and interpretation using Landsat and MODIS data. Remote Sens Environ 170:328–339

Barnes BB, Hu C, Schaeffer BA, Lee Z, Palandro DA, Lehrter JC (2013b) MODIS-derived spatiotemporal water clarity patterns in optically shallow Florida Keys waters: a new approach to remove bottom contamination. Remote Sens Environ 134:377–391

Basly L, Wald L (2010) Remote sensing and air quality in urban areas. In: Laurini R, Tanzi T (Eds) Second International Symposium on TeleGeoProcessing, May 2000, Sophia Antipolis, France, p. 213–219

Bechle MJ, Millet BD, Marshall JD (2013) Remote sensing of exposure to NO2: satellite versus ground-based measurement in a large urban area. Atmos Environ 69:345–353

Belluco E, Camuffo M, Ferrari S, Modenese L, Silvestri S, Marani A, Marini M (2006) Mapping salt-marsh vegetation by multispectral and hyperspectral remote sensing. Remote Sens Environ 105:54–67

Bellwood DR, Hughes TP (2001) Regional-scale assembly rules and biodiversity of coral reefs. Science 292(5521):1532–1535. doi:101126/science1058635

Bierman P, Lewis M, Ostendorf B, Tanner J (2011) A review of methods for analysing spatial and temporal patterns in coastal water quality. Ecol Indic 11:103–114

Blough NV, Del Vecchio R (2002) Chromophoric DOM in the coastal environment. In: Hansell DA, Carlson CA (Eds) Biogeochemistry of Marine Dissolved Organic Matter, Academic, San Diego, CA

Boyd CE, Schmittou HR (1999) Achievement of sustainable aquaculture through environmental management. Aquacult Econ Manage 3(1):59–69

Buczak A, Koshute P, Babin ST, Feighner BH, Lewis SH (2012) A data-driven epidemiological prediction method for dengue outbreaks using local and remote sensing data. BMC Med Inform Decis Mak doi:101186/1472-6947-12-124

Bukata RP (2005) Satellite Monitoring of Inland and Coastal Water Quality: Retrospection, Introspection, Future Directions. CRC Press, Boca Raton FL

Burke L, Reytar K, Spalding M Perry A (2011) Reefs at risk revisited. World Resources Institute Washington p 130

Carrick NA, Ostendorf B (2007) Development of a spatial decision support system (DSS) for the Spencer Gulf penaid prawn fishery, South Australia. Environ Modell Softw 22:137–148

Chakalall B, Mahon R, McConney P, Nurse L, Oderson D (2007) Governance of fisheries and other living marine resources in the Wider Caribbean. Fish Res 87:92–99

Chen PY, Chen CC, Chu L, McCarl B (2015) Evaluating the economic damage of climate change on global coral reefs. Global Environ Change 30:12–20

Chen Z, Hu C, Conmy RN, Muller-Karger F, Swarzenski P (2007a) Colored dissolved organic matter in Tampa Bay, Florida. Mar Chem 104(1–2):98–109

Chen Z, Hu C, Muller-Karger F (2007b) Monitoring turbidity in Tampa Bay using MODIS/Aqua 250-m imagery. Remote Sens Environ 109:207–220

Cho L (2005) Marine protected areas: a tool for integrated coastal management in Belize. Ocean Coast Manage 48:932–947

Chollett I, Muller-Karger FE, Heron S, Skirving W, Mumby PJ (2012) Seasonal and spatial heterogeneity of recent sea surface temperature trends in the Caribbean Sea and southeast Gulf of Mexico. Mar Pollut Bull 64:956–965

Chuang TW, Henebry GM, Kimball JS, VanRoekel-Patton DS, Hildreth MB, Wimberly MC (2012) Satellite microwave remote sensing for environmental modeling of mosquito population dynamics. Remote Sens Environ 125:147–156

Chust G, Galparsoro I, Borja A, Franco J, Uriarte A (2008) Coastal and estuarine habitat mapping using LIDAR height and intensity and multi-spectral imagery. Estuar Coast Shelf Sci 78:633–643

Cloern JE, Foster SQ, Kleckner AE (2013) Review: Phytoplankton primary production in the world's estuarine-coastal ecosystems. Biogeosciences Discussions 10:17725–17783

Colwell RR (1996) Global climate and infectious disease: the cholera paradigm. Science 274(5295):2025–2031

Colwell RR (2004) Infectious disease and environment: cholera as a paradigm for waterborne disease. Int Microbiol 7:285–289

Dabrowska-Zielinska K, Gruszczynska M, Lewinski S, Hoscilo A, Bojanowski J (2009) Application of remote and *in situ* information to the management of wetlands in Poland. J Environ Manage 90:2261–2269

Dahl T, Stedman S (2013) Status and trends of wetlands in the coastal watersheds of the Conterminous United States 2004 to 2009. US Department of the Interior Fish and Wildlife Service and National Oceanic and Atmospheric Administration National Marine Fisheries Service (p 46)

Devlin M, Bricker S, Painting S (2011) Comparison of five methods for assessing impacts of nutrient enrichment using Estuarine case studies. Biogeochemistry 106:177–205

Van Dolah FM (2000) Marine algal toxins: origins health effects and their increased occurrence. Environ Health Persp 108(1):131–141

Dowd M (2005) A bio-physical coastal ecosystem model for assessing environmental effects of marine bivalve aquaculture. Ecol Model 183:323–346

Eakin CM, Nim CJ, Brainard RE, Aubrecht C, Elvidge C, Gledhill DK, Muller-Karger F, Mumby PJ, Skirving WJ, Strong AE, Wang M, Weeks S, Wentz F, Ziskin D (2010) Monitoring Corals from Space. Oceanography 23(4):118–133

Epstein PR, Ford TE, Colwell RR (1993) Health and climate change: marine ecosystems. Lancet 342:1216–1219

Evans RD, Murray KL, Field SN, Moore JAY, Shedrawi G, Huntley BG, Fearns P, Broomhall M, McKinna LIW, Marrable D (2012) Digitise this! A quick and easy remote sensing method to monitor the daily extent of dredge plumes. PloS One 7(12):e51668. doi:101371/journalpone0051668

Fanning L, Mahon R, McConney P (2009) Focusing on living marine resource governance: the Caribbean large marine ecosystem and adjacent areas project. Coast Manage 37:219–234

Faure V, Cheikh AI, Herve D, Cury P (2000) The importance of retention processes in upwelling areas for recruitment of Octopus Vulgaris: the example of the Arguin bank (Mauritania). Fish Oceanogr 94:343–355

Fiedler PC (1983) Satellite remote sensing of the habitat of spawning anchovy in the southern California Bight. Calif Coop Ocean Fish Invest 24:202–209

Fleming LE, Kirkpatrick B, Backer LC, Bean JA, Wanner A, Reich A, Zaias J, Cheng YS, Pierce R, Naar J, Abraham WM, Baden DG (2007) Aerosolized red-tide toxins (brevetoxins) and asthma. Chest 131(1):187–194

Food and Agriculture Organization of the United Nations (FAO) (2015) World Food Situation FAO Rome, Italy

Gardner TA, Cote IM, Gill JA, Grant A, Watkinson AR (2003) Long-term region-wide declines in Caribbean corals. Science 301:958–960

Garni R, Tran A, Guis H, Baldet T, Benallal K, Boubidi S, Harrat Z (2014) Remote sensing land cover changes and vector-borne diseases: Use of high spatial resolution satellite imagery to map the risk of occurrence of cutaneous leishmaniasis in Ghardaïa, Algeria. Infect Genet Evol 28:725–734

Ghioca-Robrecht DM, Johnston CA, Tulbure MG (2008) Assessing the use of multiseason Quickbird imagery for mapping invasive species in a Lake Erie coastal marsh. Wetlands 28:1028–1039

Giri C, Ochieng E, Tieszen LL, Zhu Z, Singh A, Loveland T, Masek J, Duke N (2011) Status and distribution of mangrove forests of the world using earth observation satellite data. Global Ecol Biogeogr 20:154–159

Glasgow HB, Burkholder JM, Reed RE, Lewitus AJ, Kleinman JE (2004) Real-time remote monitoring of water quality: a review of current applications and advancements in sensor telemetry and computing technologies. J Exp Mar Biol Ecol 300:409–448

Goodman JA, Purkis SJ, Phinn SR (eds) (2013) Coral Reef Remote Sensing: A Guide for Mapping, Monitoring and Management. Springer, Dordrecht, p 436

Goreau TJ, Hayes RL (1994) Coral bleaching and ocean "hot spots". Ambio 100(23):176–180

Goreau TJ, McClanahan T, Hayes R, Strong A (2000) Conservation of coral reefs after the 1998 global bleaching event. Conserv Biol 14 (1):5–15

Green EP, Mumby PJ, Edwards AJ, Clark CD (1996) A review of remote sensing for the assessment and management of tropical coastal resources. Coast Manage 24:1–40

Habtes SY (2014) Variability in the Spatial and Temporal Patterns of Larval Scombrid Abundance in the Gulf of Mexico. Dissertation, University of South Florida

Hay SI (2011) An overview of remote sensing and geodesy for epidemiology and public health application. Adv Parasit 47:1–35

Hedley JD, Roelfsema CM, Chollett I, Harborne AR, Heron SF, Weeks S, Skirving WJ, Strong AE, Eakin CM, Christensen TRL, Ticzon V, Bejarano S, Mumby PJ (2016) Remote sensing of coral reefs for monitoring and management: a review. Remote Sens 8 (118):1–40. doi:103390/rs8020118

Herrero J, Castañeda C (2009) Delineation and functional status monitoring in small saline wetlands of NE Spain. J Environ Manage 90:2212–2218

Heumann B (2011) Satellite remote sensing of mangrove forests: recent advances and future opportunities. Prog Phys Geog 35:87–108

Ho AJ, Grant SB, Surbeck CQ, DiGiacomo PM, Nezlin NP, Jian S (2005) Coastal water quality impacts of stormwater runoff from an urban watershed in Southern California. Environ Sci Technol 39(16):5940–5953

Hochberg EJ (2011) Remote sensing of coral reef processes. In: Dubinsky Z, Stambler N (eds) Coral reefs: an ecosystem in transition. Springer, Dordrecht, p 25–35

Hoegh-Guldberg O, Bruno JF (2010) The impact of climate change on the world's marine ecosystems. Science 328:1523–1528

Hu C, Luerssen R, Muller-Karger FE, Carder KL, Heil CA (2007) On the remote monitoring of Karenia brevis blooms of the west Florida shelf. Cont Shelf Res 28:159–176

Huq A, West PA, Small EB, Huq MI, Colwell RR (1984) Influence of water temperature salinity and pH on survival and growth of toxigenic Vibrio cholerae serovar O1 associated with live copepods in laboratory microcosms. Appl Environ Microb 48(2):420–424

IOCCG (2009) Remote sensing in fisheries and aquaculture.In: Forget M-H, Stuart V and Platt T (ed) Reports of the International Ocean-Colour Coordinating Group 8 IOCCG, Dartmouth, Canada

Jang E, Im J, Sunghyun H, Lee S, Park Y (2016) Estimation of water quality index for coastal areas in Korea using GOCI satellite data based on machine learning approaches. Korean J Remote Sens 32 (3):221–234

Janicki A, Wade D, Pribble RJ (2000) Developing and establishing a process to track the status of chlorophyll-a concentrations and light attenuation to support seagrass restoration goals in Tampa Bay. Tampa Bay Estuary Program Technical Report # 04-00

Jia M, Zhang Y, Wang Z, Song K, Ren C (2014) Mapping the distribution of mangrove species in the core zone of Mai Po Marshes nature reserve Hong Kong using hyperspectral data and high-resolution data. Int J Appl Earth Obs 33:226–231

Kachelreiss D, Wegmann M, Gollock M, Pettorelli N (2014) The application of remote sensing for marine protected area management. Ecol Indic 36:169–177

Kalluri S, Gilruth P, Rogers D, Szczur M (2007) Surveillance of arthropod vector-borne infectious diseases using remote sensing techniques: A review. PLoS Pathog 3(10):1361–1371

Kiang R (2009) Malaria Modeling and Surveillance. Benchmark Report

Kleypas JA, MacManus JW, Menez L (1999) Environmental limits to coral reef development: where do we draw the line? Am Zool 39:146–159

Laurs RM, Fiedler PC, Montgomery DR (1984) Albacore Tuna Catch distributions relative to environmental features observed from satellites deep sea research Part A. Oceanogr Res Pap 31 (9):1085–1099

Le C, Hu C, English D, Cannizzaro J, Chen Z, Feng L, Boler R, Kovach C (2012) Towards a long-term chlorophyll-a data record in a turbid estuary using MODIS observations. Prog Oceanogr 109:90–103

Le C, Hu C, English D, Cannizzaro J, Kovach C (2013) Climate-driven chlorophyll-a changes in a turbid estuary: observations from satellites and implications for management. Remote Sens Environ 130:11–24

Lee KS, Lai YL, Lo S, Barkham T, Aw P, Ooi PL, Tai JC, Hibberd M, Johansson P, Khoo SP, Ng LC (2010) Dengue virus surveillance for early warning, Singapore. Emerg Inf Dis 16:847–849. doi:10.3201/eid1605.091006

Lindo-Atichati D, Bringas F, Goni G, Muhling B, Muller-Karger F, Habtes S (2012) Varying mesoscale structures influence larval fish distribution in the northern Gulf of Mexico. Mar Ecol Prog Ser 463:245–257

Liu G, Heron SF, Eakin CM, Muller-Karger FE, Vega-Rodriguez M et al. (2014) Reef-scale thermal stress monitoring of coral ecosystems: New 5-km global products from NOAA Coral Reef Watch. Remote Sens 6:11579–11606

Lobitz BM, Beck L, Huq A, Wood B, Fuchs G, Faruque ASG, Colwell R (2000) Climate and infectious diseases: use of remote sensing for detection of Vibrio cholera by indirect measurements. Proc Natl Acad Sci Biol 97(4):1438–1443

Longdill PC, Healy TR, Black KP (2008a) GIS-based models for sustainable open-coast shellfish aquaculture management area site selection. Ocean Coast Manage 51:612–624

Longdill PC, Healy TR, Black KP (2008b) Transient wind-driven coastal upwelling on a shelf with varying width and orientation. New Zeal J Mar Fresh 42:181–196

Longdill PC, Healy TR, Black KP (2008c) An integrated GIS approach for sustainable aquaculture management area site selection. Ocean Coast Manage 51:612–624

Longdill PC, Healy TR, Black KP, Mead ST (2007) Integrated sediment habitat mapping for aquaculture zoning. J Coast Res Special Issue 50:173–179.

Lorenzoni L, Benway HM (2013) Report of Global intercomparability in a changing and ocean: An international time series methods workshop, 28–30 Nov 2012. Ocean Carbon and Biogeochemistry (OCB) Program and International Ocean Carbon Coordination Project (IOCCP) p 61.

Lowe R, Bailey TC, Stephenson DB, Graham RJ, Coelho CAS, Carvalho MS, Barcellos C (2011) Spatio-temporal modelling of climate-sensitive disease risk: Towards an early warning system for dengue in Brazil. Comput Geosci 37:371–381

MacAlister C, Mahaxay M (2009) Mapping wetlands in the Lower Mekong Basin for wetland resource and conservation management using Landsat EMT images and field survey data. J Environ Manage 90:2130–2137

MacKay H, Finlayson CM, Fernandez-Prieto D, Davidson N, Pritchard D, Rebelo L-M (2009) The role of earth observation (EO) technologies in supporting implementation of the Ramsar Convention on Wetlands. J Environ Manage 90:2234–2242

Magris RA, Treml EA, Pressey RL, Weeks R (2015) Integrating multiple species connectivity and habitat quality into conservation planning for coral reefs. Ecography 38:001–016

Malakar N, Atia A, Gross B, Moshary F (2014) Regional estimates of ground level aerosol using satellite remote sensing and machine learning Presented at the 94th AMS Annual Meeting Atlanta, GA, 2–6 Feb 2014

May CL, Koseff JR, Lucas LV, Cloern JE, Schoellhamer DH (2003) Effects of spatial and temporal variability of turbidity on phytoplankton blooms. Mar Ecol Prog Ser 254:111–128

Maynard JA, Anthony KRN, Harvell CD, Burgman MA, Beeden R, Sweatman H, Heron SF, Lamb JB, Willis BL (2011) Predicting outbreaks of a climate-driven coral disease in the Great Barrier Reef. Coral Reefs 30:485–495

McCarthy MJ, Halls J (2014) Habitat mapping and change assessment of coastal environments: an examination of WorldView-2 QuickBird and IKONOS satellite imagery and airborne LiDAR for mapping barrier island habitats. Int J GeoInf 3:297–325

McCarthy MJ, Merton EJ, Muller-Karger FE (2015) Improved coastal wetland mapping using very-high 2-meter spatial resolution imagery. Int J Appl Earth Obs 40:11–18

Meaden GJ, Aguilar-Manjarrez J (2013) Advances in geographic information systems and remote sensing for fisheries and aquaculture CD–ROM version FAO Fisheries and Aquaculture Technical Paper No 552, Rome FAO p 425

Méndez-Lázaro P, Muller-Karger FE, Otis D, McCarthy MJ, Peña-Orellana M (2014) Assessing climate variability effects on dengue incidence in San Juan Puerto Rico. Int J Environ Res Public Health 11(9):9409–9428

Mohan M, Kandya A (2015) Impact of urbanization and land-use/land-cover change on diurnal temperature range: a case study of tropical urban airshed of India using remote sensing data. Sci Total Environ doi:101016/jscitotenv201411006

Morabito M, Crisci A, Gioli B, Gualtieri G, Toscano P, Di Stefano V, Orlandini S, Gensini GF (2015) Urban-hazard risk analysis: mapping of heat-related risks in the elderly in major Italian cities. PLoS ONE doi:101371/journalpone0127277

Muller-Karger F, Varela R, Thunell R, Scranton M, Bohrer R, Taylor G, Capelo J, Astor Y, Tappa E, Ho TY, Walsh JJ (2001) Annual cycle of primary production in the Cariaco Basin: response to upwelling and implications for vertical export. J Geophys Res Oceans 106(C3):4527–4542

Mustapha MA, Saitoh SI (2008) Observations of sea ice interannual variations and spring bloom occurrences at the Japanese scallop farming area in the Okhotsk Sea using satellite imageries. Estuar Coast Shelf Sci 77:577–588

Nath SS, Bolte JP, Ross LG, Aguilar-Manjarrez J (2000) Applications of geographical information systems (GIS) for spatial decision support in aquaculture. Aquacult Eng 23:233–278. doi:101016/S0144-8609(00)00051-0

Noren F, Haamer J, Lindahl O (1999) Changes in the plankton community passing a Mytilus edulis mussel bed. Mar Ecol Prog Ser 191:187–194

Ortiz-Lozano L, Espejel I, Granados-Barba A, Arceo P (2007) A functional and integrated approach of methods for the management of protected marine areas in the Mexican coastal zone. Ocean Coast Manage 50:379–391

Ozesmi SL, Bauer ME (2002) Satellite remote sensing of Wetlands. Wetl Ecol Manag 10:381–402

Paciorek CJ, Liu Y (2009) Limitations of remotely sensed aerosol as a spatial proxy for fine particulate matter. Environ Health Persp 117:6

Pascual M, Rodó X, Ellner SP, Colwell RR, Bouma MJ (2000) Cholera dynamics and El Niño-Southern Oscillation. Science 289:1766–1769

Pereira HM, Leadley PW, Proenca V, Alkemade R, Scharlemann JPW, Fernandez-Manjarres JF, Araujo MB, Balvanera P, Biggs R, Cheung WWL, Chini L, Cooper HD, Gilman EL, Guenette S, Hurtt GC, Huntington HP, Mace GM, Oberdorff T, Revenga C, Rodrigues P, Scholes RJ, Sumaila UR, Walpole M (2010) Scenarios for global biodiversity in the 21st century. Science 300:1496–1501

Pettorelli N, Chauvenet ALM, Duffy JP, Cornforth WA, Meillere A, Baillie JEM (2012) Tracking the effect of climate change on ecosystem function using protected areas: Africa as a case study. Ecol Indic 20:269–276

Pettorelli N, Laurance WF, O'Brien TG, Wegmann M, Nagendra H, Turner W (2014) Satellite remote sensing for applied ecologists: opportunities and challenges. J Appl Ecol 51:839–848

Pitois S, Jackson MH, Wood BJB (2000) Problems associated with the presence of cyanobacteria in recreational and drinking waters. Int J Environ Heal Res 10:203–218

Pollock FJ, Lamb JB, Field SN, Heron SF, Schaffelke B, Shedrawi G, Bourne DG, Willis BL (2014) Sediment and turbidity associated with offshore dredging increase coral disease prevalence on nearby reefs. PloS One doi:101371/journalpone0102498

Quansah JE, Rochon GL, Quagrainie KK, Amisah S, Muchiri M, Ngugi C (2007) Remote Sensing Applications for Sustainable Aquaculture in Africa. IEEE International geoscience and remote sensing symposium 1255–1259

Raabe E, Roy L, McIvor C (2012) Tampa Bay coastal wetlands: nineteenth to twentieth century tidal marsh-to-mangrove conversion. Estuar Coast 35:1145–1162

Radiarta IN, Saitoh SI (2008) Satellite-derived measurements of spatial and temporal chlorophyll-a variability in Funka Bay southwestern Hokkaido, Japan. Estuar Coast Shelf Sci doi:101016/jecss200804017

Radiarta IN, Saitoh SI (2009) Biophysical models for Japanese scallop *Mizuhopecten yessoensis* aquaculture site selection in Funka Bay Hokkaido Japan using remotely sensed data and geographic information system. Aquac Int doi:101007/s10499-008-9212-8

Randolph K, Wilson J, Tedesco L, Li L, Pascual DL, Soyeux E (2008) Hyperspectral remote sensing of cyanobacteria in turbid productive water using optically active pigments chlorophyll-a and phycocyanin. Remote Sens Environ 112:4009–4019

Rinner C, Hussain M (2011) Toronto's urban heat island—exploring the relationship between land use and surface temperature. Remote Sens doi:103390/rs3061251

Ritchie JC, Zimba PV, Everitt JH (2003) Remote sensing techniques to assess water quality. Photogramm Eng Rem S 69(6):695–704

De La Rocque S, Michel V, Plazanet D, Pin R (2004) Remote sensing and epidemiology: examples of applications for two vector-borne diseases. Comp Immunol Microb 27:331–341

Rodó X, Pascual M, Doblas-Reyes FJ, Gerhanov A, Stone DA, Giorgi F, Hudson PJ, Kinter J, Rodríguez-Arias MA, Dtenseth NC, Alonso A, García-Serrano J, Dobson AP (2013) Climate change and infectious diseases: can we meet the need for better prediction? Clim Change 118:625–640

Rose JB, Epstein PR, Lipp EK, Sherman BH, Bernard SM, Patz JA (2001) Climate variability and change in the United States: potential impacts on water- and foodborne diseases caused by microbiologic agents. Environ Health Persp 109(2):211–220

Rueda-Roa D (2012) On the spatial and temporal variability of upwelling in the southern Caribbean Sea and its influence on the ecology of phytoplankton and of the Spanish sardine (*Sardinella aurita*). Dissertation, University of South Florida

Sale PF, Agardy T, Ainsworth CH, Feist BE, Bell JD, Christie P, Hoegh-Guldberg O, Mumby PJ, Feary DA, Saunders MI, Daw TM, Foale SJ, Levin PS, Lindeman KC, Lorenzen K, Pomeroy RS, Allison EH, Bradbury RH, Corrin J, Edwards AJ, Obura DO, Sadovy de Mitcheson YJ, Samoilys MA, Sheppard CRC (2014) Transforming management of tropical coastal seas to cope with challenges of the 21st century. Mar Pollut Bull 85:8–23

Santos A, Miguel P (2000) Fisheries Oceanography using satellite and airborne remote sensing methods: a review. Fish Res 49:1–20

Schaeffer BA, Hagy JD, Conmy RN, Lehrter JC, Stumpf RP (2012) An approach to developing numeric water quality criteria for coastal waters using the SeaWiFS satellite data record. Environ Sci Technol 46:916–922

Schaeffer BA, Schaeffer KG, Keith D, Lunetta RS, Conmy R, Gould RW (2013) Barriers to adopting satellite remote sensing for water quality management. Int J Remote Sens 34(21):7534–7544

Shamir E, Georgakakos PK (2014) MODIS Land Surface Temperature as an index of surface air temperature for operational snowpack estimation. Remote Sens Environ doi:org/101016/jrse201406001

Sherman K, O'Reilly J, Belkin IM, Melrose C, Friedland KD (2011) The application of satellite remote sensing for assessing productivity in relation to fisheries yields of the world's large marine ecosystems. ICSE J Mar Sci 68:667–676

Small A, Adey W, Spoon D (1998) Are current estimates of coral reef biodiversity too low? The view through the window of a microcosm. Atoll Res Bull 458:1–20

Somerfield PJ, Jaap WC, Clarke KR, Callahan M, Hackett K, Porter J, Lybolt M, Tsokos C, Yanev G (2008) Changes in coral reef communities among the Florida Keys 1996–2003. Coral Reefs 27:951–965

Soto Ramos I, Muller-Karger FE, Hu C, Wolny J (2017) Characterization of Karenia brevis blooms on the West Florida Shelf using ocean color satellite imagery: Implications for bloom maintenance and evolution. J Appl Remote Sens doi:10.1117/1.JRS.11.012002

Soto Ramos IM, Muller-Karger F, Hallock P, Hu C (2011) Sea surface temperature variability in the Florida Keys and its relationship to coral cover. J Mar Biol doi:101155/2011/981723

Speelman EC, Checkley W, Gilman RH, Patz J, Calderon M, Manga S (2000) Cholera incidence and El Niño-related higher ambient temperature. Jama-J Am Med Assoc 283(23):3072–3074

Steyn H (2010) An overview of small satellite activities in South Africa 1st Nanosat Symposium 11 June 2010

Stuart V, Platt T, Sathyendranath S (2011) The future of fisheries science in management: a remote-sensing perspective. ICSE J Mar Sci 68:644–650

Stumpf RP, Culver ME, Tester PA, Tomlinson M, Kirkpatrick GJ, Pederson BA, Truby E, Ransibrahmanakul V, Soracco M (2003) Monitoring Karenia brevis blooms in the Gulf of Mexico using satellite ocean color imagery and other data. Harmful Algae 2:147–160

Thomas Y, Mazurié J, Pouvreau S, Bacher C, Gohin F, Struski C Le Mao P (2006) Modelling the growth of *Mytilus edulis* according to farming practices and environmental parameters Application to 2003–2004 data in the bay of Mont Saint-Michel IFREMER Report RINT/LERMPL/06–16 (www.faoorg/fishery/gisfish/id/4373)

Thompson A, Schroeder T, Brando VE, Schaffelke B (2014) Coral community responses to declining water quality: Whitsunday islands great barrier Reef Australia. Coral Reefs 33(4):923–938

Thomson MC, Mason SJ, Phindela T, Connor SJ (2005) Use of rainfall and sea surface temperature monitoring for malaria early warning in Botswana. Am J Trop Med Hyg 73:214–221

Turner M, Gannon R (2014) Values of Wetlands. North Carolina State University http://wwwwatercncsuedu/watershedss/info/wetlands/valueshtml Accessed 21 Apr 2014

Vega-Rodriguez M, Muller-Karger FE, Hallock P, Quiles-Perez GA, Eakin CM, Colella M, Jones DL, Li J, Soto I, Guild L, Lynds S, Ruzicka R (2015) Influence of water-temperature variability on

stony coral diversity of Florida Keys patch reefs. Mar Ecol Prog Ser 528:173–186

Vincenzi S, Caramori G, Rossi R, De Leoa GA (2006) GIS-based habitat suitability model for commercial yield estimation of *Tapes philippinarum* in a Mediterranean coastal lagoon (Sacca di Goro Italy). Ecol Model 193:90–104

Walter C (2015) "BleachWatch Current Conditions Report" Mote Marine Laboratory and Florida Keys National Marine Sanctuary 2015 Accessed Sep 11 2015

Wang S, Fang L, Zhang X, Wang W (2015) Retrieval of aerosol properties for fine/coarse mode aerosol mixtures over Beijing from PARASOL measurements. Remote Sens doi:103390/rs70709311

White-Newsome JL Brines SJ, Brown DG, Dvonch T, Gronlund CJ, Zhang K, Oswald EM, O'Neill MS (2013) Validating satellite-derived land surface temperature with *in Situ* measurements: a public health perspective. Environ Health Persp doi: org/101289/ehp1206176

Wigbels L (2011) Using Air Observation Data to Improve Health in the United States: Accomplishments and future challenges Report to Center for Strategic and International Studies ISBN: 978-0-89206-668-1

Wirt KE, Hallock P, Palandro D, Semon Lunz K (2015) Potential habitat of Acropora spp on reef of Florida Puerto Rico and the US Virgin Islands. Global Ecol Conservation 2:242–255

Wofsy SC (1983) A simple model to predict extinction coefficients and phytoplankton biomass in eutrophic waters. Limnol Oceanogr 28:1144–1155

Wolf T, McGregor G (2013) The development of a heat wave vulnerability index for London, United Kingdom. Weather Clim Extrem 1:59–68

World Health Organization (2001) A Framework for field research in Africa Malaria early warning systems. WHO/CDS/RBM/2001.32

Xu Z, Liu Y, Ma Z, Li S, Hu W, Tong S (2014) Impact of temperature on childhood pneumonia estimated from satellite remote sensing. Environ Res 132:334–341

Yan X, Shi W, Zhao W, Luo N (2015) Mapping dustfall distribution in urban areas using remote sensing and ground spectral data. Sci Total Environ 506–507:604–612

Young SG, Tullis JA, Jackson C (2013) A remote sensing and GIS-assisted landscape epidemiology approach to West Nile virus. Appl Geogr doi:org/101016/japgeog201309022

Zhang T, Yang X, Hu S, Su F (2013) Extraction of coastline in Aquaculture coast from multispectral remote sensing images: object-based region growing integrating edge detection. Remote Sens doi: 103390/rs5094470

Zhao J, Hu C, Lapointe B, Melo N, Johns EM, Smith RH (2013) Satellite-observed Black Water events off Southwest Florida: implications for Coral Reef health in the Florida Keys National Marine Sanctuary. Remote Sens 5(1):415–431